



UNIVERSITÀ DEGLI STUDI DI SALERNO



UNIVERSITÀ DEGLI STUDI DI SALERNO

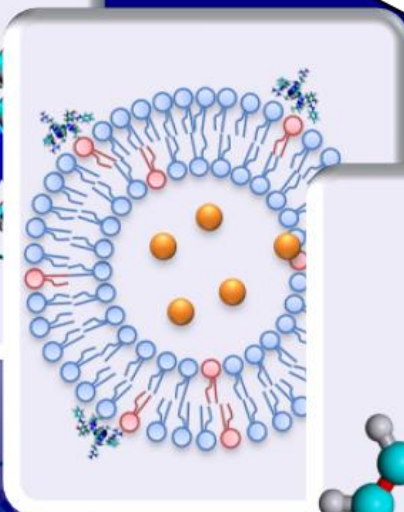
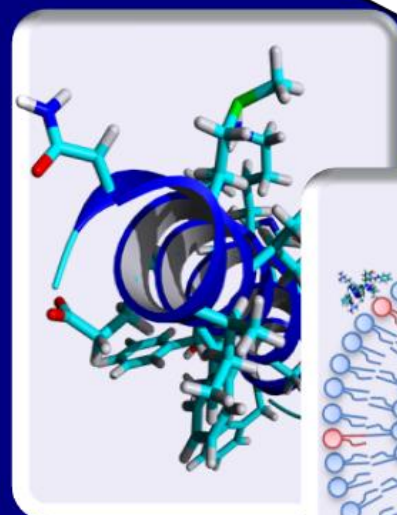
Dipartimento di Farmacia

Dottorato di ricerca

in Scienze farmaceutiche

Ciclo XII — Anno di discussione 2014

***Design and development of new polymeric materials
with potential antimicrobial and/or antifungal
activity***



Lucia Sessa



UNIVERSITÀ DEGLI STUDI DI SALERNO



UNIVERSITÀ DEGLI STUDI DI SALERNO
Dipartimento di Farmacia

Dottorato di ricerca
in Scienze Farmaceutiche
Ciclo XII — Anno di discussione 2014

Coordinatore: Chiar.mo Prof. *Gianluca Sbardella*

**DESIGN AND DEVELOPMENT OF NEW
POLYMERIC MATERIALS WITH POTENTIAL
ANTIMICROBIAL AND/OR ANTIFUNGAL
ACTIVITY**

settore scientifico disciplinare di afferenza: CHIM/03

Dottorando

Dott. Lucia Sessa

Tutori

Chiar.ma Prof.ssa Simona Concilio

Chiar.mo Prof. Pio Iannelli

To my family...

Publications

- Piotto, S. P., L. Sessa, S. Concilio and P. Iannelli. "Yadamp: Yet Another Database of Antimicrobial Peptides." *Int J Antimicrob Agents* 39, no. 4 (2012): 346-51.
- Concilio, S., S. Piotto, L. Sessa, P. Iannelli, A. Porta, E. C. Calabrese, M. R. Galdi and L. Incarnato. "Antimicrobial Polymer Films for Food Packaging." *AIP Conference Proceedings* 1459, no. 1 (2012): 256-258.
- Piotto, S., S. Concilio, L. Sessa, P. Iannelli, A. Porta, E. C. Calabrese, M. R. Galdi and L. Incarnato. "Novel Antimicrobial Polymer Films Active against Bacteria and Fungi." *Polymer Composites* 34, no. 9 (2013): 1489-1492.
- Piotto, S., S. Concilio, L. Sessa, A. Porta, E. C. Calabrese, A. Zanfardino, M. Varcamonti and P. Iannelli. "Small Azobenzene Derivatives Active against Bacteria and Fungi." *Eur J Med Chem* 68, (2013): 178-84.
- Bruno, A., C. Borriello, T. Di Luccio, G. Nenna, L. Sessa, S. Concilio, S. Haque and C. Minarini. "White Light-Emitting Nanocomposites Based on an Oxadiazole–Carbazole Copolymer (Poc) and Inp/Zns Quantum Dots." *Journal of Nanoparticle Research* 15, no. 11 (2013): 1-10.
- Sessa, L., S. Piotto, S. Concilio, T. Robinson, A. Küchler and P. Walde. "A Novel Photoresponsive Peptide with Antimicrobial Activity: A Biophysical Study." (*submitted*).

Conferences

- Sessa, L. , S. Concilio, S. Piotto, A. Porta, E. C. Calabrese and P. Iannelli. "Novel Materials with Antibacterial and Antifungal Activity." In *II International Conference on Antimicrobial Research (ICAR)*. Lisbon, Portugal, 21-23 November 2012.
- Piotto, S., L. Sessa, S. Concilio and P. Iannelli. "Molecular Simulation of Membrane Interacting Novel Antimicrobial Compounds." In *II International Conference on Antimicrobial Research (ICAR)*. Lisbon, Portugal, 21-23 November 2012.
- Sessa, L., S. Concilio, S. Piotto and P. Iannelli. "Engineered Amps for Nano Drug Delivery Systems." In *1st Workshop on Bio Nano Materials (BIONAM2013)* Department of Pharmacy, University of Salerno, 18 October 2013.
- Concilio, S., L. Sessa, S. Piotto and P. Iannelli. "Smart Materials for Biomedical Applications " In *1st Workshop on Bio Nano Materials (BIONAM2013)*. Department of Pharmacy, University of Salerno, 18 October 2013.

Table of contents

Table of contents	I
--------------------------------	----------

Abstract	V
-----------------------	----------

Part I. Design of new polymers inspired by AMPs

Chapter 1. Antimicrobial peptides: an overview	3
---	----------

1.1. Background	3
-----------------------	---

1.2. What are AMPs?	3
---------------------------	---

1.3. Classification by secondary structure	4
--	---

1.4. Principal families of cationic antibacterial peptides and their activity spectrum.....	9
---	---

1.5. Antimicrobial activity: mechanism of action.....	11
---	----

1.6. Bacterial resistance strategy.....	16
---	----

1.7. Limits of the antimicrobial peptides as therapeutic agents	18
---	----

1.8. AMPs in clinical trial	19
-----------------------------------	----

Chapter 2. Collection and building of a new AMPs database	23
--	-----------

2.1. Introduction.....	23
------------------------	----

2.2. Data collection	24
----------------------------	----

2.3. Database content	33
-----------------------------	----

2.4. Web database design: an overview	34
---	----

2.5. Using YADAMP.....	36
------------------------	----

Chapter 3. Development of a modified antimicrobial peptide..... 39

- 3.1. Design of modified antimicrobial peptides 39
- 3.2. Our approach..... 40
- 3.3. Chemical modification of natural amino acid with a photoactive ligand. 42
- 3.4. Selection of an AMP as template..... 46

Chapter 4. Investigation of the different membrane interaction..... 51

- 4.1. Aim of the work 51
- 4.2. Materials used 52
- 4.3. Effect of synthetic peptides on GUVs membrane permeability 62
- 4.4. Effect of synthetic peptides on LUVET membrane permeability 67
- 4.5. LUVETs characterization..... 86

Chapter 5. Conclusion e discussion 91**Part II. Development of new antimicrobial and antifungal compounds****Chapter 6. Small azobenzene derivatives active against bacteria and fungi..... 97**

- 6.1. Introduction..... 97
- 6.2. *In silico* screening 100
- 6.3. Azo compounds synthesis 104
- 6.4. Thermal and optical properties..... 115
- 6.5. Antimicrobial activity 118

Chapter 7. Structure modifications using A4 as lead compound..... 127

- 7.1. Introduction..... 127
- 7.2. Synthesis of A4 analogues with modified second ring 130
- 7.3. Synthesis of A4 analogues with modified first ring 133
- 7.4. Thermal and optical properties of A4 analogues compounds 135
- 7.5. Antimicrobial activity of A4 analogues compounds..... 137

Chapter 8. Conclusions and outlook..... 139**Part III. Development of new antimicrobial and antifungal polymer films****Chapter 9. Novel antimicrobial polymer films active against bacteria and fungi..... 143**

- 9.1. Introduction..... 143
- 9.2. Thin film preparation techniques 146
 - 9.2.1. Mold-casting method 147
 - 9.2.2. Solvent casting method 147
- 9.3. Material used..... 148
- 9.4. Experimental part: film preparation..... 153
- 9.5. Thermal characterization of the films 161
- 9.6. Summary of films characteristics..... 167
- 9.7. Microbiological Characterization 169
- 9.8. Conclusions and outlook..... 175

Appendix-a MatLab Scripts 179**Appendix-b Fmoc-azoTyr characterization..... 193**

Appendix-c Dynamic light scattering results.....	195
Appendix-d ¹H NMR spectra of azo compounds	201
Appendix-e Thermogravimetric characterization of azo compounds..	205
Appendix-f Thermal characterization of azo compounds.....	207
Appendix-g UV-Vis spectra of azo compounds.....	211
Appendix-h Thermal characterization of thin films	213
Abbreviations, Acronyms and Symbols	217
Reference.....	223

Abstract

This PhD project is focused on the development of new polymeric materials with antibacterial and antifungal activity.

The first part of the work was dedicated to the synthesis and the insertion of a modified amino acid into an antimicrobial peptide (AMP), with the aim to retain the action mechanism on bacterial membranes. Understanding the mechanism of action of AMPs is important for the rational design of new drugs. For this reason, I have collected structural properties, antimicrobial activity values and biological origin of antimicrobial peptides from published data. I have calculated the most relevant chemical physical properties like charge, hydrophobic moment, helicity, flexibility, isoelectric point, Boman and instability index and penetration capabilities. This data collection work permitted us to create YADAMP (www.yadamp.unisa.it), a web database with detailed informations on AMPs. YADAMP database contains the highest number of active sequences with proven antimicrobial activity. YADAMP permitted me to do a work of data mining that end up with the choice of a peptide, a defensin, to be used as template for developing a new photoresponsive peptide. The peptide, hereafter indicated as ALY, is a short α -helix, membrane active AMP with a tyrosine in the sequence. I have developed the modified analogue replacing the tyrosine by a modified tyrosine with azobenzene group in the side chain. The modified amino acid, named Fmoc-azoTyr, was synthesized according to the classic scheme of diazocoupling reactions. I have chosen the azobenzene group because it permits a reversible *trans* to *cis* photochemical isomerization. The photo-induced switch will, potentially, permit to turn on or off the peptide antimicrobial activity. As described in the following part, we have already confirmed the antimicrobial and antifungal activity of azobenzene group.

Therefore, the modified peptide might have a broader spectrum of activity due to the azobenzene presence, and it might act as a prodrug, generating *in vivo* the antimicrobial azo compound. I evaluated the difference in membrane permeability due to the introduction of the modified amino acid performing studies of membrane permeability during a period in the group of Prof. Peter Walde at the Swiss Federal Institute of Technology (ETH Zurich). Calcein leakage assays showed that the modified amino acid introduced into active sequence increased the membrane permeability of a suspension of giant unilamellar vesicles compared to the unmodified peptide at the same conditions. I have prepared large unilamellar vesicles formed by POPC/POPG (mixture 90:10 mol/mol), that contain HRP enzyme, by mechanical extrusion and I performed measurements of enzyme leakage after interaction with the peptide. In this assay the membrane permeability was associated with an increase in enzyme activity. Preliminary results of enzyme leakage showed a greater membrane perturbation with time-dependence enzyme leakage from LUVs after interaction with modified peptide.

The second part of my research work was focused on the design and the synthesis of antimicrobial low molecular weight molecules with antimicrobial and antifungal activity. I used the phytoalexin resveratrol as template to design a new class of active compounds with azobenzene structure. I selected the best candidates by preliminary *in silico* test of ADMET properties and then I synthesized the azo compounds with lowest *in silico* toxicity values (A1, A2, A3, A4, A5, B10 and B11) according to the classic scheme of diazocoupling reaction. The antimicrobial activity and the thermal stability of each compound were evaluated. The majority of synthesized compounds exhibited high antibacterial activity against *S. aureus* and antifungal activity against *C. albicans*, but they were inactive against Gram-negative bacteria such as *P. aeruginosa* and *S. Typhimurium*. The different antibacterial activities of synthesized azo compounds suggest that these molecules interact with protein

receptors and that the interaction with membranes is of minor importance. To validate this hypothesis, I carried out structural modifications of azo compounds to enhance their biological activity. I have used the best antimicrobial azo compounds named A4 (4'-hydroxy-(4-hydroxy-3,5-dimethyl)-azobenzene) as lead compound to synthesize several analogues having modifications on the first and on the second azobenzene ring. This includes the moving of the phenolic hydroxyl group from *para*- to *meta*-position, the removal of the phenolic hydroxyl group, and the replacement of the phenolic hydroxyl group by the methoxy or the methyl group. In this way I obtained molecules with antibacterial and antifungal activity higher than lead compound.

The antimicrobial activities of these azo compounds and their thermal stability are very promising and indicate that these molecules may have interesting and therapeutically significant applications. A possible application is the insertion of azo compounds into polymeric matrices to produce composites with low production cost, good processability, and antimicrobial potential. Using solvent casting and mold casting methods, I realized active antimicrobial and antifungal films using polyolefins (such as PP and LLDPE) and biodegradable polymers (such as PLA, PVA and Mater-B), by introducing different percentages of antimicrobial azo dyes in polymer matrices. The obtained thin films retained the proprieties of the pure matrices without azo compounds such as thermal proprieties, flexibility and transparency; also I prepared transparent amorphous films, as confirmed by X-Ray analysis. The films exhibited antimicrobial activity and the capability to inhibit biofilms formation of *S. aureus* and *C. albicans*. Concentration of 0.01% (w/w) permitted the preparation of active, uncolored and transparent films. This is the first time that novel azobenzene based antimicrobial compounds have been added into polymer films. These preliminary tests confirmed that the new materials realized in this thesis are promising for future applications in the field where

an intrinsic antimicrobial ability of the material is required, like biomedical tools, antibacterial surfaces, and films for food packaging. Spectrophotometric investigation of the azo compound release from the polymer matrices is currently undergoing.

Part I.

Design of new polymers inspired by AMPs

Chapter 1. Antimicrobial peptides: an overview

1.1. Background

Since the discovery of the penicillin, the subsequent development of new antibiotics has considerably improved the public health. However, starting from the 80s, a slowdown was observed. First, very few antibiotics were discovered, but improvements within existing classes were still suggested. Second, a resistance to almost all antibiotics was observed in clinical use. However, the use and overuse of antibiotics has causing the emergence of multidrug-resistant microorganisms. Due to mutations and adaptation in bacteria, traditional antibiotics became more inefficient and the elimination of adapted strains has become increasingly difficult [1].

This is the reason why antimicrobial peptides (AMPs) are receiving much attention as a class of new antibiotics. Traditional antibiotics generally target a specific physiological process of bacteria, such as DNA replication, cell wall synthesis, etc. Instead, most AMPs target the bacterial cell membrane without specific receptors. Consequently their membrane interaction and broad activity spectra are becoming an ideal approach to overcome the resistance resulting from bacterial mutations [2].

1.2. What are AMPs?

The term AMP is generally used to define a large number of small proteins produced by multicellular organisms that are able to kill or to inhibit growth of various microorganisms [3]. They are small peptides, highly variable, with 12–50 amino acids, mostly in their common L configuration. Due to the presence of basic amino acids as Lys and Arg, they are positively charged, with net charge from + 2 to + 9. AMPs possess approximately 50% hydrophobic

residues, which allow an amphipathic conformation that permits them to interact with bacterial membranes [4]. These molecules are able to kill or inhibit a variety of organisms, including Gram-positive and Gram-negative bacteria, fungi, viruses, protozoa, parasites [5]. More than two thousand natural AMPs have been isolated and characterized from different sources and several thousands of synthetic variants have been developed.

1.3. Classification by secondary structure

AMPs can be divided into many subtypes following different criteria: origin, amino acid sequence, size, structure, biological action, mechanism of action and others; but it has been shown that secondary structure is the only meaning criterion to order them [6]. The secondary structure of AMPs include four major classes, α -helix, β -sheet stabilized by two or more disulfide bridges, extended helices with a predominance of one or more amino acids and loop structures with one disulfide bridge. As one of most widely distributed AMPs, α -helical antimicrobial peptides (α AMPs) have been thoroughly investigated.

1.3.1. α -helical antibacterial peptides

The α -helical peptides family is the largest, the most common in nature and the most studied class of cationic peptides. They have been found in plants, vertebrates and invertebrates. This subgroup contains linear peptides with antimicrobial activity, generally formed of less than forty amino acid residues other than cysteine [7]. They are highly positively charged and present notable amphipathic behavior. In aqueous solution these peptides are unstructured and fold into their α -helical configuration after binding the bacterial membrane. Here they could be absorbed onto bacterial surface or inserted into it. A direct correlation between α -helical conformation and antibacterial activity has been established [8].

Some known families are cecropins, andropins, melittins and ceratotoxins from insects; or magainins, bombinins, dermaseptins, esculentins and buforins II from amphibians.

Figure 1.1 shows two known example such as Magainin 2 from frogs and LL-37 from humans. The structures were taken from the RCSB Protein Data Bank (<http://www.pdb.org/>) and personally modified using YASARA software. The protein are colored by secondary structure elements, which means that α -helices are blue, β - strands are red, turns are green and random coil is cyan.

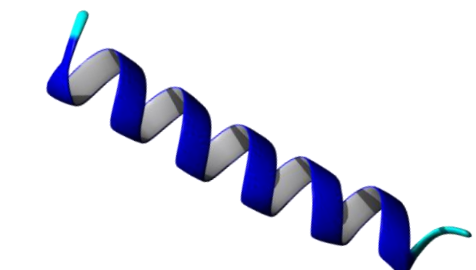
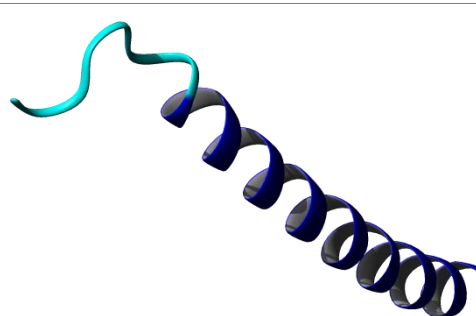
a)		<p><i>Name</i> magainin 2 <i>Chain</i> GIGKFLHSAKKFGKAFVGEI MNS <i>Source</i> Xenopus laevis</p>
b)		<p><i>Name</i> Cathelicidin LL-37 <i>Chain</i> LLGDFFRKSKEKIGKEFKRIV QRIKDFLRNLVPRTES <i>Source</i> Homo sapiens</p>

Figure 1.1. 3D model structures representing to the structure of magainin 2, PDB ID: 2MAG (a); LL-37, PDB ID: 2K6O (b).

1.3.2. β -sheet antibacterial peptides

This subgroup is formed of β -sheet peptides that are conformationally forced and stabilized because of the presence from one to five disulfide bridges [7]. They adopt a sort of cyclic conformation. They already exist in their β -sheet conformation in aqueous solution and may be more stabilized after binding the bacterial membrane. The number of disulfide bridges has an impact on the overall structure as well as on the activity of the peptide. It has been shown that the cyclic structure is essential for antibacterial activity [9].

Some known examples with 2 disulfide bonds are protegrins from porcine leukocytes, or tachyplesins from horseshoe crabs, while examples with 3 disulfide bonds are defensins from several human tissues humans; finally peptides with more than 3 disulfide bonds are drosomycins in fruit flies. *Figure 1.2* shows an example for each category, as reported for α -helical peptide. The structures are colored by secondary structure elements.

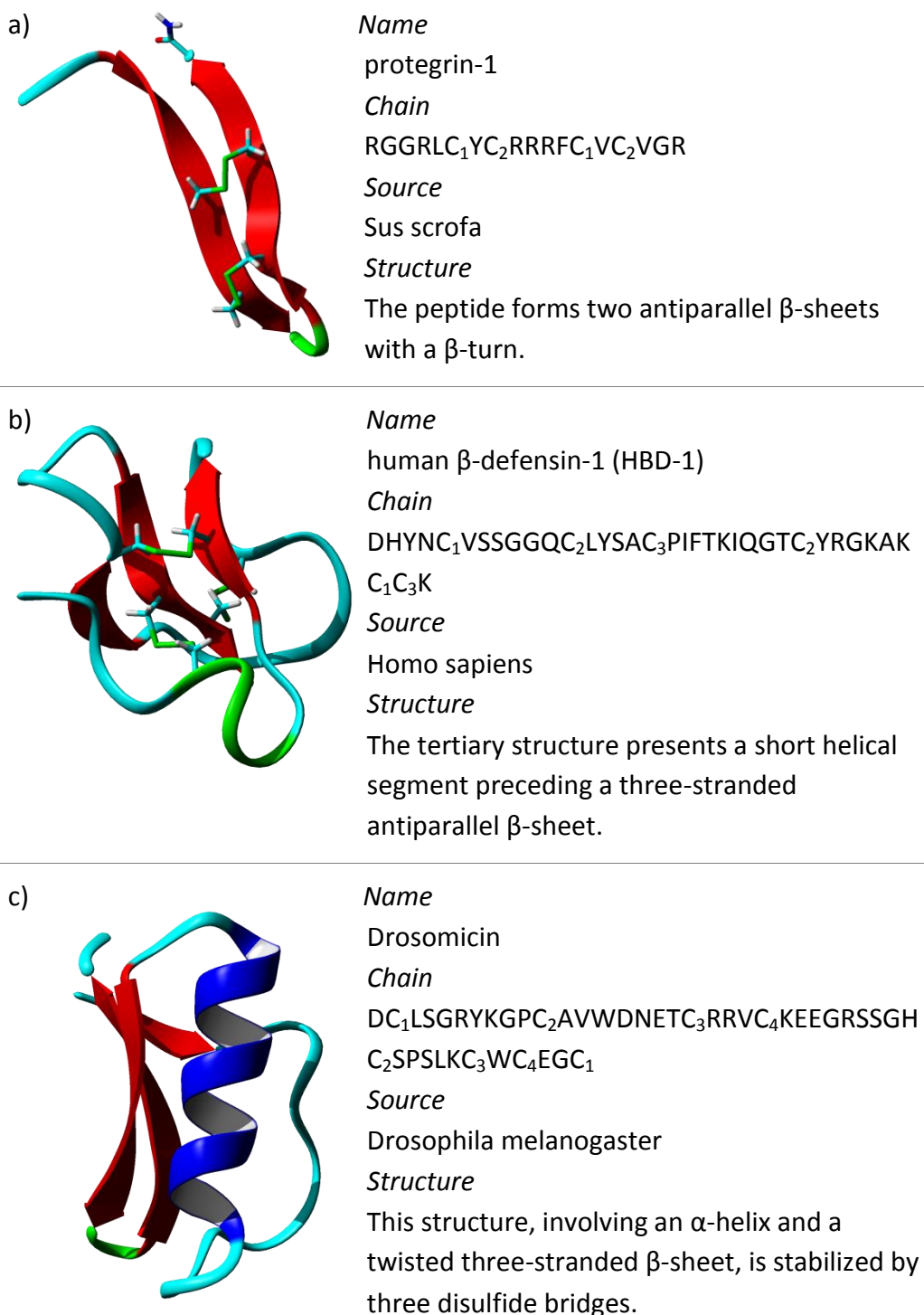
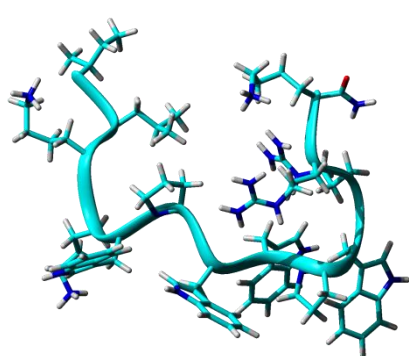


Figure 1.2. 3D model structures representing to the structure of protegrin-1, PDB ID: 1PG1 (a); HBD-1, PDB ID: 1KJ5 (b) and Drosomycin, PDB 1MYN (c).

1.3.3. Linear extended antibacterial peptides

Linear extended peptides are very flexible in solution but they do not fold into regular secondary structure. These peptides are characterized by an overexpression of one or more amino acids, especially Arg, Trp or Pro residues. Some of them are rich in histidine residues, like histatin found in human saliva [10], others, such as abaecin and apidaecins from honeybees, are rich in proline residues or as prophenin from pigs, rich in proline and phenylalanine and indolicidin from cattle, rich in tryptophan and arginine residues (*Figure 1.3*).



Name

Cathelicidin-4

Chain

ILPWKWPWWPWRR

Source

Bos taurus

Structure

No regular secondary structure elements.

Figure 1.3. 3D model structures representing to the structure of Indolicidin derivative, PDB ID: 1QXQ

1.3.4. Loop antibacterial peptides

This is a quite small group of peptides which adopt a loop formation with one intramolecular disulfide bridge, often in the C-terminal part. Bactenecin, isolated from bovine neutrophils, is the first peptide in this group [11], other examples are peptides extracted from the frog skin, such as ranalexin or brevinin which contain a C-terminal loop and a long N-terminal tail, or thanatin from insect hemocytes (*Figure 1.4*).

**Name**

Thanatin

ChainGSKKPVPIIYC₁NRRTGKC₁QRM**Source**

Podisus maculiventris (Spined soldier bug)

Structure

Thanatin adopts a well-defined anti-parallel beta-sheet structure from residue 8 to the C-terminus, including the disulfide bridge.

Figure 1.4. 3D model structures representing to the structure of Thanatin, PDB ID: 8TFV

1.4. Principal families of cationic antibacterial peptides and their activity spectrum

A variety of different natural peptides have been identified and isolated from many organisms in addition, modified and mimetic peptides have been designed and synthesized.

Amongst the multi-drug resistant bacteria responsible for nosocomial infections are *Staphylococcus aureus*, *Pseudomonas aeruginosa* and *Escherichia coli*. In this paragraph, the principal families of cationic AMPs active against these pathogens will be described.

1.4.1. Magainins

The name magainin derives from the Hebrew *magain* meaning shield. Magainins 1 and 2 were the first AMPs extracted thirty years ago from the skin of the African frog *Xenopus laevis* [12]; they can be found within amphibian skin as well as mammals. They are composed of 23 amino acids, exhibit a net charge of +4 and differ by two residues in position 10 and 22. They adopt an amphipathic α -helical structure and present a broad

antimicrobial activity spectrum against Gram-positive and Gram-negative bacteria with a MIC (Minimum Inhibitory Concentration) value between 50 and 150 $\mu\text{g mL}^{-1}$. Different analogues have been synthesized and they showed enhanced activity. Their mechanism of action follows the toroidal pore model to permeabilize the bacterial membrane [13].

1.4.2. Cathelicidins

Cathelicidins are cationic peptides constituted by a highly conserved *N*-terminal domain of approximately 100 residues, named cathedin and with a structurally variable antimicrobial domain at the *C*-terminus. They have been isolated in neutrophilic granules and epithelial cells of many invertebrate and vertebrate species, including reptiles, fishes, birds, mammals and humans [14-16].

Among the most studied cathelicidins are SMAP-29 and LL-37. SMAP-29 has been isolated in sheep and is, nowadays, one of the most potent AMP known: its MIC against some bacteria being below 1 $\mu\text{g mL}^{-1}$. It is composed of 29 residues, adopts an α -helical conformation and presents an amphipathic nature [17]. Its antibacterial activity is attributed to its *N*-terminal amphipathic α -helix. The only cathelicidin found in humans is LL-37, a cationic α -helical peptide formed by 37 amino acids with two leucine residues at the beginning. LL-37 disrupts the bacterial membrane through the toroidal pore model or through the carpet model [18].

1.4.3. Defensins

Defensins are cationic peptides rich in cysteine residues, adopting β -sheet structures. The first peptides were discovered in 1983 in rabbits [19] and only two years later in humans [20]. Since these discoveries many similar peptides were isolated from other organisms.

They have broad spectra of activity due to interact and disrupt the lipid membranes by multimerizing and forming pores, with subsequent lysis of the microbes.

Mammalian defensins contain three stabilizing disulfide bridges formed by six cysteine residues [21]. They are classified into three subclasses: α -defensins and β -defensins, adopting a triple-stranded β -sheet conformation, and θ -defensins, adopting a total circular conformation.

In contrast, insect defensins contain an α -helix domain bound to a β -sheet region via a disulfide bridge.

Plant defensins, commonly called as thionines, may contain up to eight cysteines, thus forming up to four disulfide bridges. They also contain both α -helix and β -sheet domains.

It is known that AMPs found in humans or in mammals are not limited to cathelicidins and defensins, but other anionic peptides into histatins and dermcidins families were also found in some tissue.

1.5. Antimicrobial activity: mechanism of action

1.5.1. Reaching of the site of action

Regardless of the precise mechanism, the interaction with the cell membrane is the key step for all AMPs [22]. For Gram-negative and Gram-positive bacteria, the bactericidal process of cationic AMPs is stepwise and generally rapid. Initially, driven by electrostatic forces, AMPs diffuse toward the cell membrane even from a relatively long distance. It is hypothesized that the negative charge on the outer bacterial envelope and the strong electrochemical gradient of the bacterial cytoplasmic membrane both contribute to the attraction of cationic AMPs [23].

Before looking at the mode of action, it is necessary to understand the membrane biology of bacteria, fungi and eukaryotic membranes, which are the primary targets for most AMPs.

Universally, all cell membranes can be seen as fluid mosaics of proteins and phospholipids, which are arranged as bilayers with hydrophobic and hydrophilic domains. However, a significant lipid compositional difference exists between the prokaryotic and eukaryotic membranes as well as among cell types.

Bacterial membranes (*Figure 1.5*) are made up of negatively charged phospholipids such as phosphatidylglycerol (PG), cardiolipin (CL), or phosphatidylserine (PS) [24], which are stabilized by divalent cations such as Mg^{+2} or/and Ca^{+2} . Even though there is not much difference in lipid composition, Gram-negative bacteria differ from Gram-positive bacteria as the former have a smaller peptidoglycan layer and an outer membrane, in addition to a cytoplasmic membrane containing lipopolysaccharide (LPS), which acts as permeability barrier [25].

Interestingly, some peptides binding to Gram-negative bacterial membranes induce Mg^{2+} ion displacement between the LPS, thus destabilizing the membranes arrangement.

In contrast to bacteria, fungal membranes are rich in phosphomannans and other related constituents such as negatively charged phosphatidylinositol (PI), phosphatidylserine (PS) and diphosphatidylglycerol (DPG), which give a higher negative charge surface to the membranes [26].

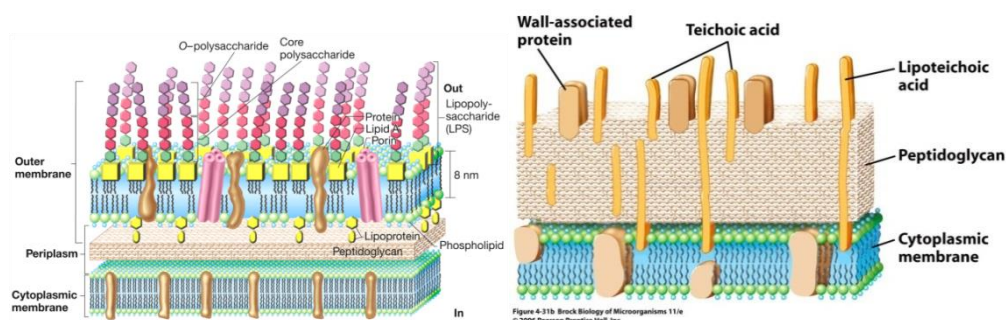


Figure 1.5. Schematic structure of Gram-negative (on the left) and Gram-positive (on the right)[27]

On the other hand, mammalian membranes are rich in zwitterionic phospholipids with neutral net charge, including phosphatidylethanolamine (PE), phosphatidylcholine (PC), or sphingomyelin (SM). Moreover, cholesterol is present in significant amounts in mammalian membranes and can reduce the activity of AMPs by affecting the fluidity and dipole potential of phospholipids, in addition to stabilizing the lipid bilayers and delaying the binding of peptides to the membranes. Therefore, sterol in the mammalian membranes is thought to be involved in the specificity of action of the antimicrobial peptides [28], in addition membrane potential and asymmetric distribution of phospholipids in eukaryotic membranes contribute to prevention of AMPs binding [29].

1.5.2. Proposed models

After reaching the bacterial surface, cationic peptides competitively displace divalent cations due to different binding affinities. Divalent cations act as stabilizers for the LPS by binding the anionic phosphate groups. The loss of Mg^{2+} and Ca^{2+} results in the disturbance of the rigid outer membrane and promotes the uptake of more molecules. During this process, many linear AMPs fold into an amphipathic structure due to the hydrophobic environment of the cell membrane. The amphipathic nature of AMPs is essential for further

interaction with the hydrophobic components of the membrane. Consequently, the peptides contact the cytoplasmic membrane and disrupt the lipid bilayer in multiple ways.

During this folding process, it is proposed that AMPs adopt a parallel orientation to the membrane. Moreover, there is an accumulation of the peptides on the surface of the membrane, until a threshold in peptide interfacial concentration is reached. Parameters influencing the threshold concentration include the propensity of peptide self-assembly, peptide charge, amphipathicity and hydrophobicity, as well as membrane fluidity and composition [30, 31].

An overview of the widely accepted models proposed to clarify the membrane permeabilization is given in *Figure 1.6*: they include the carpet model, barrel-stave model and toroidal-pore model and all of them need the interaction of cationic AMPs with the negatively charged outer membrane surface in a parallel orientation.

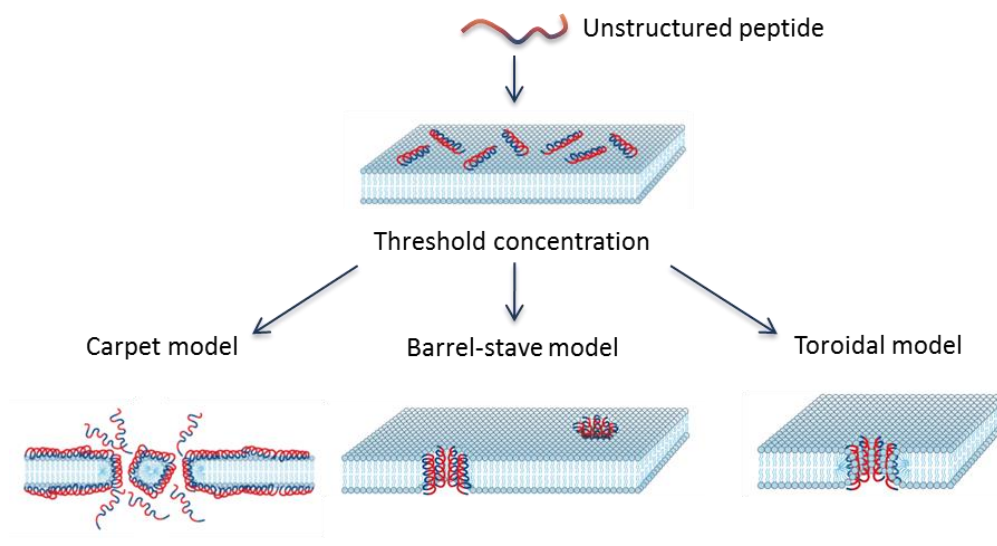


Figure 1.6. Three expected models of interaction between cationic AMPs and cytoplasmic membrane [7].

a) In the carpet model the peptides initially associate with the membrane, align parallel to the surface of bilayer and cover the surface. This orientation destabilizes the packing of phospholipids and causes a change in membrane fluidity because of the moving of phospholipids by peptides. Thus, the stability of the local membrane is disturbed. When a threshold peptide concentration is reached, the membrane will break down due to unfavorable energetics. The general features of the carpet model include that peptides remain in contact with the lipid head groups with consequent membrane dissolving [32].

b) Barrel-stave model was first proposed by Ehrenstein and Lecar in 1977. According to this model, a variable number of individual peptide molecules are arranged to form a barrel-like pore or channel. In this mechanism, peptide hydrophobic surfaces interact with the acyl chains of lipid in the membrane, generating an aqueous pore consisting of at least four peptides. A crucial step in this model is that peptides have to recognize each other in the membrane bound state. It is highly energetically unfavorable for a single peptide to traverse the membrane, hence the peptides aggregate on the surface until the threshold concentration is reached, and then insert into the hydrophobic core of the membrane by undergoing a conformational phase transition, forcing polar-phospholipids head groups aside to induce localized membrane thinning. This event is followed, by additional recruitment of peptides around or into the channel, leading to an increase in pore size and stabilization, thus killing the microbe by leakage of intracellular components. Aggregation may be required simply because the amount of stabilization that one peptide provides is not sufficient for pore formation and stronger binding of peptides to pores could be due to packing reasons as lipid head groups are less tightly packed in pores [33].

c) Toroidal pores can be formed by a much greater variety of peptides. Prior to formation of both barrel-stave and toroidal pores, the peptide adsorbs

parallel to the membrane surface [34]. When a certain concentration on the surface is reached, the peptide either inserts perpendicularly into the membrane, or induces a positive curvature strain in the membrane, resulting in an opening, the so-called toroidal pore. The hydrophilic regions of the peptides keep the association with lipid head groups and the hydrophobic peptide regions associate with the hydrophobic core of the membrane lipids. Thus, the peptides and lipids together form well-defined pores, with the hydrophilic regions of the peptides and phospholipids head groups facing the center of the pore and producing an aqueous pore [23].

The effect of barrel-stave and toroidal mechanism is that peptides or other molecules could be translocated into the cytoplasm, resulting in enzyme inhibition or DNA and RNA binding.

Numerous AMPs are found to show antifungal activity and the mechanisms of action involve cell disruption by binding of the outer membrane. Moreover antifungal peptides interfere with cell wall synthesis [35]. AMPs also possess antiviral activity by interacting with virus proteins [36, 37] and different AMPs with antiparasitic activities have been discovered [38].

1.6. Bacterial resistance strategy

Presumably, bacteria have been exposed to AMPs for millions of years, but the development of resistance against AMPs has occurred to a much less degree.

Inability to develop resistance to AMPs is based on two points. Firstly, the bacterial membrane has to be modified and this is really hard for the microorganisms. Secondly, due to the presence of huge numbers of AMPs in the host, it is difficult for microbes to develop resistance against all peptides at the same time.

More recently, however, a few resistance mechanisms in bacteria against AMPs have been discovered and investigated. They include: surface modification, external trapping of AMPs, and active efflux of AMPs or proteolytic degradation.

The simplest way for a bacterium to increase its resistance towards AMPs is to reduce the negative net charge of its outer membrane. A small number of bacteria have developed some mechanisms to stop the first step of AMPs action in which they reduce the electrostatic interaction with the cationic peptides. These modifications concern the teichoic acid of peptidoglycan in Gram positive or the lipid A moiety of LPS in Gram negative bacteria. For example, some *Staphylococcus aureus* transport positively charged D-alanines residues from the cytoplasm to the anionic teichoic acids of the bacterial wall. These modified teichoic acids could have a role in the protection of some bacteria against antimicrobial peptides [39].

Other resistance mechanisms could involve the production of extracellular proteases, which are able to degrade cationic peptides. Interestingly, some bacteria such as *Pseudomonas sp.* and *S. epidermidis*, use other methods in addition to protease production, such as forming biofilms to prevent AMP insertion and pore formation [40]. AMP insertion and pore formation are prevented by this increased hydrophobicity of the membrane.

It has also been shown that ATP-Binding Cassette (ABC) transporters import AMPs into the bacteria, while efflux pumps export them. Overexpression of these efflux pumps can explain resistance to AMPs [41].

In conclusion, it is important to keep in mind that the primary target of an AMP is the bacterial membrane. To develop resistance against them, the bacteria should redesign their whole membrane a very long process. Considering that AMPs are part of the innate immune system, and that bacteria have had a huge time-span to adapt to their killing mechanisms, the resistance

phenomenon is extremely difficult. However, it is worth to notice that, among microbes, only bacteria have shown resistance mechanisms against AMPs.

1.7.Limits of the antimicrobial peptides as therapeutic agents

AMPs have many advantages which make them potential substitute of conventional antibiotics. They have broad spectra of activity, are efficient towards multi-resistant bacteria and are not hindered by resistance. However AMPs possess different disadvantages that limit their development as therapeutic agents. Briefly, these limits are:

- *Hemolytic activity for eukaryotic cells*

Since the mechanism of action involves membrane interactions, the antimicrobial peptides could interact with eukaryotic cells and lyse them. It was observed that some natural AMPs with amidated C-terminal show higher hemolytic effect [42]. It is known that the process of amidation stabilizes the helix formations after membrane binding [43, 44]. To decrease the unwanted effect Ulrich *et al.* have prepared the deamidated analogues observing a decrease of hemolytic effect, maintaining the antimicrobial activity [45].

- *Broad activity spectrum*

As already stated, antimicrobial peptides possess broad spectrum of activity, but this could be a problem in term of destruction of the microflora during the therapy with consequent risk of diarrhea and other infections [46].

- *Protease susceptibility*

Proteolytic stability is essential for therapeutic use of AMPs because they are rapidly inactivated by proteases in the human body. This problem can be overcome using different strategies. Considering that AMPs taken into account in this thesis do interact with bacterial membranes, the most frequent modification includes the replacing of natural amino acids with D-amino acids

in the antimicrobial sequence, in this case the proteases cannot hydrolyze the unnatural residues and the modified peptide is consequently more active [47]. Designing polymeric analogues, such as amphiphilic arylamide polymers that mimic the AMPs structures, is another good strategy to increase the stability against proteases. In addition these peptide mimetics could be prepared in an easy and less expensive way [48]. Finally, in some studies has been observed that peptide cyclization improves the serum stability of AMPs [49].

- *Salt sensitivity*

AMPs are inactive in presence of high salt concentrations. The mechanism of inactivation is not so clear, but the general idea is that the interaction with the salt occurs after the interactions with cell membranes, when AMPs organize in the secondary structure [50]. Therefore, it is necessary to develop new AMPs with the secondary structure more stable.

- *High cost of production*

If we compare the cost of production of traditional antibiotics with the cost of the production of AMPs, the last one is really higher. Compared with the cost of traditional antibiotics, circa 1\$/g, an AMP produced by fermentation can cost more than \$400/g [2]. The high cost slowed the development of novel AMP drugs.

1.8.AMPs in clinical trial

Several companies are currently attempting to developed AMP-based drugs, but to date, none of them have reached the market. Nevertheless, many antimicrobial peptides are currently being tested in clinical trials. At the moment I am writing this thesis, a few peptides or mimetics are in (or have completed) clinical trials as antimicrobial or immunomodulatory agents. In *Table 1.1* a list of AMPs into clinical trials is given, obtained by the web database of the U.S. National Institutes of Health [51].

Table 1.1. List of AMP into clinical trials and their current status

Peptide name	Company	Structure	Phase of study	Development for treatment of
Omiganan	Cadence Pharmaceuticals	analogue of indolicidin	Completed Phase III	preventing catheter infections/ colonization in patients with Central Venous Catheters
			Completed Phase II	topical skin antisepsis in healthy adult subjects
hLF1–11	AM-Pharma	aminoterminal amino acids 1–11 of human lactoferrin	Completed Phase II	<i>Candida</i> infection
PMX-30063	Polymedix	oligomeric and small molecule mimetics of AMPs	Completed Phase II	acute bacterial skin and skin structure infections (ABSSSI) caused by <i>S. aureus</i>
PAC 113	Pacgen Biopharmaceuticals Corporation	from histatin 3 and histatin 5	Completed Phase II	oral candidiasis in HIV seropositive patients

DPK-060	Pergamum	structurally derived from the endogenous human protein kininogen	Phase II	Atopic Dermatitis with an extension program in external otitis
OP-145	Octoplus	from cathelicidin antimicrobial peptide LL-37	Phase II	chronic otitis media
CLS001	Cutanea Life Sciences	Cationic AMP pentahydrochloride	currently recruiting participants for Phase II	Rosacea
LTX-109	Lytix Biopharma AS	synthetic antimicrobial peptidomimetic	currently recruiting participants for Phase II	Impetigo
HB1345	HelixBiomedix	Lipohexapeptide	Phase I	skin infections
POL-7080	Polyphor Ltd	protein epitope mimetics of the antimicrobial peptide protegrin I	Phase I	Pseudomonas specific antibiotic
NZ2114	Novozymes	defensin-like AMP plectasin	Preclinical	pneumonia and septicaemia

The story of Pexiganan is interesting. It derives from magainin-2 and was developed by MacroChem Corporation in the 90s. It entered in Phase III trials

(ClinicalTrials.gov Identifier: NCT00563433) and was tested as topical cream vs. oral Ofloxacin in the Treatment of Infected Diabetic Ulcers. It was rejected by the Food and Drug Administration (FDA) in 1999 because its efficiency towards infected diabetic foot ulcers did not offer any improvement over the conventional treatment with ofloxacin, a fluoroquinolone antibiotic. Pexiganan is, however, now getting a new life as Locilex by Dipexium Pharmaceuticals of White Plains, New York. This company is negotiating with FDA to bring Pexiganan through clinical trials, as a way of treating bacterial infections associated with diabetic foot ulcers, particularly when the bacteria are resistant to standard antibiotics (ClinicalTrials.gov Identifier: NCT01594762).

Chapter 2. Collection and building of a new AMPs database

2.1. Introduction

After 30 years of intensive research on AMPs, an accepted and universal model of action is still lacking. This is not due to lack of scientific research, but rather to the simple fact that a comprehensive model does not exist. AMPs utilize a wide variety of mechanisms, such as altering the membrane equilibrium, creating pores, disrupting the membrane, docking a protein receptor and so on. The first requirement to conduct a quantitative structure-activity relationship (QSAR) study of a series of peptides is to cluster those expected to act in the same way. A correct QSAR investigation is simply impossible if the same analysis set includes peptides acting with different mechanisms, such as membrane disruption or enzyme inhibition. In recent years, many novel AMPs have been discovered and characterized. Most of these data have been included in web databases. Unfortunately, several noteworthy features of AMPs, such as minimum inhibitory concentrations (MIC) or their spectrum of activity, are not always included in public databases. The need to have a more extended collection of AMPs, together with the need for physical-chemical parameters, motivated me and my research group to create a new web database called YADAMP: Yet another database of antimicrobial peptides [52]. It permits a quick and easy search of peptides on the base of their activity (expressed as MIC against several bacterial strains) and their structure. The philosophy behind YADAMP is to facilitate the access to important information on AMPs, to allow extensive QSAR analysis and the creation of the activity model against a particular bacterial target. With YADAMP, it is possible to create a uniform subset of

AMPs that is still large enough to allow meaningful statistical analysis. The database can be accessed via a web-based browser at:

<http://www.yadamp.unisa.it>.

2.2.Data collection

YADAMP collects data on AMPs scattered in scientific papers or web databases, providing structural data and information on antimicrobial activities. In YADAMP, a user can obtain information about peptide name, amino acid sequence, length, presence of disulfide bridges, date of discovery, activity and taxonomy. In addition, the most relevant chemical-physical properties were calculated such as charge, hydrophobic moment, helicity, flexibility, isoelectric point, Boman index, instability index and penetration capabilities.

2.2.1. Sequences

Sequences of active AMPs were mainly extracted from the scientific literature and were compared with data in public databases (UniProtKB/Swiss-Prot [53], APD [54], CAMP [55]). Each of the collected sequence was validated with literature available data. To facilitate future QSAR studies of antimicrobial peptides for peptide design, I also collected sequences of synthetic peptide derivatives. I collected relevant information on 2525 active sequences. Collecting and annotating large numbers of sequences is a perilous job as it can propagate errors in the original papers that might have been corrected later, or because it can introduce new errors from manual annotations. For this reason, YADAMP is frequently updated.

2.2.2. MIC values

More important, YADAMP is mainly focused on peptides activities. In microbiology, the MIC is the lowest concentration of an antimicrobial that will

inhibit visible growth of a microorganism. The MIC is necessary to perform a statistical analysis of peptides. YADAMP permits the selection of AMPs with the lowest MIC value. Experimental MIC values (expressed in μM) were manually extracted from careful reading the original papers. MIC values expressed in $\mu\text{g}/\text{mL}$ were converted to μM to allow a quick comparison, using the formula:

$$\text{Concentration } \mu\text{M} = \frac{\text{Concentration } \left(\frac{\mu\text{g}}{\text{mL}}\right)}{\text{middleweight aminoacidi (150)} * \text{peptide lenght}} * 1000$$

The most intensively studied organisms are *Escherichia coli*, *Pseudomonas aeruginosa* and *Salmonella enterica* serotype *Typhimurium* amongst Gram-negative organisms and *Staphylococcus aureus* and *Micrococcus luteus* amongst Gram-positives. These organisms are also the primary source of infections in humans. For these reasons, in YADAMP the fields corresponding to these MIC values are added, by default, to the Result page. There are also two areas reporting the activity against *Bacillus subtilis* and the fungus *Candida albicans* owing to their high frequency. Data against all other bacteria were inserted in fields: Other Gram⁻, Other Gram⁺ and Other for fungi and yeast. In addition, for each peptide, we added in YADAMP the link to the references from which information were extracted in order to check the data and the antibacterial assay conditions.

2.2.3. Biological classification

Biological classification is a method of scientific taxonomy used to group and categorize organisms into groups having attributes or traits in common. Taxonomy materials are important to understand and identify sequence patterns conserved across species. It is a hierarchical classification, in which each level is named rank. The data about taxonomic information was extracted

from NCBI Taxonomy database [56]. YADAMP permits a selection for five main ranks: phylum, class, order, family, and genus.

2.2.4. Calculated parameters

As already stated, YADAMP was created to be a resource for QSAR investigations on AMPs, thus, for an accurate QSAR analysis, it is essential to group peptides sharing some features, such as similar secondary structure, flexibility or charge. For this reason, YADAMP enriches the experimental data with some theoretical information.

Following descriptions about calculation performed, however in the *Appendix-a* it is possible to read the MATLAB scripts associated with each parameter computed.

i. Charge

AMPs can act in very different pH conditions, depending on the tissue in which the bacteria are grown. I have calculated the charge of each peptide at three different pH values (pH 5, 7 and 9) by the formula:

$$Charge = \sum_i N_i \frac{10^{pKa_i}}{10^{pH} + 10^{pKa_i}} - \sum_j N_j \frac{10^{pH}}{10^{pH} + 10^{pKa_j}}$$

where N_i is the number of the N -terminus and of the side chains of arginine, lysine and histidine. The j -index refers to the C -terminus and the aspartic acid, glutamic acid, cysteine and tyrosine amino acids. pKa_i and pKa_j values refer to amino acids labeled with the index i and j .

This algorithm has some limitations, such as:

- the residues are assumed to be independent of each other;
- N - and C -termini have fixed pKa values;
- only the 20 natural amino acids are considered;
- the resulting net charge depends on what pKa values were used.

I used pKa value taken from Lehninger Principles of Biochemistry [57].

A quick inspection at the database reveals that, mainly because of the wide variation in lysine abundance, the charge of certain peptides can largely vary at different pH. Peptides acting as antimicrobial compounds do not always experiment the neutral pH, so this parameter can be decisive for peptide simulations in specific tissues.

ii. Isoelectric point

The isoelectric point (pI) is the pH at which a protein has no net electrical charge. Below the pI proteins carry a net positive charge and above it they have a net negative charge. Theoretical pI values were calculated using a free online tool [58]. According to Bjellqvist et al. [59] it was assumed that the same pK value could be used for an amino acid residue in all polypeptides and in all positions in the peptide except for *N*- or *C*-terminally placed amino acids. For the pK values of the *N*-terminal amino groups the effect of the different substituents on the α -carbon were taken into account.

iii. Boman index

Most authors have agreed that a potential AMP should possess a positive net charge to facilitate binding to bacterial phospholipids as well as a certain degree of amphipathicity to allow molecule adaptation to a bacterial membrane. These criteria are not enough to predict the ability of a peptide to interact with cell membrane. Boman [60] introduced a parameter which shows a certain degree of discrimination between membrane-interacting and protein-interacting peptide. They established the tendencies of amino acids to leave water and move in a nonpolar condensed phase calculating the distribution coefficients for each side chain of the natural amino acids at pH 7. I calculated the Boman index for all sequences, as the sum of the free energies (kcal/mol)

of the respective amino acid side chains for transfer from cyclohexane to water divided by the total number of residues.

$$\text{Boman index} = \sum_i \frac{\text{free energies (kcal/mol)}}{\text{residues number}}$$

The free energies values were taken from Radzeka and Wolfenden [61].

iv. Hydrophobicity

Hydrophobicity is another critical characteristic of amino acid residues that determines protein folding, protein subunit interaction, binding to receptors, and interactions of proteins and peptides with biological membranes. Calculation of hydrophobicity assigns a numerical hydrophobicity value to each type of amino acid, and then relates these hydrophobicities in a particular protein or fragment with some aspect of structure or function. The hydrophobicity of an amino acid residue is not a property that can be easily defined or simply measured. Nevertheless, several groups have attempted to derive numerical hydrophobicity scales using a variety of experimental and computational methods. The distribution of hydrophobic residues in amphipathic peptides is revealed by the hydrophobic moment, which depends on the spatial conformation of the peptide. The hydrophobic dipole moment can be estimated from a known peptide sequence, assumed that the polypeptide backbone follows some periodic arrangements such as an α -helix or a strand from a β -sheet. It is represented by the vectorial sum of all the hydrophobicity indices, divided by the number of residues. I estimated the hydrophobic moment in according to three different hydrophobic scales: CCS [62]; Kyte–Doolittle [63]; and Eisenberg [64], reporting in the web database the three different results for each peptide. For this calculation it was assumed that the hydrophobicity of each residue i can be represented by a vector of

length H_i , having a direction perpendicular to the axis of the helix or strand of beta structure.

The value of estimated hydrophobic dipole moment (μ_H) is:

$$\mu_H = \left(\left(\sum_i H_i \cos(i\delta) \right)^2 + \left(\sum_i H_i \sin(i\delta) \right)^2 \right)^{1/2}$$

where δ is the angle separating side chains along the backbone (e.g. $\delta = 100^\circ$ for an α -helix).

Finally, I calculated the mean hydrophobicity as the total hydrophobicity (sum of all residue hydrophobicity indices) divided by the number of residues.

$$\text{mean } H = \sum_i \left(\frac{\mu H_i}{\text{residues number}} \right)$$

v. *Helicity*

The secondary structure of a peptide is crucial for the investigation. If it is not experimentally available, peptide structure prediction is essential. In YADAMP, the prediction is based upon the DSC (Discrimination of protein Secondary structure Class) algorithm from King and Sternberg [65]. The method extracts the maximum information from the primary sequence and allows the prediction of the secondary structure from multiply aligned homologous sequences and linear statistics. The DSC Method is accessible as ‘Secondary Structure Prediction’ (SSP) option in Discovery Studio from Accelrys.

The DSC method gave the following results:

001		ALRLAIRKR			
DSC-SEC		HHHHHHCCC			
PROB-H		779998421			
PROB-E		000001000			
PROB-C		331111689			
NO.	RES	DSC-SEC	PROB-H	PROB-E	PROB-C
1	a	H	0.723	0.020	0.257
2	l	H	0.723	0.020	0.257
3	r	H	0.877	0.004	0.119
4	l	H	0.905	0.015	0.080
5	a	H	0.893	0.032	0.075
6	i	H	0.751	0.065	0.0184
7	r	C	0.366	0.042	0.592
8	k	C	0.185	0.021	0.794
9	r	C	0.087	0.020	0.893

The first section of the report shows 5 lines for each sequence:

1. the sequence
2. the predicted secondary structure type, DSC_SEC
3. the probability of being helix, PROB_H
4. the probability of being beta strand, PROB_E
5. the probability of being coil, PROB_C

Values of PROB_H, PROB_E, and PROB_C are between 0 and 9, with 9 being the highest probability.

The second section of the report shows similar information for each residue, but the probabilities are shown in real number values for each residue. I calculated the Helicity probability via a Perl script by summing of PROB-H number and dividing by the number of residues.

vi. Flexibility

The molecular flexibility of proteins is a crucial factor in determining their biological activity, including binding affinity, and for the theoretical understanding of peptide dynamics. The identification of regions in proteins

with the highest conformational flexibility and rigidity is essential for predicting the mechanism of protein folding. Consequently, there is considerable interest in predicting the flexibility or, conversely, the rigidity of peptides from their amino acid sequence. Obviously, prediction of the secondary structure of an AMP is a hard task due to the different conformations that a peptide shows in different chemical environments. Moving from the water bulk into the membrane, the structure of peptides varies considerably. I calculated the flexibility of α -AMPs according to a conformational flexibility scale for amino acids in peptides [66], which provides an absolute measure for the time scale of conformational changes in short unstructured peptides as a function of the amino acid type. This experimental scale derived from kinetic measurements of the collision frequency between the two ends of short random-coil polypeptides. These peptides were labeled with a fluorescent probe at the *C*-terminus and Trp as a fluorescence quencher at the *N*-terminus. The fluorescence lifetimes of fluorescent probe/Trp peptides provide the quenching rate constants (k_q), which measure the *end-to-end* collision frequency. The authors have shown different collision frequencies when the probe and the quencher were separated by different amino acids. This arrangement allowed them to correlate the collision frequency with the type of amino acid and build up a flexibility scale.

In YADAMP the flexibility was calculated by formula:

$$Flexibility = \sum_i \frac{k_q}{residues\ number}$$

For amino acids not found in the Huang work, I estimated missing values by comparison with reported k_q constants.

vii. Instability index

A peptide cannot show activity if it is not sufficiently resistant to proteases. The instability index predicts the *in vivo* half-life of the peptide; this was added to YADAMP to investigate the correlation between activity and *in vivo* stability. To estimate the instability values I inspired in Guruprasad work [67]. They made a statistical analysis of 12 unstable and 32 stable proteins to reveal patterns in the occurrence of certain dipeptides. Some dipeptides appeared particularly frequent in stable proteins, whereas other dipeptides were common in unstable proteins. The contribution of each of the dipeptides towards instability was obtained by summing the instability weight values corresponding to the conditions satisfied by the dipeptide and termed as the dipeptide instability weight value (DIWV). I calculated the instability index (II), using the DIWV values for all 400 combinations reported in the Guruprasad paper by equation:

$$II = \left(\frac{10}{L}\right) \sum_{i=1}^{L-1} DIWV(x_i y_{i+1})$$

where $x_i y_{i+1}$ is a dipeptide, L is the length of the sequence and 10 is a scaling factor.

viii. CPP

This parameter is the acronym of Cell Penetrating Peptides and is an estimate of the tendency for a peptide to penetrate a cell membrane. The parameter can take values between 0 and 1, where 1 corresponds with the highest probability of a peptide to penetrate a membrane, and 0 indicates the impossibility to enter a membrane. To predict this ability I used a free online tool [68] in which I inserted the peptide sequences. The limit of this web server is that the prediction is limited to peptide with length between 5 and 30 amino acids.

2.3.Database content

YADAMP contains a large number of manually annotated sequences of AMPs. To date, it contains 2525 sequences of active peptides with length between 5 and 96 amino acids; amongst them, 469 sequences have one or more disulfide bridges. In cases in which the active structure of a peptide is not experimentally known, an estimation of helicity was made by an automated script. From helicity estimations, 1362 sequences have a helicity index >5 , in a range between 0 and 9, in which 9 corresponds with the highest probability of α -helix secondary structure. The action mechanism of many peptides involves interaction with the membrane, therefore hydrophobic moment is a key parameter to characterize AMPs. In my collection, there are 619 sequences with mean hydrophobic moments >3.0 calculated using the CCS scale.

YADAMP has the largest collection of MIC values of AMPs. It contains 1015 sequences with an experimentally verified action against *E. coli* (the bacterium with the largest data set). Other bacteria well represented in YADAMP are *S. aureus* (957 sequences), *P. aeruginosa* (438 sequences), *B. subtilis* (253 sequences), *S. Typhimurium* (149 sequences) and *M. luteus* (129 sequences). Furthermore, there are 251 sequences active against other Gram-negative bacteria and 363 sequences active against other Gram-positive bacteria. Fungi are represented by *C. albicans* (486 sequences), but there are 128 sequences active against other fungi or yeast. A specific peptide may have activity against different bacteria, so it can be included twice or more. Finally YADAMP includes 911 sequences extracted from Amphibia, the most important source for active peptides, 260 sequences from Insecta, 277 sequences from Mammalia, 158 sequences from Magnoliopsida and 294 synthetic sequences.

2.4. Web database design: an overview

The web interface of YADAMP (*Figure 2.1*) is designed to offer a simple but practical use of the database.

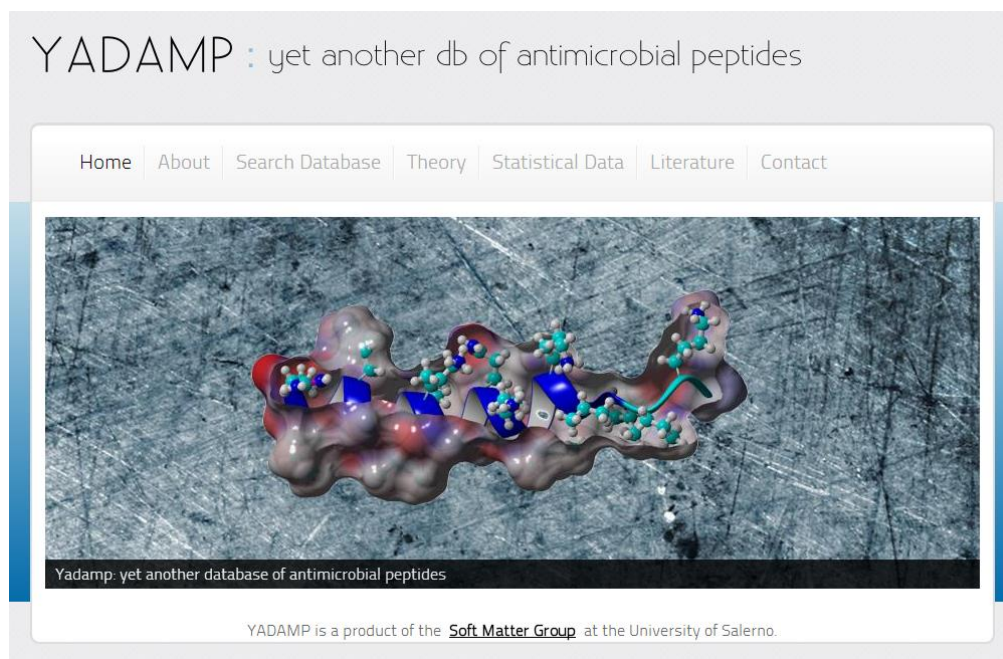


Figure 2.1. Screenshot of YADAMP Homepage

It includes seven sections:

- Home
- About

In this section is possible to read the philosophy behind YADAMP and eventually news.

- Search Database

In this section is possible to query the database by length, sequence, name, taxon, or discovery period. Any query can be made combining as many fields as the user likes with AND and OR operators. We have provided the option to search structural parameters such as the presence of disulfide bridges, the value of charge at pH 7, the mean hydrophobic moment, the instability or

propensity to α -helix conformation. More importantly, it is possible to select AMPs with a proven activity against five organisms, chosen because of their importance and because they are a common target of AMPs. In this way, it is extremely easy to build sets of AMPs with characteristics suitable for further investigation.

- Theory

This section offers a description of the theoretical terms, included the references.

- Statistical Data

It provides an estimate of the database content and the date of the last update.

- Literature

This section provides an automatic visualization of the 50 most recent papers through RSS (Rich Site Summary). It is due to the extraordinary interest in AMPs, as reflected by the high number of publications in this field.

- Contact

In this section is possible to send an e-mail for opinion and suggestions or to report eventual errors.

2.5. Using YADAMP

As an example of use, I simulated here the search of structural elements in peptides effective against *E. coli*. To develop a model of action against this bacterium, it is necessary to choose sequences sharing the same target (for example peptides acting on the cell membrane or against the cell wall), and it is critical to quantify the effectiveness of this action.

The screenshot shows the YADAMP search interface. At the top, there are navigation links: Home, About, Search Database, Theory, Statistical Data, Literature, and Contact. Below these is a yellow instruction box: "To make a search you MUST select at least one operator (the fields on the left columns) and you MUST enter a value in the corresponding field in the right column. The description of the fields can be find in the THEORY page".

The main search area is a table with columns for field names, operators, and values. The fields are grouped into three color-coded sections: blue (structural properties), light blue (biophysical properties), and light green (MIC values). The bottom section is light brown and contains taxonomic filters.

Field	Operator	Value
NAME		
SEQUENCE	LIKE	
LENGHT	>	
AND		
HELICITY	>	5
FLEXIBILITY	>	
DISULFIDE BRIDGES		<input type="checkbox"/> (check for yes)
INSTAB. INDEX	>	
BOMAN INDEX	>	
AND		
MEAN HYD. MOM.	>	2
CHARGE pH 7	>	
Delta G	>	
CPP	>	
MLP	>	
AND		
MIC <i>E. coli</i>	<	40
MIC <i>P. aeruginosa</i>	>	
MIC <i>S. aureus</i>	>	
MIC <i>B. subtilis</i>	>	
MIC <i>C. albicans</i>	>	
PHYLUM		Actinobacteria
CLASS		Actinobacteria
ORDER		Actinomycetales
FAMILY		Aclopidae
GENUS		Acalolepta
Date	>	

At the bottom of the form are three buttons: "Query YADAMP!", "Blast SEQUENCE", and "Reset".

Figure 2.2. Screenshot of Search database page

As shown in Figure 2.2, it is possible to make a query to select peptides with a similar secondary structure (in this case with helicity >5), amphipathic (with hydrophobic moment > 2) and active against *E. coli* (MIC $< 40 \mu\text{M}$).

The query result page shows recovers of 391 sequences for further investigation (*Figure 2.3*). The peptides are listed by ID order and by clicking on this number detailed information for each selected peptide are accessible.

YADAMP : yet another db of antimicrobial peptides

Home | About | Search Database | Theory | Statistical Data | Literature | Contact

Result of Query (391 items found)
[Back to Query Manager](#)

ID	NAME	LENGTH	DATE	PAPER	PDB
46	Synthetic_5	9	1994	Novel synthetic antimicrobial peptides effective against methicillin-resistant Staphylococcus aureus	4L
SEQ: RLKLLLRK					
49	Modified defensin_2	9	1999	Purification, cDNA cloning and modification of a defensin from the coconut rhinoceros beetle, Oryctes rhinoceros	4L
SEQ: ALWLAIRKR					
50	Modified defensin_4	9	1999	Purification, cDNA cloning and modification of a defensin from the coconut rhinoceros beetle, Oryctes rhinoceros	4L
SEQ: AWLLAIRKR					
51	Modified defensin	9	1999	Purification, cDNA cloning and modification of a defensin from the coconut rhinoceros beetle, Oryctes rhinoceros	4L
SEQ: ALLLAIRKR					
70	Synthetic_4	10	1994	Novel synthetic antimicrobial peptides effective against methicillin-resistant Staphylococcus aureus	5L
SEQ: RLKLLLRK					

Figure 2.3. Query result page

The example of page about detailed information is given in *Figure 2.4*. To facilitate the immediate interpretation of the results, we separated the information by colors. In the blue section (*Figure 2.4*) I reported data about ID YADAMP, name and eventually number of disulfide bridges. In the green section I put the value of calculated parameters and the sequence of the peptide. In the orange section there are the activity values and in the second blue section there are taxonomic information, date of discovery and the link to papers in which I extracted the activity value. Finally, since some peptides possess an amphipatic helix structure, it is interesting to visualize the amphiphilic region in a sequence. Thus I used the helical-wheel Java applet [69] to obtain a projection of the amino acids side chains along the helix axis

(Figure 2.4, bottom). Each residue is numbered and colored according to its chemical nature.

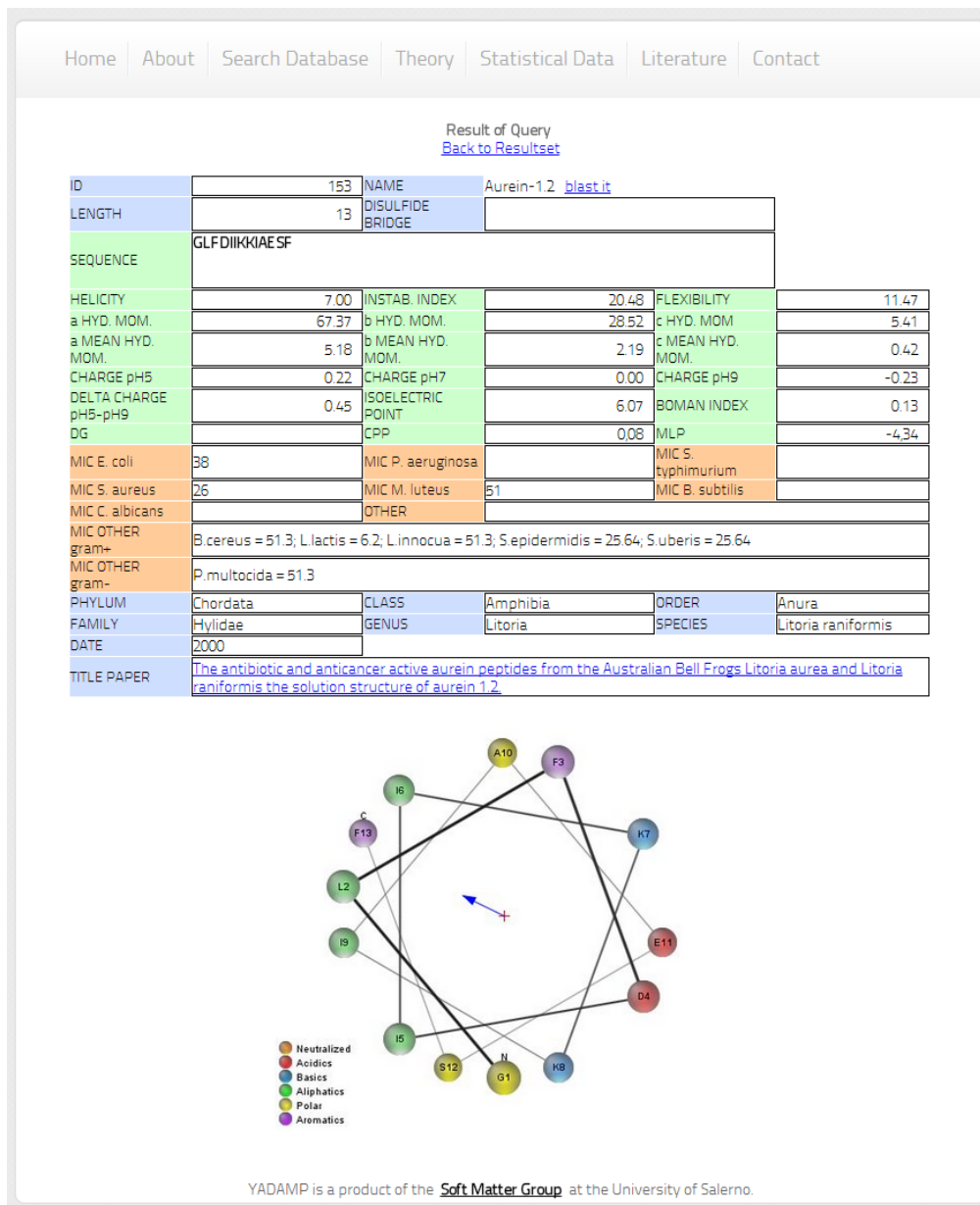


Figure 2.4. Experimental and predicted data of a particular antimicrobial peptide

Chapter 3. Development of a modified antimicrobial peptide

3.1. Design of modified antimicrobial peptides

Due to the discussed limits of AMPs in the clinical therapy, some chemical modifications or sequence optimization are needed. In the last years many molecules that mimic AMPs function and structure have been synthesized, resulting in a number of distinctive AMPs classes, briefly reported in the following.

3.1.1. AMPs mimetics

This class is formed by synthetic molecules such as β -peptides, peptoids or arylamides. These compounds possess the same chemical-physical feature of AMPs, mimic the same mechanism of action but, lacking the peptide bonds, they are more stable *in vivo* [70, 71].

3.1.2. Hybrid AMPs

As suggested by the name, these molecules are the result of the combination of the active portions of two or three AMPs [72]. In this way it is possible to increase the antimicrobial activity towards a specific target.

3.1.3. AMPs congeners

A congener peptide is a modified AMP obtained by swapping out of a particular amino acid in the active sequence or by truncating of the *N*-terminus or the *C*-terminus ends. The goal is to individuate the residues responsible for the activity and to reach the smallest sequence length [73].

3.1.4. Cyclotides and stabilized AMPs

They are cyclic peptides of about thirty amino acids isolated from plants. They possess a characteristic head-to-tail ring structure stabilized from three disulfide bonds [74]. The high stability and microbiological activity as anti-HIV and insecticidal give them promising potential application as new stable peptide-based drugs [75].

3.1.5. AMP conjugates

AMPs can be coupled to an antibody or a ligand for a receptor on a definite bacterial pathogen, in this case they could be used at lower concentrations inducing lower side effects or could reach a specific target [76, 77].

3.1.6. Immobilized AMPs

Finally AMPs can be incorporated in different materials or adsorbed to surfaces where they still retain their ability to bind and kill bacteria. Immobilized peptides appear to interact and disrupt microbial membranes with high affinity in a similar fashion to native peptides in solution [78]. These classes of molecules are advertised to have selective or ‘targeted’ antimicrobial activities, improved retention or unique abilities that allow them to bind to specific surface. These groups of new peptides have smart medical and industrial application potentials, for example for treating antibiotic-resistant bacterial infections and septic shock, to preserve food or to sanitize surfaces both *in vitro* and *in vivo*.

3.2. Our approach

There is an urgent need for unconventional, molecular approaches to control antimicrobial function. Light is an attractive external trigger for the control of biological functions [79, 80] because it offers highly spatiotemporal resolution,

it is relatively non-invasive and it does not lead to sample contamination. Furthermore, its intensity and wavelength can be regulated with very high precision.

I decided to take advantage of the special properties of light by designing photoresponsive antimicrobial peptide. The control of biological function by light is enabled by the incorporation of molecular photo-switches into biomolecules and bioactive compounds [81]. These molecules undergo a light-induced, reversible change in their structure that results in a change in their properties (for example, geometry, polarity, flexibility or degree of conjugation).

A part of this PhD thesis was dedicated to synthesizing and inserting modified amino acids into active AMPs sequence. The modified amino acids are based on azobenzene structure. Azobenzene and many of its derivatives are characterized by reversible isomerization from the more stable *trans* form to the less stable *cis* isomer, upon irradiation with UV light (see *Figure 3.1*), the two isomers differing in geometry and dipole moment. Azobenzene group was created as side chain in the structure of aromatic amino acids such as tyrosine and phenylalanine. The first reason was to exploit photochemical isomerization, by introducing photoactive compounds into biomolecules; this modification could change the functioning of biological systems, as already exemplified by the photocontrol of enzyme activity [82], receptor affinity [83], transport through membrane pores [84], or even the motility of an entire organism [85]. I supposed that, by placing an azobenzene moiety in AMP sequence, the whole chain of peptide could change its conformation upon irradiation with a suitable light. So this molecular switch could help to turn on/off the antimicrobial activity of AMPs. Moreover, in a recent work [86] I demonstrated the antimicrobial and antifungal activity of azobenzene containing small molecules. Thus I supposed that the azo-modified peptide

could have a broad spectrum of activity due to the presence of similar azobenzene moiety in its structure.

3.3. Chemical modification of natural amino acid with a photoactive ligand

Here I report the chemical modification of a tyrosine with a photoactive ligand such as azobenzene group. Azobenzene undergoes isomerization from *trans* to *cis* upon irradiation with UV or visible light. The intense absorption at 320 nm due to the π - π^* transition of the *trans* isomer decreases during such an isomerization, while the absorption maximum due to the *cis* isomer at 430 nm which is due to the n - π^* transition increases [87]. Photoinduced isomerism of azobenzene proceeds with large structural modification as reflected in the change in geometry and dipole moment. The result of the isomerization from *trans* to *cis* is a contraction of the structure (Figure 3.1) with a considerable change in dipole moment, approximately from zero to 3 D [88].

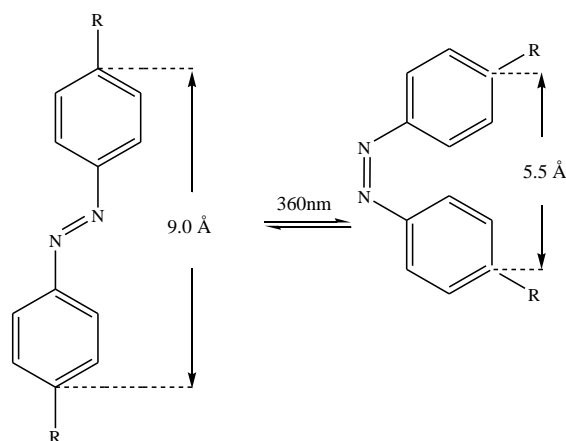


Figure 3.1. Photoinduced isomerism of Azobenzene from *trans* isomer (on the left) to *cis* isomer (on the right)[87]

The first azo-amino acid was synthesized by Bose and was incorporated into *E. coli* proteins to photoregulate the DNA binding affinity of *E. coli* catabolite

activator protein (CAP) [89]. The photoisomerizable amino acid phenylalanine-4'-azobenzene (AzoPhe) showed a distinct absorbance peak at 334 nm corresponding to the *trans* azobenzene chromophore. Irradiation of the compound at 25 °C with 334 nm light led to a decrease in the 334 peak and an increased absorbance at 420 nm, consistent with a photostationary state of approximately 45% *trans*, 55% *cis* azobenzene (Figure 3.2). The isomerized amino acid was then irradiated with 420 nm light, resulting in complete conversion back to the 334 nm band. These results showed that azo-amino acids could be selectively incorporated into proteins and undergo reversible *cis-trans* photoisomerization.

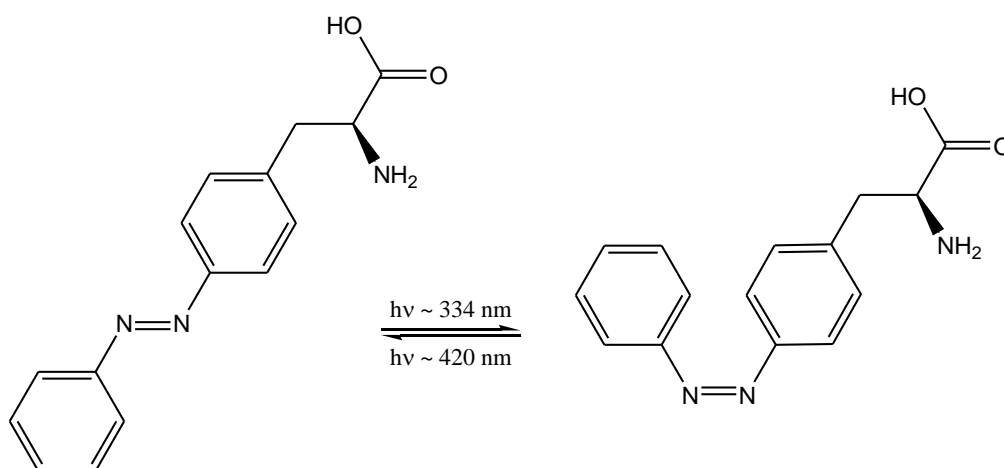


Figure 3.2. Photoinduced isomerism of AzoPhe from *trans* isomer (on the left) to *cis* isomer (on the right) [89]

3.3.1. Synthesis of unnatural tyrosine

Azo-amino acid 3-(p-tolyldiazenyl)-N-Fmoc-tyrosine is a modified tyrosine (in the following abbreviated in Fmoc-azoTyr). It was synthesized according to the classic scheme of diazocopulation reactions, as illustrated in the Figure 3.3.

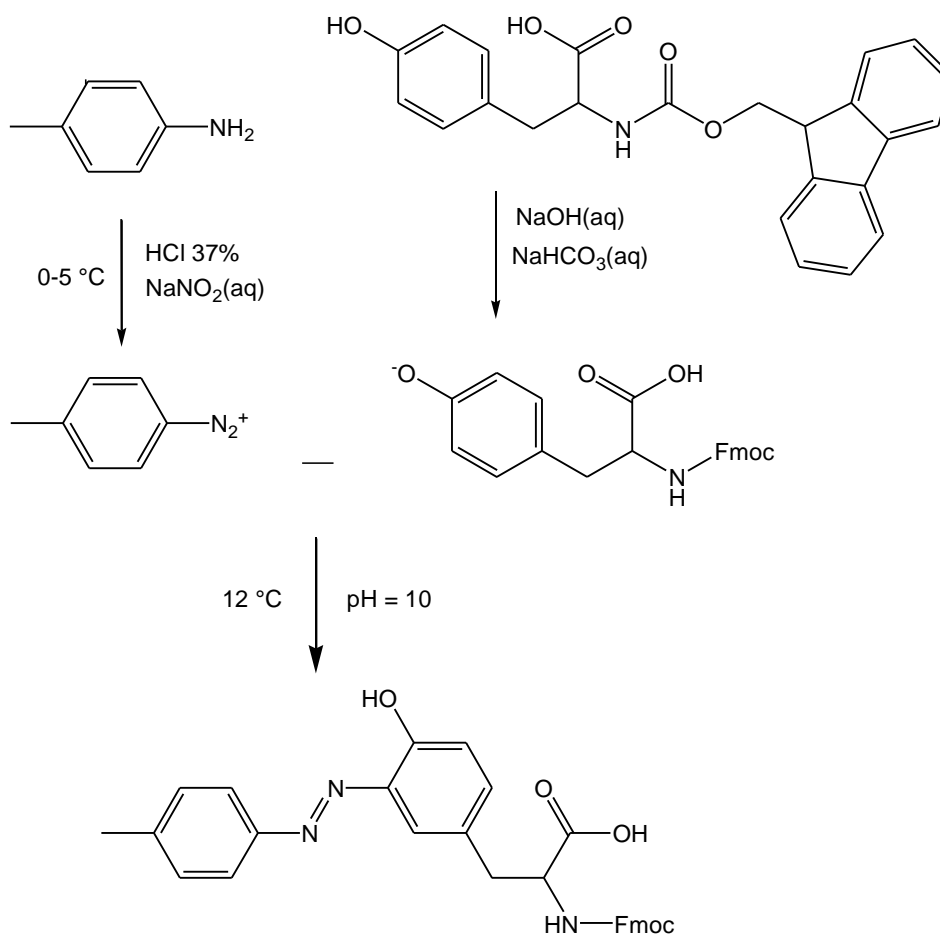


Figure 3.3. Synthesis scheme of modified azo-amino acid

The procedure was the following: 1.19 g of p-toluidine (0.011 mol) was suspended in a solution containing 19.2 mL of water and 4.8 mL of HCl 37% (w/w). The suspension was cooled at 0-5 °C in a water-ice bath. A cold solution of 0.85 g of sodium nitrite (0.012 mol) dissolved in 2.4 mL of water was added drop-wise, obtaining a suspension of the diazonium salt (solution A). The p-toluidine became completely soluble during sodium nitrate solution addition.

A basic solution containing 0.09 g of NaOH and 0.34 g of NaHCO₃ in 100 mL of water was prepared (pH = 9-10). Then, 2 g of N-Fmoc-L-tyrosine (0.0049 mol) were added to 22 mL of this basic solution (solution B).

Solution A was added drop-wise to solution B, under stirring at 12 °C and maintaining pH = 10 by addition of portions of the basic solution previously prepared. The system was left reacting for 20 min, keeping the same conditions of pH and temperature. Then a dark red precipitate of the azo compound was formed. The filtered crude precipitate was dried under vacuum and washed in 200 mL of chloroform. The purified azo compound was collected as a red powder. Yield 90%.

The ^1H NMR spectrum (reported in the section *Appendix-b*) was made in DMSO- d_6 . Chemical shift values confirmed the expected structure. Methyl group was confirmed as a sharp signal at δ 2.4 ppm, protons of the tyrosine methylene group were visible between δ 2.94-3.13 ppm. The signals in the range δ 3.83-4.37 ppm were recognized to the methyl protons of the Fmoc-group and to the α -carbon atom of the amino acid group. In the range δ 6.54-7.87 ppm was possible to observe the aromatic protons attributed to the azobenzene and Fmoc group. Also was possible to discern the proton of the carboxylic group at δ 11.26 ppm.

3.3.2. Optical and thermal properties of Fmoc-azoTyr

The UV absorption spectrum of Fmoc-azoTyr was recorded in DMF solution on a Perkin-Elmer Lambda 19 spectrophotometer (spectrum reported in *Appendix-b*). In the 300-500 nm region, the spectrum showed two bands centered around 334 and 400 nm, related respectively to the π - π^* and n - π^* electronic transitions of the azobenzene chromophore [90]. The sample was completely soluble in the solvent used, so by the Beer-Lambert law was possible to calculate the molar extinction coefficient (ϵ_{max}). Using a cell path length of 1 cm and modified amino acid concentration of 4.1×10^{-6} M, the molar extinction coefficient for wavelength at the absorption maximum $\lambda_{\text{max}} = 334$ nm was $\epsilon_{\text{max}} = 36805 \text{ M}^{-1} \text{ cm}^{-1}$. Also, the spectral region 240 - 300 nm showed a typical absorption of the Fmoc group.

From Differential Scanning Calorimetry (DSC) I studied the thermal behavior of synthesized azo-amino acid (*Appendix-b*). In the heating run at 10 °C, under nitrogen flow, the compound showed a melting peak at 190 °C (melting enthalpy $\Delta H_m = 24.8$ J/g), and immediately after underwent thermal degradation.

3.4. Selection of an AMP as template

3.4.1. Criteria of selection

YADAMP database was employed to select active antimicrobial peptide to be used as template in order to develop a new photoresponsive peptide. I performed the query using the following criteria (*Figure 3.4*):

- a) presence of one tyrosine in the sequence, to replace with Fmoc-azoTyr;
- b) amino acid sequence length less than 10 residues to facilitate the next step of peptide synthesis;
- c) helicity value greater than 4.5 (in a scale range between 0 and 9, in which 9 corresponds with the highest probability of α -helix secondary structure);
- d) charge value higher than 2 to select a positively antimicrobial peptide;
- e) cell penetrating potential value higher than 0.5 (in a scale range between 0 and 1, in which 1 corresponds with the highest probability of a peptide to penetrate a membrane and 0 indicates the impossibility to enter a membrane). This was an important parameter to select a membrane active peptide.
- f) MIC values less than 15 μ M against a Gram-negative and a Gram-positive bacterium such as respectively *E. coli* and *S. aureus*.

YADAMP : yet another db of antimicrobial peptides

Home | About | Search Database | Theory | Statistical Data | Literature | Contact

To make a search you MUST select at least one operator (the fields on the left columns) and you MUST enter a value in the corresponding field in the right column. The description of the fields can be find in the THEORY page

AND	NAME	LIKE	Y
AND	SEQUENCE		
AND	LENGHT	<=	10
AND	HELICITY	>	4.5
	FLEXIBILITY	>	
	DISULFIDE BRIDGES		<input type="checkbox"/> (check for yes)
	INSTAB. INDEX	>	
	BOMAN INDEX	>	
	MEAN HYD. MOM.	>	
AND	CHARGE pH 7	>	2
	Delta G	>	
AND	CPP	>	0.5
	MLP	>	
AND	MIC E. coli	<	15
	MIC P. aeruginosa	>	
AND	MIC S. aureus	<	15
	MIC B. subtilis	>	
	MIC C. albicans	>	
	PHYLUM		Actinobacteria
	CLASS		Actinobacteria
	ORDER		Actinomycetales
	FAMILY		Acetivibaceae
	GENUS		Acetivibacter
	Date	>	

Query YADAMP | Blast SEQUENCE | Reset

YADAMP is a product of the [Soft Matter Group](#) at the University of Salerno.

Figure 3.4. Screenshot of search database page, during peptide selection

3.4.2. Selected AMP

I selected a synthetic peptide from Ishibashi work [91]. It is a synthesized oligopeptide based on the amino acid sequence of *Allomyrina dichotoma* defending. Selected peptide has the amino acid sequence ALYLAIKRR, (it will be abbreviated in ALY).

ALY is a short peptide formed by 9 amino acids ($mW = 1103.361 \text{ gmol}^{-1}$). From literature data it shows antimicrobial activity with MIC values of $3 \mu\text{gmL}^{-1}$ against *S. aureus* and $30 \mu\text{gmL}^{-1}$ against *Methicillin-resistant Staphylococcus aureus* (MRSA), also it is active against Gram-negative such

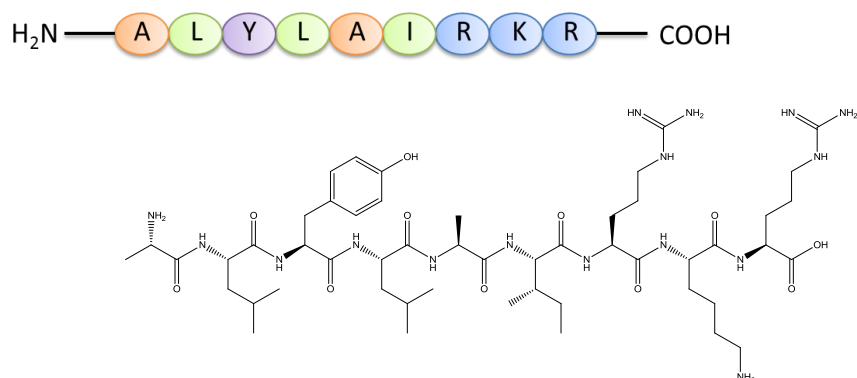
as *E. coli* and *P. aeruginosa* isolated from patients with MIC value of 4 $\mu\text{g mL}^{-1}$.

Its antibacterial effect could be due to peptide interaction with bacterial membranes as suggested liposomal membrane permeability assays [91] that showed an increase in membrane permeability proportionally to the increment of the peptide concentration. Also the peptide did not show any hemolytic activity and cytotoxic activity.

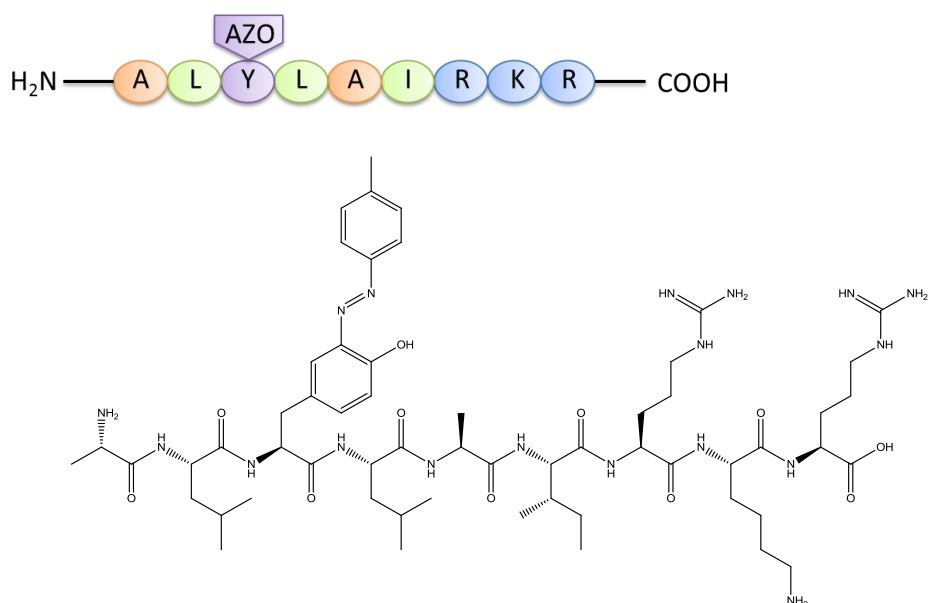
Therefore, it was used as a template to study the impact of the incorporation of azo-amino acids on membrane permeability.

3.4.3. Peptide structures

- *ALY* (unmodified peptide)



- *azoALY* (modified peptide)



The unmodified peptide ALY and the modified peptide azoALY were synthesized in the laboratory of Prof. P. Campiglia, at the University of Salerno, according to the solid phase approach [92]. The synthetic procedure was the same for both analogues.

Briefly, the first N^α-Fmoc-AA-OH was coupled to Wang resin previously swollen in 4 mL DMF for 2 h. Then the following protected amino acids were then added stepwise N^α-Fmoc-Arg(Pbf)-OH, N^α-Fmoc-Lys(Boc)-OH, N^α-Fmoc-Ile-OH, N^α-Fmoc-Ala-OH, N^α-Fmoc-Leu-OH, N^α-Fmoc-Tyr-OH for ALY peptide and N^α-Fmoc-AzoTyr for azoALY.

Each coupling reaction was accomplished using a 3-fold excess of amino acid with HBTU and HOBT in the presence of DIEA. The N^α-Fmoc protecting groups were removed by treating the protected peptide resin with a 25% solution of piperidine in DMF for 30 min.

The peptide resin was washed three times with DMF, and the next coupling step was initiated in a stepwise manner. All reactions were performed under an Ar atmosphere. The peptide resin was washed with DCM (3×), DMF (3×), and DCM (4×), and the deprotection protocol was repeated after each coupling step. The N-terminal Fmoc group was removed as described above, and the peptide was released from the resin with TFA/Et₃SiH/H₂O (90:5:5) for stirring 3 h. The resin was removed by filtration, and the crude peptide was recovered by precipitation with cold anhydrous ethyl ether to give a powder of crude synthesized peptide.

Both peptides were purified by RP-HPLC on a semipreparative C18-bonded silica column (Vydac 218TP1010, 1.0 cm × 25 cm) using a gradient of CH₃CN in 0.1% aqueous TFA (from 10 to 90% in 45 min) at a flow rate of 1.0 mL/min. The product was obtained by lyophilisation of the appropriate pooled fractions after removal of the CH₃CN by rotary evaporation as a white powder for ALY and yellow powder for azoALY. Analytical RP-HPLC indicated purity >98% and molecular weights were confirmed by ESI-MS (Electrospray ionization).

Chapter 4. Investigation of the different membrane interaction

4.1. Aim of the work

Published data about ALY peptide show that this antimicrobial peptide acts by binding to lipid membranes [91]. The modified amino acid introduced (azoTyr) could influence this interaction with an increase or decrease in membrane permeability. Thus, in the period I spent at ETH Zuerich, in the laboratory of Prof. Peter Walde, at Dept. of Materials, I investigated the different interaction of ALY and azoALY peptides with liposome membranes using two different approaches.

On one hand, I estimated the calcein leakage induced by both peptides using a suspension of POPC/POPG (mixture 90:10 mol/mol) giant unilamellar vesicles (GUVs). This is a typical assay to investigate the interaction between peptides and membranes in which a fluorescent probe (calcein) is used, and the release may be assayed by means of its fluorescence intensity. Large amount of leakage indicates that the substance strongly interacts with lipid membranes, inducing instability in the structure of vesicles and lipid membranes.

On the other hand, I performed measurements of leakage of enzyme entrapped in a suspension of POPC/POPG (mixture 90:10 mol/mol) of large unilamellar vesicles (LUVs), after peptide interaction. This is a complex and uncommon assay for detecting a permeability increase. I used enzyme containing vesicles and the change of the membrane permeability was associated with an increase in enzyme activity. I also used chromogenic substrates that allow a convenient determination of the catalytic activity using UV-Vis spectrophotometer.

4.2. Materials used

4.2.1. AMPs solutions

A stock solution of the unmodified ALY peptide was prepared in this way: a few μg of compound were solubilized in 1 mL of MilliporeQ water. It was soluble after 3 min vortex. The peptide concentration was calculated from the absorbance at 275 nm (Figure 4.1) using $\epsilon = 1400 \text{ M}^{-1} \text{ cm}^{-1}$ for the single tyrosine chromophore [93]. The solution was filtered through a $0.22 \mu\text{m}$ pore size syringe filter.

In the same way a stock solution of modified azoALY peptide was prepared. The modified compound was immediately soluble in MilliQ water and the concentration was calculated from the absorbance at 334 nm using $\epsilon = 36805 \text{ M}^{-1} \text{ cm}^{-1}$ for the single modified tyrosine amino acid. The molar extinction coefficient was obtained from quantitative UV-Vis spectrum of the corresponding azo-amino acid (paragraph 3.3.2). The solution was filtered through a $0.22 \mu\text{m}$ pore size syringe filter.

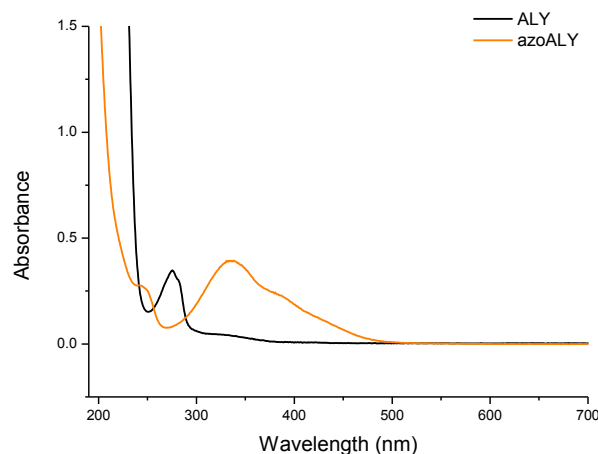


Figure 4.1. UV-Vis spectrum of unmodified ALY peptide (—) and modified azoALY peptide (—) in MilliQ water

From literature data, the MIC of ALY is close to 4 μM towards Gram-positive bacteria such as *Staphylococcus aureus* and Gram-negative bacteria such as *Escherichia coli* and *Pseudomonas aeruginosa*.

The goal of this work was to investigate the different membrane interactions of both peptides, for this reason I chose a peptide concentration values similar to the MIC for the enzyme release assays. However for calcein release tests I selected 1 μM and 50 μM , to estimate the effect on the membrane of a peptide concentration lower and higher than active one.

4.2.2. HRPC enzyme

i. Structure of peroxidase

The most widely used peroxidase in analytical chemistry is the horseradish peroxidase isolated from horseradish root. It is also commercially the most easily available form of highly purified peroxidase. Seven major isoenzymes of horseradish peroxidase have been isolated and the isoenzyme C (HRPC) is the predominant isoenzyme in horseradish. The total molecular weight of HRPC is about 42.100, which included the following components: the apoenzyme, the heme prosthetic group, two bound calcium ions, and 8 carbohydrate chains.

HRPC consists of 308 amino acid residues with eight neutral carbohydrate side chains attached to 8 asparagine residues [94]. The carbohydrate moiety of HRPC accounts for about 18% of the whole molecular weight, but they do not appear to influence the catalytic activity of the enzyme. A possible biological role of carbohydrates is to minimize aggregation or precipitation of the enzymes in the endoplasmic reticulum [95].

A characteristic feature of heme containing plant peroxidases is the presence of at least two histidine residues and in most cases of eight cysteine residues. The cysteine residues seem to be involved in four intramolecular disulfide

bonds stabilizing the three-dimensional structure of the protein. The two histidine residues occur in highly conserved regions, one coordinated at the heme iron and the other close to the postulated catalytic site [96].

HRPC contains two different types of metal center, iron (III) protoporphyrin IX (usually referred to as the ‘heme group’) and two calcium atoms (*Figure 4.2 a*). Both iron and calcium are essential for the structural and functional integrity of the enzyme.

The heme group is attached to the enzyme at His170 (the proximal histidine residue) by a coordination bond between the histidine side-chain and the heme iron atom. The second axial coordination site (on the so-called distal side of the heme plane) is unoccupied in the resting state of the enzyme but available to hydrogen peroxide during enzyme turnover (*Figure 4.2 b*).

The two calcium binding sites are located at positions distal and proximal to the heme plane and are linked to the heme-binding region by a network of hydrogen bonds. Loss of calcium results in decreases of both enzyme activity and thermal stability [97].

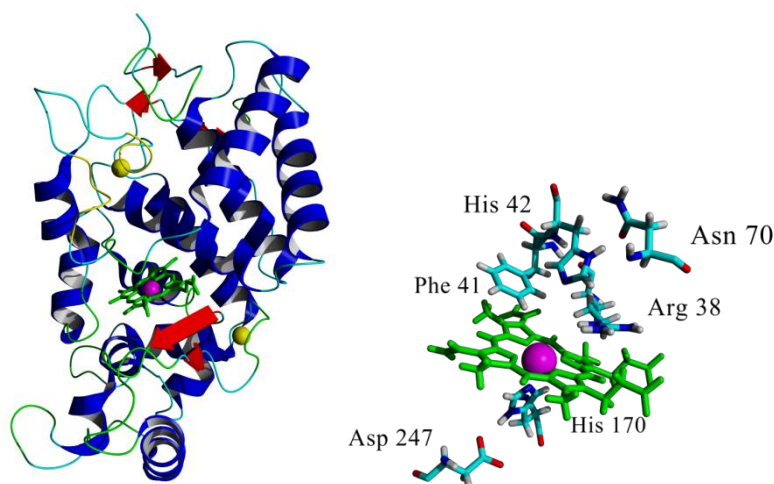


Figure 4.2. a) 3D representation of the X-ray crystal structure of horseradish peroxidase isoenzyme C (pdb code 1H5A). The heme group (colored in green with the Fe atom in magenta) is located between the distal and proximal domains which each contain one calcium atom (shown as yellow spheres). α -helical and β -sheet regions of

the enzyme are shown in blue and red, respectively. b) Key amino acid residues in the heme-binding region of HRPC. The heme group and heme iron atom are shown in green and magenta respectively, the remaining residues in atom colors.

Based on the strong absorption of the heme group between 350 and 450 nm, one can easily measure the concentration of HRP by UV/Vis-spectroscopy. The UV/Vis spectrum of the HRPC used in this work is shown in *Figure 4.3*.

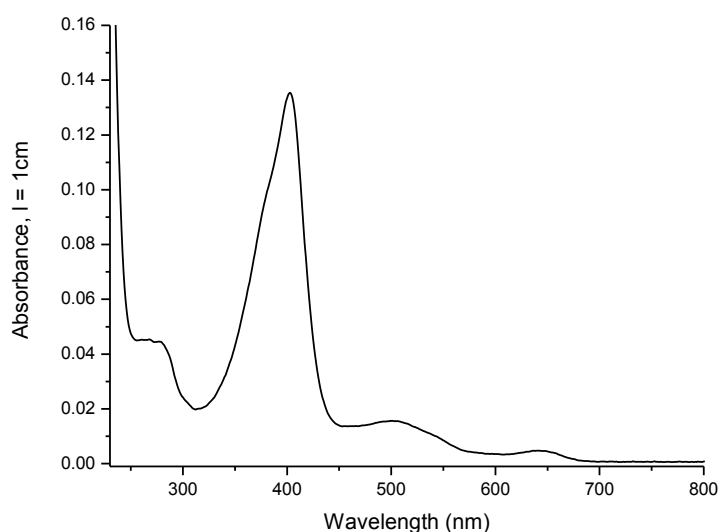


Figure 4.3. UV/Vis-spectrum of 1.41 μM HRPC in 10 mM MES buffer, pH = 5. RZ = 3.09 measured with a Jasco V760 spectrophotometer, $l = 1$ cm.

The Soret band has an absorption maximum at $\lambda = 403$ nm ($\epsilon_{403\text{nm}} = 102000$ $\text{M}^{-1} \text{cm}^{-1}$) [98]. Besides the Soret band at 403 nm and peaks centered on 500 and 640 nm, there is an additional band at 280 nm caused by absorption of the amino acids tryptophan and tyrosine [99]. Knowing that pure peroxidase contains only one tryptophan, one can define a ratio of those absorbance at 403 nm and 280 nm to estimate the purity of HRPC.

The enzyme purity is commonly indicated by an RZ (Reinheitszahl) value, defined as follow:

$$\text{RZ} = \frac{A_{403\text{nm}}}{A_{280\text{nm}}}$$

whereby $A_{403\text{nm}}$ and $A_{280\text{nm}}$ are the absorbance measured at 403 nm and 280 nm.

Good preparations of HRPC should have $\text{RZ} \geq 3.0$. The RZ value of an HRPC preparation only indicates the purity of the enzyme preparation, without, however, guaranteeing the enzymatic activity of the preparation.

Generally the HRPC has a slightly alkaline isoelectric point of $\text{pI} = 8.8$ and it is stable in the range of pH 5-10 at temperature below 50 °C.

ii. Reaction kinetics and mechanism

Horseradish peroxidase (E.C. 1.11.1.7, Donor: hydrogen peroxide oxidoreductase) catalyzes the oxidation of a variety of compounds by hydrogen peroxide or other peroxide compounds. UV/Vis-spectroscopy is the most convenient method for the determination of the catalytic activity of HRPC. Most reactions catalyzed by HRPC and other horseradish peroxidase isoenzymes can be expressed by the following equation, in which AH_2 and $\text{AH}\cdot$ represent a reducing substrate and its radical product, respectively.



This equation indicates that two major functions can be ascribed to the enzyme: to catalyze the conversion of hydrogen peroxide to water, and to catalyze the oxidation of a substrate molecule to a free radical product. Typical reducing substrates include aromatic phenols, phenolic acids, indoles, amines and sulfonates [100].

The mechanism of catalysis of horseradish peroxidase, in particular the C isoenzyme, has been investigated extensively.

The first step in the catalytic cycle is the reaction between H_2O_2 and the Fe (III) resting state of the enzyme to generate Compound I (Figure 4.4), a high oxidation state intermediate comprising a Fe (IV) oxoferryl center and a porphyrin-based cation radical, overall 2 electron-transfer processes.

Compound I is, in turn, reduced by a hydrogen donor via a one-electron transfer process to form a second enzyme intermediate called Compound II and a donor radical. Then the Compound II is again reduced by a hydrogen donor via a one-electron process to the native enzyme and another donor radical. The two donor radicals can combine to form a stable final product.

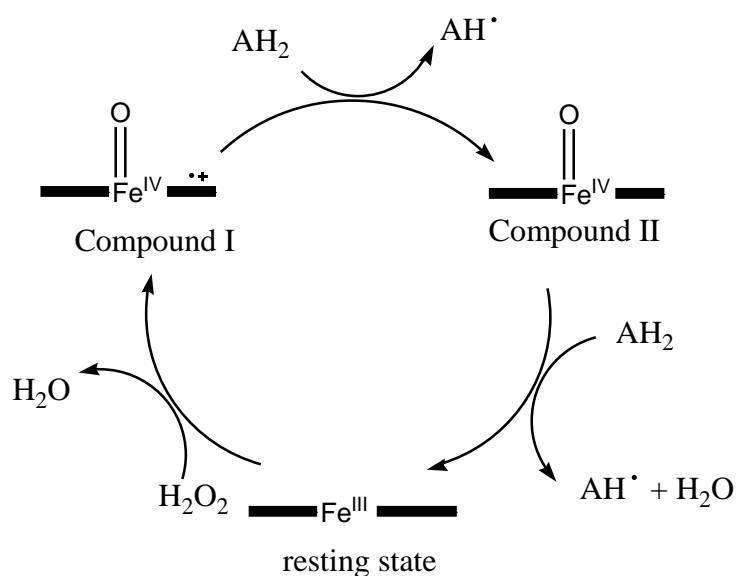


Figure 4.4. The catalytic cycle of HRP with a generic substrate (AH_2). Modified by [100]

iii. ABTS^{2-} as substrate for HRP

2,2'-Azino-bis(3-ethylbenzothiazoline-6-sulfonic acid) diammonium salt, called in this thesis ABTS^{2-} , is frequently used as sensitive chromogenic substrate for the quantification of horseradish peroxidase (Figure 4.5).

ABTS^{2-} (I) can undergo a one-electron oxidation to give the metastable radical anion $\text{ABTS}^{\cdot-}$ (II), which slowly disproportionates giving (I) and an

azoproduct (III). This last chemical change takes several hours, so it does not affect the measurements of enzyme activity carried out in this thesis that took into account only the first five minutes of the reaction.

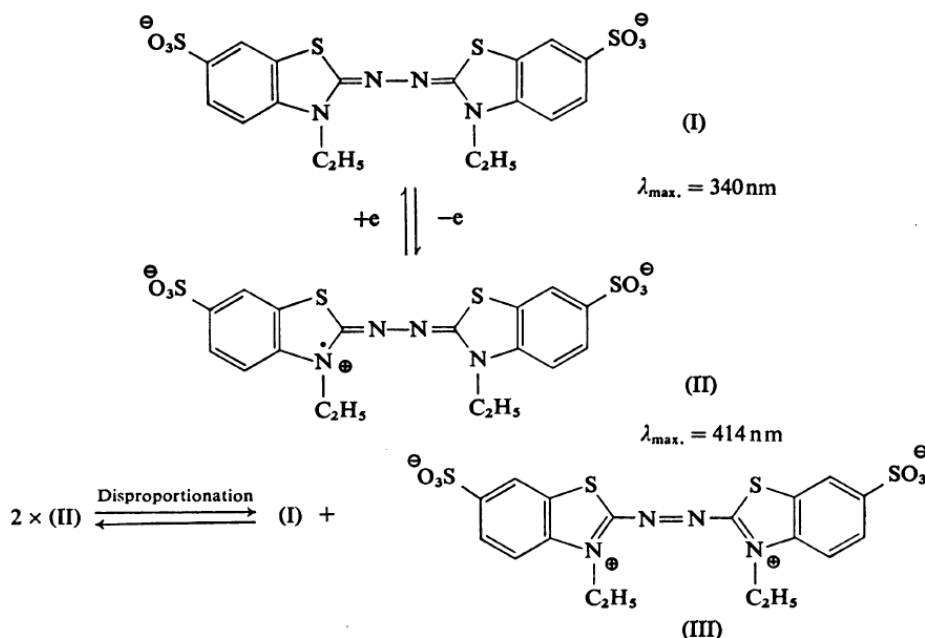


Figure 4.5. Chemical oxidation of ABTS²⁻ Modified by [101]

ABTS²⁻ has an absorption maximum at 340 nm ($\lambda = 3.6 \times 10^4 \text{ M}^{-1} \text{ cm}^{-1}$). Depending on the experimental conditions, the HRP catalyzed oxidation of ABTS²⁻ can lead to the formation of the radical anion ABTS^{•-}, which has an absorption maximum at 414 nm ($\lambda = 3.6 \times 10^4 \text{ M}^{-1} \text{ cm}^{-1}$) together with other three peaks at 650, 735 and 814 nm. Therefore, the activity of HRP can be measured spectrophotometrically by following the rate of reaction product formation.

4.2.3. Giant unilamellar vesicles GUVs

In collaboration with Dr. Tom Robinson at the Department of Chemistry and Applied Biosciences, ETH Zurich, I focused on the understanding of the membrane interaction and perturbation by the natural antimicrobial peptide

ALY and its analogue azoALY, using the single GUV method. Peptide membrane interactions are involved in numerous crucial biological processes, such as antimicrobial defense mechanisms, viral translocation, membrane fusion, functions of membrane proteins, transport of therapeutic compounds, disruption of integrity of membranes, and others. During peptide membrane interactions, both the peptide and the membrane may experience a series of structural changes. Thus, theoretical and experimental studies of peptide membrane interactions constitute a challenging topic of research and complete understanding of the relationship between the structure of the peptide and the mechanism of interaction with lipids, as well as molecular details of this process, still remain elusive. However, it is of paramount importance to reveal the biological functions of membrane active peptides and to design peptides with tailored functionalities that may be exploited for therapeutic applications. The complexity of a biological membrane is overwhelming and the multiple processes that occur simultaneously within this unique environment are just beginning to be understood. Biological membranes are mainly composed of proteins and lipids which do not form a single homogeneous mixture, being some regions more enriched in some components of the mixture. The membrane bilayer of different organisms can be very different. Many different model systems have been created that retain the essential lipid bilayer structure, but simplify the system so that the roles of individual components can be assessed and their organization and dynamics can be visualized [102].

Giant unilamellar vesicles (GUVs) represent an excellent model system for cell membranes and have become an important tool in biophysical research. They have diameters of 1–100 μm and their applications are numerous and include membrane protein research, artificial cells, membrane fusion, drug discovery and nano-science [103].

GUVs have been used for investigations of the physical and biological properties of vesicle membranes such as elasticity and shape change. The

shape of a single GUV and its physical properties in water can be measured in real time. Therefore, GUVs have a great advantage over smaller liposomes such as LUVs and small unilamellar vesicles (SUVs) in investigating the physical properties and structural changes of liposomes.

4.2.4. Unilamellar vesicles

In the laboratory of Prof. Peter Walde, at ETH Zurich, I spent 7 months to learn basic knowledge about vesicles preparation and characterization methods. Lipid vesicles [104] (also called liposomes or simply vesicles) are polymolecular aggregates formed in aqueous solution from the dispersion of bilayer-forming amphiphilic molecules. Under osmotically balanced conditions, they are spherical in shape and contain one or more (concentric) lamellae, in which the hydrophobic part of the molecule forms the hydrophobic interior of the bilayer and the hydrophilic part (the polar head group) is in contact with the aqueous phase.

The physical properties of lipid vesicles may vary depending on how and under which conditions lipid vesicles of a certain amphiphile (or mixture of amphiphiles) are prepared. A controlled reduction in size and lamellarity of vesicles can be achieved by using track-etch polycarbonate membranes, which contain almost cylindrical pores of a defined size [105, 106]. The vesicles suspension can be forced to pass through these membranes under moderate pressure (usually 10 times) in order to obtain a mechanical transformation of the large vesicles into smaller ones [106, 107]. The whole process is called ‘extrusion technique’ and the corresponding vesicles are called VET (vesicles prepared by the extrusion technique). Usually, the extrusion starts with membranes containing relatively large pores (mean diameter 400 nm), followed by an extrusion through smaller pores (200 nm and often finally 100 nm). The corresponding obtained vesicle preparation are called VET₁₀₀, where ‘100’ indicates the mean pore diameter (in nm) used for the final extrusions.

VET₁₀₀ are mainly unilamellar and rather monodisperse with a mean diameter of 100 nm [106].

In the case of VET₂₀₀, VET₄₀₀, or VET₁₀₀₀, the vesicles are characterized by a lower degree of unilamellarity and a lower degree of monodispersity [106]. In addition to the high degree of reproducibility of the preparation, one advantage of the extrusion technique is certainly the fact that no organic solvent is directly involved.

Of course, it is necessary that all mechanical treatments of lipid vesicles are carried out above T_m (main lamellar chain-melting phase transition temperature), in the fluid state of the membranes. Below T_m , the saturated hydrophobic chains exist predominately in a rigid, extended all *trans* conformation, similar to their crystalline state (*Figure 4.6*). Above T_m , the chains are rather disordered with a lot of gauche conformations in the hydrocarbon chains, making the bilayer fluid (mechanically treatable), and characterized by high lateral and rotational lipid diffusion, rather similar to a liquid [108].

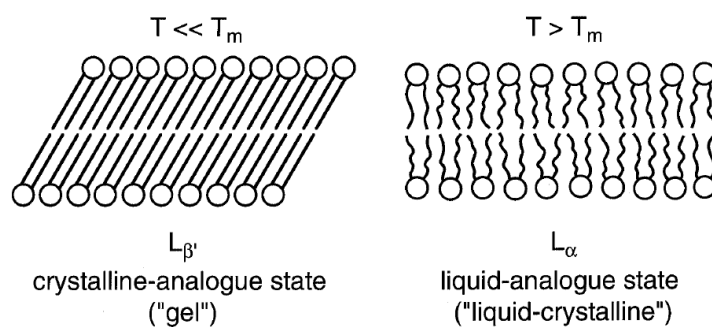
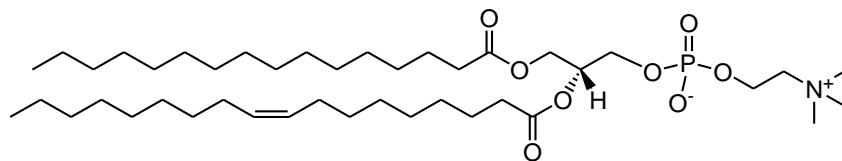


Figure 4.6. Schematic representation of the lipid arrangement in a planar bilayer below and above the T_m

Many bacterial cell membranes are anionic because they are composed of a significant percentage of negatively charged phospholipids. Therefore, vesicles containing POPC/POPG (90:10) (*Figure 4.7*) are a rough mimic of a generic anionic bacterial membrane.

POPC 1-palmitoyl-2-oleoyl-sn-glycero-3-phosphocholine $T_m = -2.5 \pm 2.4$ °C [109]



POPG 1-palmitoyl-2-oleoyl-sn-glycero-3-phospho-(1'-rac-glycerol) (sodium salt) $T_m = 0.8$ °C [110].

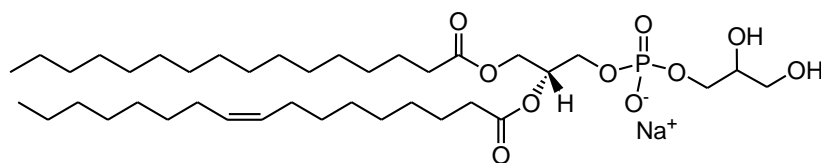


Figure 4.7. Chemical structures of lipid used for GUVs and LUVs preparation

4.3. Effect of synthetic peptides on GUVs membrane permeability

4.3.1. Formation of GUVs

Among the different ways of preparing GUVs, electroformation is the most favorable, due to the unilamellarity of the obtained vesicle membranes and the fast production time [111]. Once formed, they can be investigated using standard optical microscopy and even spectroscopic techniques such as fluorescence correlation spectroscopy.

In this work, GUVs were created by electroformation following the Angelova procedure [112]. The cell used for vesicles preparation (Figure 4.8) consisted of two conductive indium tin oxide (ITO) coated glasses separated by a 1.5 mm thick silicone rubber spacer to maximize the yield of vesicles.

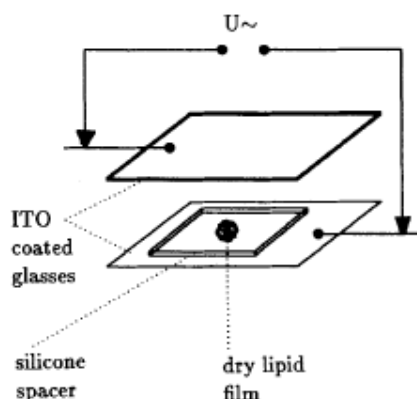


Figure 4.8. Sketch of the cell for the vesicles preparation[112]

POPC/POPG lipids (9:1 mol/mol) were dissolved in chloroform/methanol (9:1 v/v) at a concentration of 1 mM. The orange-red fluorescent dye, DiI, was added at a concentration of 1 μ M. A drop of 2.5 μ L of the mixture was deposited on one of the conductive coated glasses, and this was repeated in 12 locations. The lipid film was then dried under vacuum overnight and then hydrated with MilliQ water containing 10 μ M calcein. The chambers were sealed by a second ITO slide and held at 60 $^{\circ}$ C within a custom-built heating device. GUVs were formed by applying 0.7 V at a frequency of 10 Hz for 4 h using a function generator. After applying 1 V at 4 Hz for 30 min to detach the vesicles from the surface, harvesting was achieved by careful pipetting. GUVs were stored at room temperature and used within 48 h.

For the release analysis of calcein from GUVs, I used a technique developed by Dr. Tom Robinson: a microfluidic platform able to trap single GUVs in parallel [113]. The device consists of an array of chambers each containing a trap and therefore allowing up to 60 vesicles of a similar size to be immobilized simultaneously without compromising their integrity. As an additional feature, Robinson's group integrated "donut" shaped valves positioned above the traps that can be lowered by pressurizing a separate microchannel network. The traps are made of polydimethylsiloxane (PDMS)

and each trapped vesicle is isolated from the rest of the channel network, leading to a defined microenvironment where the GUV experienced no shear stress.

By exchanging the solution inside the chip and subsequently opening the valves, it is possible to perform fast kinetic studies. To investigate the membrane perturbation and subsequent transport of calcein across the membrane, GUVs containing fluorescent calcein were trapped. Due to the hydrophilic nature of calcein, it does not permeate the membrane and remains encapsulated. Once trapped, the GUVs remain stable for long time periods (at least 12 h).

4.3.2. Microscopic observation of GUVs

The fluorescence intensity of the calcein within three separate vesicles was monitored using a confocal laser scanning microscope (Axiovert 200 M, Zeiss). *Figure 4.9 (a)* shows a trapped GUV between the two PDMS posts in a flow rate of $0.625 \mu\text{L min}^{-1}$ with calcein fluorescence visible both inside and outside. The solution was then exchanged with MilliQ water and as shown in *Figure 4.9 (b)*, after this washing only calcein fluorescence inside GUV is visible.

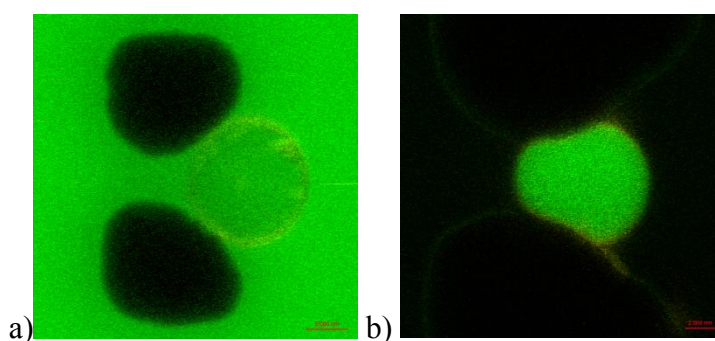


Figure 4.9. Confocal fluorescence images (a) before washing with MilliQ water and (b) after washing. Scale bar: $5 \mu\text{m}$ (a) and $2 \mu\text{m}$ (b)

The aqueous solution outside the donuts was then exchanged with an aqueous solution of peptide. With a total flow rate of $5 \mu\text{L min}^{-1}$, the valves were opened and closed for 2 s to rapidly expose the GUV to the membrane protein. The experiments were carried out using two different concentrations: $1 \mu\text{M}$ and $50 \mu\text{M}$ of both peptides.

Figure 4.10 shows an image series after the addition of $50 \mu\text{M}$ azoALY, where it is visible that calcein diffuses out of the GUVs and the calcein fluorescence decreases accordingly.

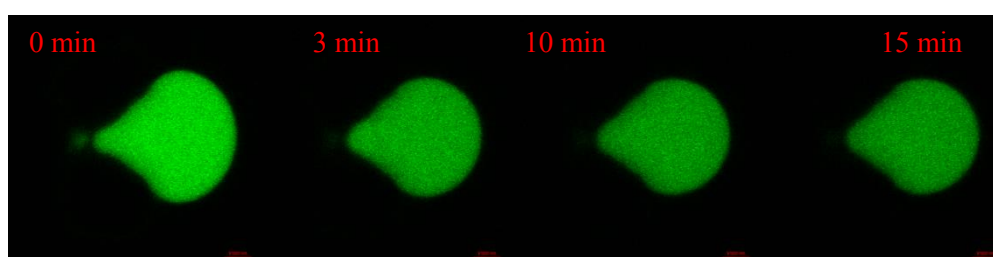


Figure 4.10 Confocal fluorescence images of calcein being released from GUV with $50 \mu\text{M}$ azoALY. Scale bar: $5 \mu\text{m}$

After 15 minutes of interaction the GUVs preserved their shape, so I excluded the destruction of the membrane or pore formation. However a considerable amount of calcein was still extant in the vesicles.

4.3.3. Calcein leakage: preliminary results

Two processes govern the release of calcein from the vesicles: (i) the membrane permeability changes by peptide membrane interaction and (ii) diffusion of calcein across the membrane due to a concentration gradient.

The GUVs analyzed were unilamellar vesicles and all had the same diameter of $12 \mu\text{m}$, in order to maintain the same surface area for comparable results. The mean pixel intensities within each GUV were normalized and plotted against time (*Figure 4.11*). The release measure in absence of the peptide was used as control, and the amount of calcein within the GUV remained constant indicating that photobleaching did not occur. Error bars are calculated from

the standard error, estimated by population standard deviation divided by the square root of the sample number. The number of individual experiments at a given peptide concentration was $n = 3$.

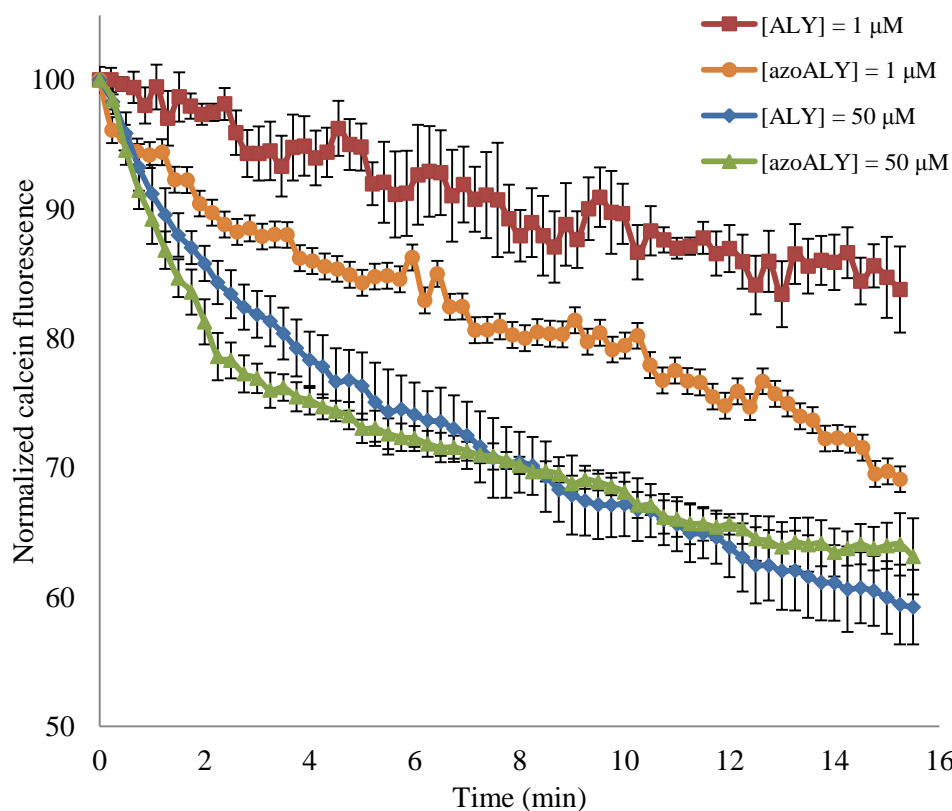


Figure 4.11. Kinetics of calcein release for 1 and 50 μM of azoALY and ALY using 3 separate vesicles. The control without peptide showed no calcein release.

At low concentrations of ALY peptide (1 μM), during the first 15 min of exposure, the calcein fluorescence undergoes a decrease of 17%. But, using the same concentration of the modified azoALY peptide, a decrease of 31% in intensity was observed at the same time. In contrast, when high concentrations were used (50 μM) it was possible to observe that azoALY had a faster effect on membrane permeability than the natural peptide. In fact, during the first three minutes of experiment, 25% of calcein leakage was observed, though after 15 minutes both peptides had the same calcein leakage.

Usually, peptide membrane interactions induce an immediate and complete material release [114, 115] by forming pore through the membrane. In my experiments, I found that there was no complete calcein release from GUVs. However, the goal of the proposed experiment was to put in evidence the difference between the behavior of the natural and the azo modified peptide.

4.4. Effect of synthetic peptides on LUVET membrane permeability

The idea was to entrap a sensitive reporter enzyme like HRPC in large unilamellar vesicles with a diameter size of 200 nm, prepared by extrusion method and then to estimate the membrane permeability increase by measuring the enzyme activity. The figure below (*Figure 4.12*) is a schematic representation of the hypothesis of work.

I needed few assumptions. First of all I excluded the presence of enzyme bound to the outer membrane of the lipid vesicles. Second I supposed that until the vesicle membrane is intact, HRPC molecules cannot cross the membrane due to their size, and substrate molecules (ABTS^{2-}) cannot enter due to their negative charge. So, in normal conditions, there is no enzyme activity.

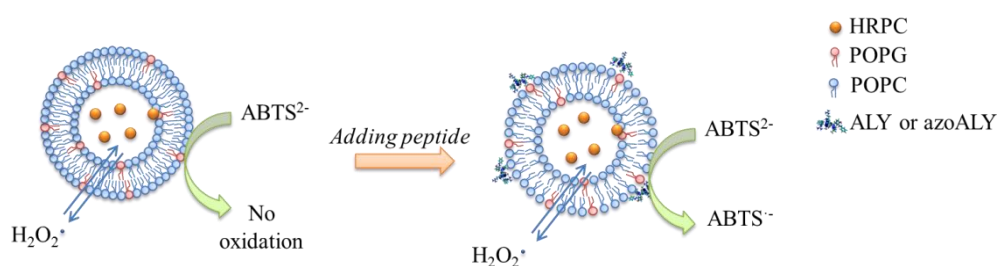


Figure 4.12. Enzyme leakage hypothesis of work

The situation could be different when a membrane interacting peptide is present, in this case the membrane perturbation by peptide interaction could

cause ABTS²⁻ uptake or HRPC release and it is possible to follow the ABTS²⁻ oxidation by spectrophotometric measurements.

4.4.1. Spectrophotometric quantification of horseradish peroxidase catalytic activity

The following reaction conditions for the spectrophotometric quantification of horseradish peroxidase (HRPC) activity were found to be appropriate: [ABTS²⁻]₀ = 0.25 mM in presence of hydrogen peroxide [H₂O₂]₀ = 80 μM at 25 °C in MES buffer pH = 5, for a total assay volume of 1 mL.

The initial formation of only one of the possible reaction products and intermediates, ABTS^{·-} (λ_{max} = 414 nm), was observed. The rate of ABTS^{·-} formation during the first 5 min of reaction was followed spectrophotometrically and found to linearly depend on the HRPC concentrations between 50 and 350 pM under the conditions used (*Figure 4.14*).

For the activity measurements three stock solutions were freshly prepared:

1. ABTS²⁻ stock solution was prepared by dissolving a few mg of ABTS²⁻ in 1 mL of MES pH = 5 buffer solution. The exact concentration was calculated by UV-absorbance (λ = 340 nm, ε = 3600 M⁻¹ cm⁻¹). The solution was kept in the dark at room temperature and was used within 8 h.
2. H₂O₂ stock solution (4 mM) was prepared by appropriate dilution with MilliQ water of a 30 wt% aqueous H₂O₂ solution.
3. Enzyme stock solution 4 mg/mL was prepared by dissolving HRPC in MES buffer pH = 5. From this concentrated solution a diluted stock solution 1 μM was prepared. Finally, for each measurement, two fresh stock solutions (100 nM and 2 nM) were prepared in plastic reaction tubes. I needed to repeat these last two preparations because I realized that for low HRPC concentration, part of the enzyme adsorbed to the reaction tube.

The activity measurements were carried out in this way: buffer to reach the assay volume of 1 mL, ABTS^{2-} (final concentration of 0.25 mM) and HRP stock solution were mixed in a reaction tube. Immediately before the spectrophotometric analysis, H_2O_2 was added (final concentration of 80 μM). The mixture was transferred into a PS cuvette (path length = 1 cm) and the development of the absorption spectrum of the reaction mixture was monitored as a function of time (Figure 4.13) using diode array spectrophotometer (Specord 5600 Analytik Jena). All measurements were repeated three times.

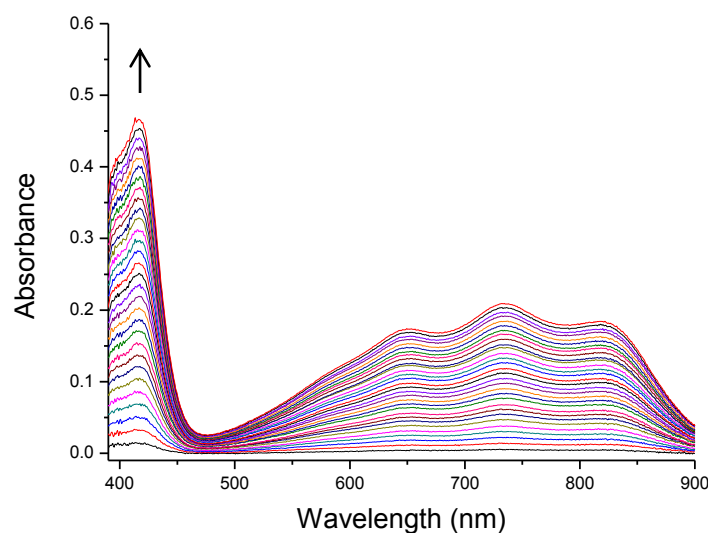


Figure 4.13. Changes of the absorption spectrum of the reaction solution as a function of reaction time, with $[\text{ABTS}^{2-}]_0 = 0.25 \text{ mM}$, $[\text{H}_2\text{O}_2]_0 = 80 \mu\text{M}$ and $[\text{HRP}] = 150 \text{ pM}$ at 25 °C (MES buffer pH = 5). The spectra were recorded at intervals of 10 sec immediately after the start of the reaction (up to 5 min).

During the investigation of membrane peptide interaction, I used Triton X-100 as control. It is a non-ionic surfactant with a hydrophilic polyethylene oxide chain and an aromatic hydrophobic group. It is able to solubilize the vesicles. However non-ionic detergents, such as Tween 20 or Triton X-100 were found

to increase the activity of horseradish peroxidase due to delay of inactivation in the course of substrate reaction [116]. Thus I measured a second calibration curve in presence of Triton X-100 (Figure 4.14).

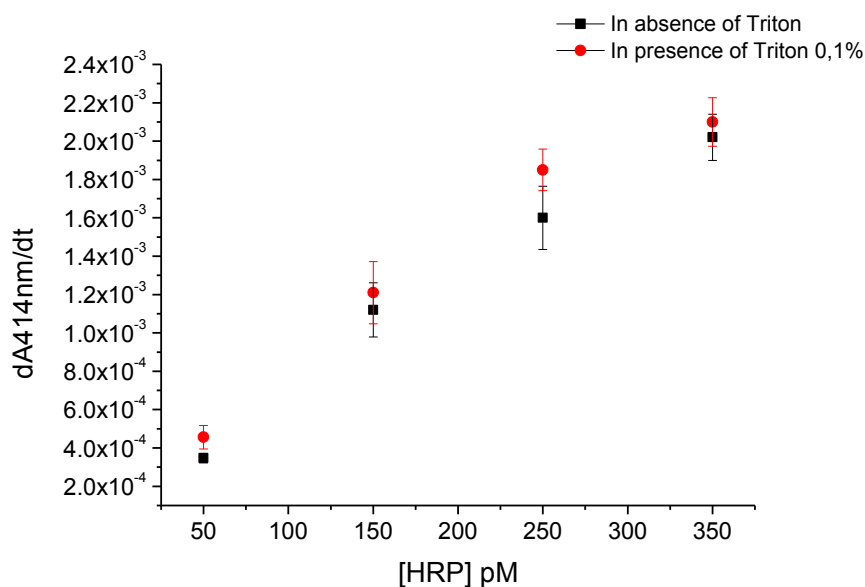


Figure 4.14. HRP concentration dependency of the absorbance of the reaction solution at 414 nm measured during the first 5 min of enzymatic reaction (—■—) without addition of detergent to substrate mixture and (—●—) with addition of Triton X-100. Each data point shown is the average from three measurements using the same stock solutions. The standard deviation is indicated with a bar. Deviation from linearity was evident for concentration higher than 350 pM HRP.

For the assay I used the same stock solutions previously described, additionally a new stock solution of Triton X-100 5% was prepared. The final surfactant concentration was 0.1% in the assay mixture containing HRP and ABTS²⁻ solutions. I waited 5 min after Triton X-100 addition, then the reaction was started adding hydrogen peroxide and the enzymatic reaction was followed by UV/Vis spectrophotometry. All measurements were repeated three times.

Linear regression of the product absorbance at $\lambda_{\max} = 414$ nm as a function of the time allows an easy determination of enzymatic activity, read as the slope of the linear fit (dA414nm/dt), see *Table 4.1*.

Table 4.1. Rate of ABTS $^{\cdot-}$ formation for HRPC concentrations between 50 and 350 pM in absence and presence of Triton X-100

	<i>dA414nm/dt</i>	<i>st. dev.</i>
1) HRPC 50 pM	3.47E-04	2.47E-05
2) HRPC 150 pM	1.12E-03	2.41E-04
3) HRPC 250 pM	1.60E-03	1.65E-04
4) HRPC 350 pM	2.02E-03	1.20E-04
5) HRPC 50 pM + Triton X-100 0.1%	4.56E-04	6.12E-05
6) HRPC 150 pM + Triton X-100 0.1%	1.21E-03	2.62E-04
7) HRPC 250 pM + Triton X-100 0.1%	1.85E-03	1.08E-04
8) HRPC 350 pM + Triton X-100 0.1%	2.10E-03	1.26E-04

Enzymatic activity for HRPC solutions from 50 to 350 pM (1-4) and adding Triton X-100 (4-8). Each data point shown is the average from three measurements and the standard deviation is also indicated.

4.4.2. Formation of enzyme containing lipid vesicles

Unilamellar vesicles 200 nm composed of POPC/POPG (mixture 90:10 mol/mol) and loaded with HRPC were prepared by mechanical extrusion. *Figure 4.15* gives a schematic summary of the method used.

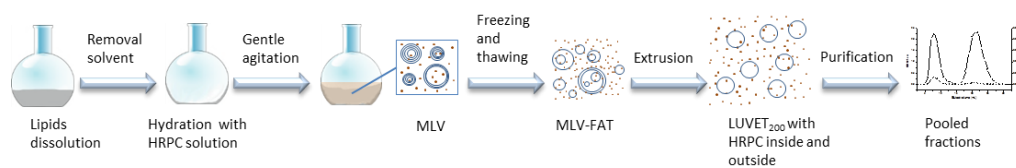


Figure 4.15. Schematic scheme for the preparation of enzyme containing lipid vesicles

A weighted amount of lipids (20 mM) was first dissolved in chloroform stabilized with ethanol and then mixed in a 100 mL round bottom flask.

The solvent was removed by rotatory evaporation at 35 °C and dried in high vacuum overnight. The obtained thin lipid film was hydrated with 3.5 mL of 20 μ M HRPC solution in 10 mM (MES) buffer (pH = 5) at room temperature. In this step lipid multilayers are formed, which results in the formation of a heterogeneous population of vesicles. Usually this phase is made by vigorous shaking with the help of a Vortex mixer above T_m of the lipids. In my case, I worked with enzyme, in order to exclude enzyme denaturation; I performed the hydration by gentle agitation of the flask.

In order to homogenize and equilibrate the enzyme containing multilamellar vesicles suspension (MLV) 10 freezing–thawing cycles were carried out, cooling the flask in liquid nitrogen for 20 seconds followed by heating in water at 50 °C for 30 seconds. The resulting vesicle suspension, abbreviated as FAT-VET (freezing and thawing extruded vesicles), is usually characterized of a higher entrapment yield and a more homogenous size distribution [117].

To reduce size and lamellarity of MLV, the vesicle suspension was first extruded 10 times through track-etch polycarbonate membranes with cylindrical pores of 400 nm size under moderate pressure (3 mbar) at room temperature, followed by extrusion with a 200 nm membrane increasing the pressure to 5 mbar at same temperature conditions because T_m of the lipids used is lower than room temperature.

The non-entrapped enzyme molecules were separated from the enzyme containing vesicles by size-exclusion chromatography. Using a 2×20 cm glass column filled with Sepharose 4B equilibrated with MES buffer (pH = 5). 2 mL of the mixture was applied and the separation was performed at a flow rate of 0.5 mL/min. If this separation step is not carefully carried out, some of the enzyme molecules will still be in the bulk aqueous solution, which may falsify the results obtained from investigations using these enzyme-containing vesicle dispersions, possibly leading to incorrect interpretations.

Turbidity measurements of each eluted fraction, performed with a spectrophotometer (*Figure 4.16*), indicate a good separation of the vesicles from the free enzyme. The optical density at 403 nm indicates two peaks, the first assigned to the turbid vesicles fraction, the second to the free HRPC with an absorption maximum at 403 nm due to the Soret band.

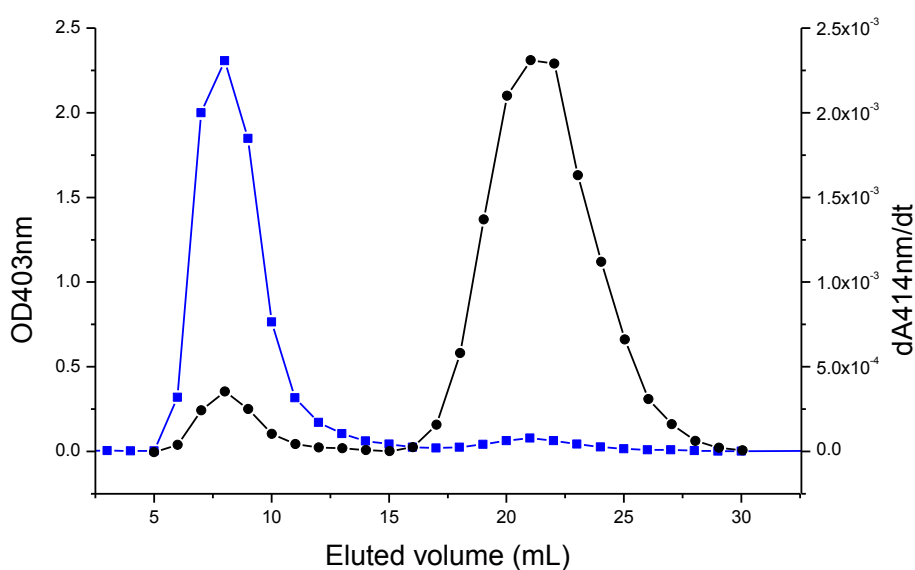


Figure 4.16. (—■—) Turbidity trend from 2nd fraction to 30th fraction (—●—) activity assay for each fraction from 5th to 30th one.

I also demonstrated that enzyme containing vesicles were stable for at least one week, measuring the enzymatic activity for the fractions from highest absorption values. *Figure 4.17* shows the enzymatic activities of the fractions 6 - 11, which were stable for one week. Addition of Triton X-100 confirmed that a considerable amount of enzyme was still entrapped in the vesicles.

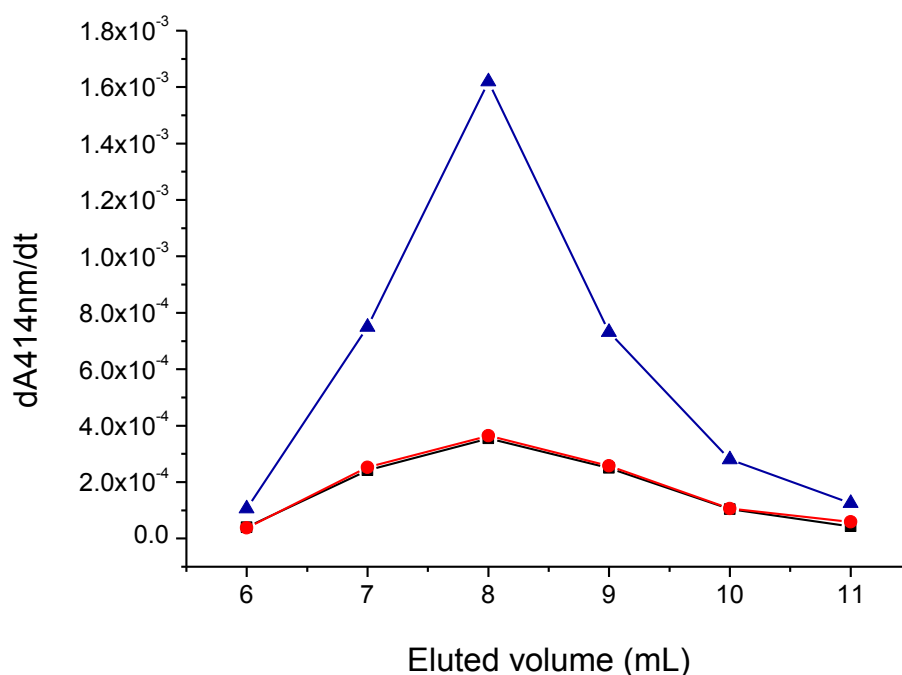


Figure 4.17. Enzymatic activity in the fractions 6 to 11 immediately after preparation (—■—), after one week (—●—) and after adding Triton X-100 one week after the preparation (—▲—).

4.4.3. Release of HRPC from negative vesicles after peptide interaction: preliminary results

The suspension of enzyme containing vesicles was used to evaluate different membrane interactions of ALY and azoALY. Moreover I performed measurements using different incubation times (0, 5, 10 min) to estimate a possible time dependence of the interactions, and to understand if and how much the membrane permeability could be influenced by peptide interaction.

I performed measurements of HRPC release (or ABTS²⁻ uptake) using the pooled fractions 6-11, yielding 6 mL of POPC/POPG vesicles containing HRPC.

The activity measurements were carried out as already described following these reaction conditions: [ABTS²⁻]₀ = 0.25 mM, [peptide] = 4 μM, [H₂O₂]₀ = 80 μM, 100 μL of pooled fraction 100x diluted and 20 μL 5% v/v Triton X-100 at 25 °C in MES buffer pH 5, for a total assay volume of 1 mL and reaction time 5 min. The results are shown in *Table 4.2*.

Table 4.2. Rate of ABTS²⁻ formation to estimate release time depending from POPC/POPG vesicles with enzyme entrapped in four different systems

		<i>Incubation Time (min)</i>		
		<i>0'</i>	<i>5'</i>	<i>10'</i>
1) POPC/POPG + HRPC entrapped 100x diluted	<i>dA414nm/dt</i>	8.93E-05	7.93E-05	8.53E-05
	<i>st. dev.</i>	5.46E-06	4.32E-06	2.46E-06
2) POPC/POPG + HRPC entrapped 2000x diluted + Triton X-100 0.1%	<i>dA414nm/dt</i>		1.47E-3	
	<i>st. dev.</i>		2.00E-05	
3) POPC/POPG + HRPC entrapped 100x diluted + ALY 4 μM	<i>dA414nm/dt</i>	1.83E-04	1.87E-04	1.85E-04
	<i>st. dev.</i>	2.07E-06	2.37E-06	2.29E-06
4) POPC/POPG + HRPC entrapped 100x diluted + azoALY 4 μM	<i>dA414nm/dt</i>	9.89E-04	1.64E-03	1.95E-03
	<i>st. dev.</i>	7.28E-06	1.77E-05	1.00E-05

Time dependent enzymatic activity for POPC/POPG vesicles with HRPC entrapped 100x diluted (1), adding Triton X-100 2000x diluted (2), adding ALY (3) and adding azoALY (4). Each data point is the average of three measurements and the standard deviation is also indicated.

As shown in *Figure 4.18*, the enzymatic activity in the pooled fraction (dilution factor 100x) is very low, and the correspondent HRPC concentration is lower than 50 pM, from the calibration curve (*Figure 4.14*). Also, the activity for this system was not time dependent, the slope value did not change for the three different incubation times. When I analyzed enzyme containing vesicles plus Triton X-100 0.1%, I observed a big increase in enzyme activity after 5 min of incubation. This big increase is normal if I consider that Triton X-100 causes immediate vesicles destruction with release of entrapped enzyme in the assay solution. Checking in the calibration curve in presence of Triton X-100, there was a release of HRPC in the range of 200 pM and considering a dilution factor 2000x, I can say that the concentration of entrapped enzyme should be around 400 nM.

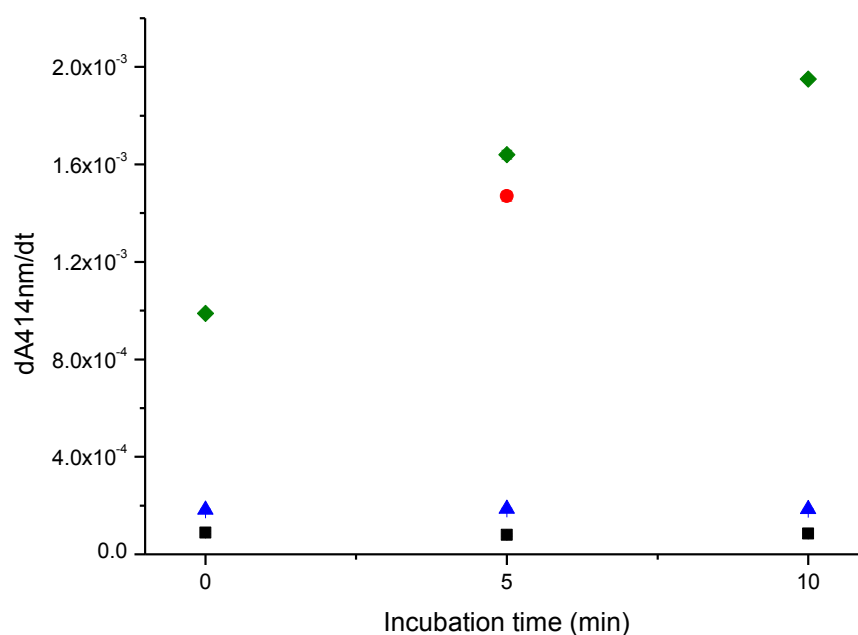


Figure 4.18. Enzymatic activity time depending for POPC/POPG vesicles with HRPC entrapped (—■—), adding Triton X-100 (—●—), adding ALY (—▲—) and adding azoALY (—◆—). Each data point shown is the average from three measurements and the standard deviation is indicated with a bar.

Analyzing the results obtained with ALY peptide, I detected a very small increase in enzyme activity caused from HRPC release or substrate uptake, with a slope value constant at three measurement times, but lower than values reported in the calibration curve. So I could only suppose that the released enzyme concentration in the assay solution was lower than 50 pM, but I could not estimate the amount of HRPC released. The situation was completely different using the modified peptide, the activity increase was time dependent with values bigger than those obtained for the unmodified peptide and lower than values obtained with Triton X-100. The slope value for 0 min of incubation corresponds to a HRPC concentration around 100 pM, for 5 min 250 pM and for 10 min 325 pM. So, considering a dilution factor 100x I could say that I had an increase of enzyme release or ABTS²⁻ uptake time dependent with an enzyme concentration in the pooled fraction of 10 nM, 25 nM and 32.5 nM respectively.

The preparation of vesicles with enzyme entrapped was repeated three more times and for each mixture I evaluated the membrane perturbation due to the ALY and azoALY action. In all cases I obtained analogous enzyme leakage.

To validate and understand the results, some controls were required.

i. First control

I checked if the presence of the peptides could influence HRP activity as ALY and azoALY peptides contain a phenol moiety (in Tyrosine) and azo-group, and, aromatic phenols, phenolic acids, indoles, amines are typical reducing substrates for HRP. I performed the activity assay as already described.

As shown in *Table 4.3* and in *Figure 4.19*, in presence of both the unmodified and modified peptide there are no changes in enzymatic activity. All measurements were repeated three times to confirm the reproducibility of the results. Moreover as shown in the UV-Vis spectra below, there is no spectrum change due to the presence of peptide: in each of them there is no shift of the characteristic peaks of the oxidized ABTS²⁻ form (414 nm, 650, 735 and 814 nm).

Table 4.3. Rate of ABTS^{·-} formation for HRP concentrations 200 pM in presence of ALY and azoALY

	<i>dA414nm/dt</i>	<i>st. dev.</i>
a) HRP 200 pM	1.50E-03	4.16E-05
b) HRP 200 pM + ALY 4 μM	1.55E-03	5.13E-05
c) HRP 200 pM + azoALY 4 μM	1.53E-03	3.00E-05

Enzymatic activity for HRP 200 pM (a), adding unmodified peptide 4 μM (b) and modified peptide 4 μM (c). Each data point shown is the average from three measurements and the standard deviation is also indicated.

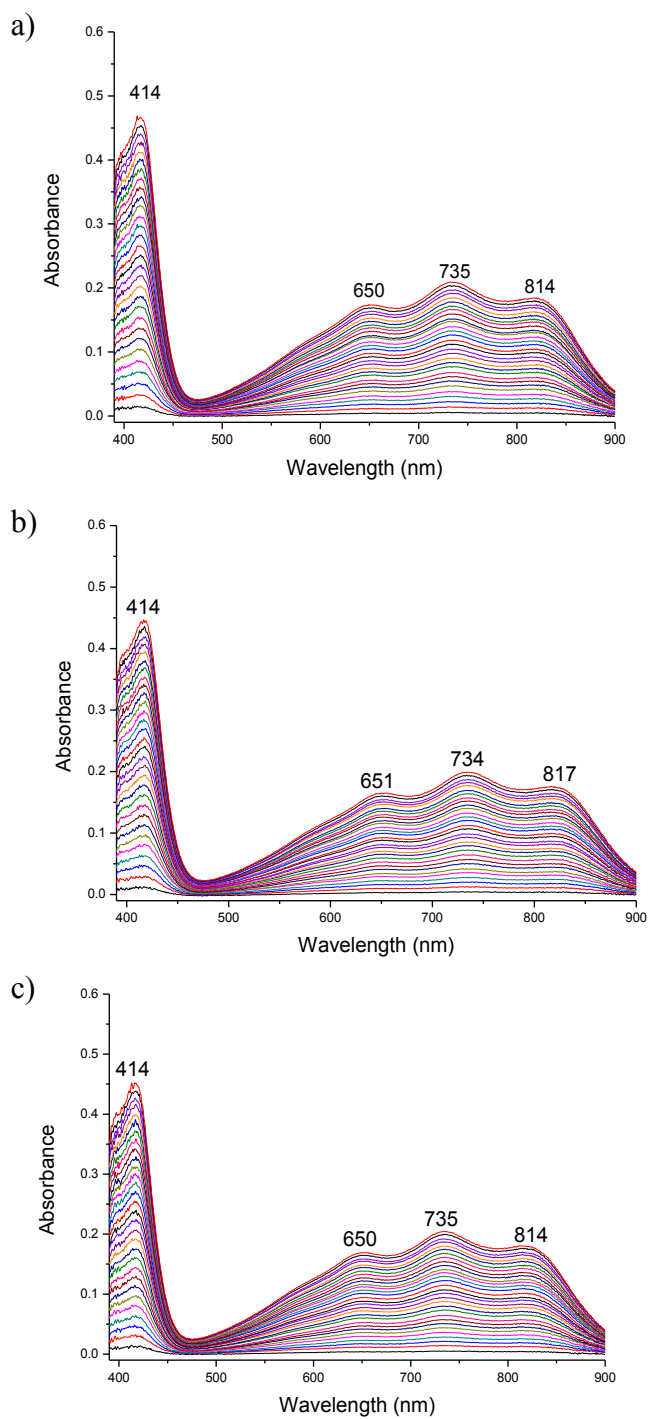


Figure 4.19. a) Activity assay $[HRP] = 200 \text{ pM}$ in absence of peptide. b) Activity assay $[HRP] = 200 \text{ pM}$ adding $[ALY] = 4 \text{ }\mu\text{M}$ c) Activity assay $[HRP] = 200 \text{ pM}$ adding $[azoALY] = 4 \text{ }\mu\text{M}$

ii. Second control

The second control was made to estimate if the enzymatic reaction was influenced by vesicles and peptide mixing. The enzymatic activity measurements were carried out for four different systems containing:

- 1) 250 pM HRPC solution;
- 2) 250 pM HRPC solution adding POPC/POPG vesicles (200 nm) 6 μ M suspension;
- 3) 250 pM HRPC solution adding POPC/POPG vesicles (200 nm) 6 μ M suspension and peptide 4 μ M solution;
- 4) 250 pM HRPC solution adding POPC/POPG vesicles (200 nm) 6 μ M and Triton X-100 0.1% suspension.

The results are reported in *Table 4.4*.

Analyzing the results, I observed that the rates are very close each other, so for these preliminary tests I could exclude enzymatic inhibition by assay mixture. However I observed an increase in activity due to Triton X-100 presence, but the value $1.81E-0.3$ is the same value obtained in the calibration curve in presence of Triton X-100 (see *Figure 4.14*).

Table 4.4. Rate of ABTS^{•-} formation for HRPC concentrations 250 pM in five different systems

	<i>dA414nm/dt</i>	<i>st. dev.</i>
1) HRPC 250 pM	1.60E-03	8.39E-05
2) HRP 250 pM + empty POPC/POPG 6 μM	1.59E-03	6.35E-05
3) HRP 250 pM + empty POPC/POPG 6 μM +ALY 4 μM	1.58E-03	1.19E-04
4) HRP 250 pM + empty POPC/POPG 6 μM + azoALY 4 μM	1.53E-03	7.37E-05
5) HRP 250 pM + empty POPC/POPG 6 μM + Triton X-100 0.1%	1.81E-03	2.16E-04

Enzymatic activity for HRPC 250 pM (a), with empty POPC/POPG 6 μM vesicles in the assay mixture (b), with empty POPC/POPG 6 μM vesicles and ALY 4 μM (c) or azoALY 4 μM (d), and with empty POPC/POPG 6 μM vesicles plus Triton X-100 0.1% in the assay mixture (d). Each data point shown is the average from three measurements and the standard deviation is also indicated.

iii. Third control

I performed a third control to evaluate how much HRPC was bound to the vesicle surface prepared without enzyme entrapped. I prepared 20 mM POPC/POPG (90:10 mol/mol) vesicles in 10 mM MES buffer pH = 5 by extrusion using 200 nm filter. After the extrusion the vesicle suspension was mixed with a solution 20 μM HRPC (in a plastic tube). The system was allowed to interact for two hours, the time that usually preparation of enzyme containing vesicles takes. The separation of the free enzyme solution was made in the same way as for enzyme containing vesicles. The fractions with the highest vesicle concentrations were identified by turbidity measurements (*Figure 4.20*) and fractions from 4 to 9 were pooled for a total volume of 6 mL.

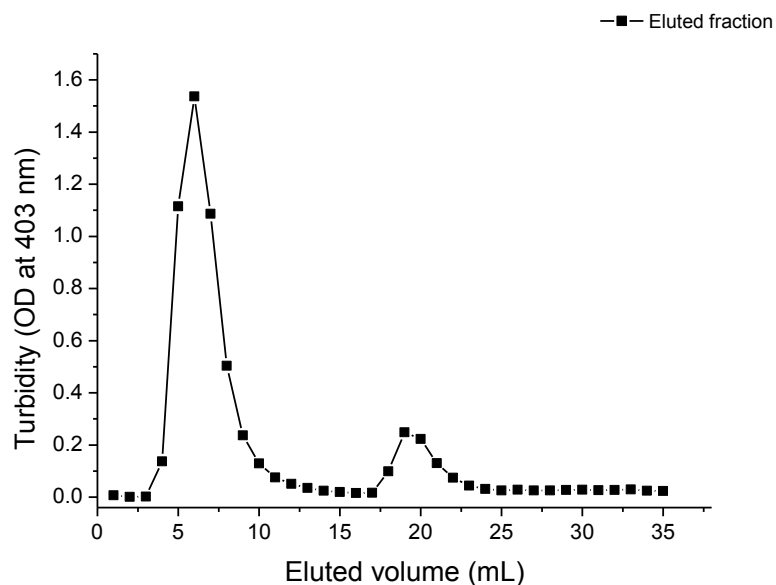


Figure 4.20. Turbidity trend of eluted fractions (from 1 to 35) from POPC/POPG vesicles mixed with HRPC solutions

The activity measurements on this suspension were carried out in presence and in absence of Triton X-100. As shown in *Table 4.5* there is no considerable enzymatic activity using empty vesicles mixed with HRPC solution.

For the slope value = $5.61\text{E-}05$, the correspondent HRPC concentration, from the calibration curve, is lower than 50 pM. When Triton X-100 was added the slope value increased ($2.17\text{E-}03$). Checking in the calibration curve made in presence of Triton X-100, the slope value could be attributed to 350 pM HRPC concentration. Considering the dilution factor 100x, the HRPC concentration in the pooled fraction was found 35 nM.

Table 4.5. Rate of ABTS^{•-} formation for POPC/POPG (9:1) LUVET₂₀₀ mixed with HRPC solution

	<i>dA414nm/dt</i>	<i>st. dev.</i>
a) POPC/POPG mixed with HRPC solution 100x diluted	5.61E-05	2.25E-06
b) Empty POPC/POPG mixed with HRPC solution 100x diluted + Triton X-100 0.1%	2.17E-03	2.52E-05

Enzymatic activity for pooled fractions of POPC/POPG LUVET₂₀₀ mixed with enzyme solution (a) and adding Triton X-100 (b). Each data point shown is the average from three measurements and the standard deviation is also indicated.

This point needed more investigation, because I still could not exclude the presence of HRPC bound to the vesicles surface. I repeated the assays using a new enzyme containing vesicle preparation, and I obtained the same results. I expected an interaction between cationic HRPC and negatively charged vesicles, so the presence of bound enzyme was not a surprise. However the increase of activity in presence of Triton X-100 suggests that the enzyme could be bound in inactive way; probably some changes in the tertiary structure after membrane binding could make the catalytic site unavailable for the reaction. This could explain the increase in activity after membrane disruption by Triton X-100. This is only a rough deduction, and more investigations are needed. A good strategy to understand the role of the negatively charged vesicles during the enzyme binding could be to make the same experiment using zwitterionic vesicles.

iv. Fourth controls

To understand the role of the negatively charged vesicles during enzyme entrapment I made the same experiments using zwitterionic vesicles.

I prepared 20 mM POPC vesicles 200 nm with entrapped HRPC solution 20 μ M in MES buffer (pH = 5). The suspension was purified by Sepharose 4B

column, applying 2 mL of the mixture. After turbidity measurements a volume of 6 mL was collected.

The activity assay conditions were unchanged, I used two different incubation time (0 and 5 min) during peptide interaction. The results are shown in *Table 4.6*.

Table 4.6. Rate of ABTS^{•-} formation to estimate release time depending from POPC vesicles with enzyme entrapped in four different systems

		<i>Incubation Time (min)</i>	
		<i>0'</i>	<i>5'</i>
1) POPC + HRPC entrapped 100x diluted	<i>dA414nm/dt</i>	8.51E-05	8.83E-05
	<i>st. dev.</i>	1.25E-5	1.87E-5
2) POPC + HRPC entrapped 2000x diluted + Triton X-100 0.1%	<i>dA414nm/dt</i>		5.12E-04
	<i>st. dev.</i>		7.82E-06
3) POPC + HRPC entrapped 100x diluted + ALY 4 μM	<i>dA414nm/dt</i>	2.11E-04	2.25E-04
	<i>st. dev.</i>	2.77E-05	1.01E-05
4) POPC + HRPC entrapped 100x diluted + azoALY 4 μM	<i>dA414nm/dt</i>	2.95E-04	3.00E-04
	<i>st. dev.</i>	6.58E-06	3.31E-05

Enzymatic activity time depending for POPC vesicles with HRPC entrapped 100x diluted (1), adding Triton X-100 2000x diluted (2), adding ALY (3) and adding azoALY (4). Each data point shown is the average from three measurements and the standard deviation is also indicated.

As shown in *Figure 4.21*, the enzymatic activity in the pooled fraction of POPC (dilution factor 100x) is very low, and checking in the calibration curve, the corresponding HRPC concentration was lower than 50 pM. Also, the

activity for this system was not time dependent, the slope value did not change for the three different incubation times. When I analyzed enzyme containing vesicles plus Triton X-100 0.1% I observed an increase in enzyme activity after 5 min of incubation. Checking in the calibration curve in presence of Triton X-100, there was a release of HRPC like 50 pM and considering a dilution factor 2000x, I can say that the concentration of entrapped enzyme should be around 100 nM.

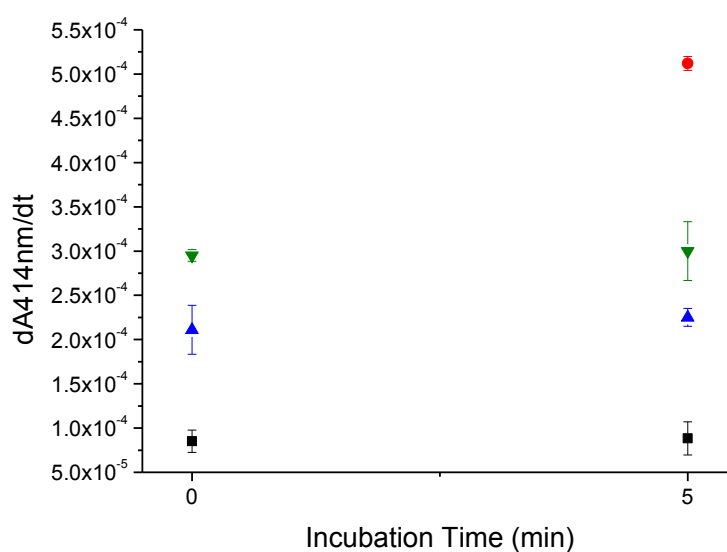


Figure 4.21. Enzymatic activity time depending for POPC vesicles with HRPC entrapped (■), adding Triton X-100 (●), adding ALY (▲) and adding azoALY (▼). Each data point shown is the average from three measurements and the standard deviation is indicated with a bar.

Analyzing the results with ALY peptide, I detected a very small increase in enzyme activity caused from HRPC release or substrate uptake, with a slope value constant at two measurement times, but lower than values reported in the calibration curve. So I could only suppose that the released enzyme concentration in the assay solution was lower than 50 pM, but I could not estimate the amount of HRPC released. The situation was not so much different using the modified peptide, the activity increase was not time

dependent but with values a bit higher than unmodified peptide. In the calibration curve it was possible to check only the slope value for 5 min of incubation and it corresponded to HRP concentration around 50 pM. Considering a dilution factor 100x, I could say that I had an increase in enzyme release or ABTS²⁻ uptake with an enzyme concentration in the pooled fraction of 5 nM.

I observed a lower enzyme entrapped in zwitterionic vesicles than negatively charged vesicles. In fact, comparing the values of concentration of enzyme leakage using Triton X-110 I observed that using zwitterionic vesicles the concentration of HRP release was 100 nM, while using negatively charged vesicles this value was 400 nM.

Consequently the enzyme release caused by azoALY and ALY was affected by the lower number of entrapped enzymes.

However last assays were repeated just once, so I don't have enough data to propose a hypothesis of mechanism of interaction. More investigations are needed to clarify the different membrane interaction, using different lipids and enzymes.

4.5.LUVETs characterization

Cryogenic transmission electron microscopy (cryo-TEM) is a tool for characterizing suspensions; it permits the direct visualization of vesicles and of eventually entrapped macromolecules. It allows the determination of the true size and of the number of lamellae of a vesicle, but it does not yield any quantitative information about the number of vesicles present in a suspension. Cryo-TEM observations were carried out in collaboration with Dr. Takashi Ishikawa at Paul Scherrer Institute (PSI), Switzerland. The suspensions (volume 5 μ L) were frozen (vitrified) in thin aqueous layers and examined at low temperature with transmission electron microscope (cryo-TEM).

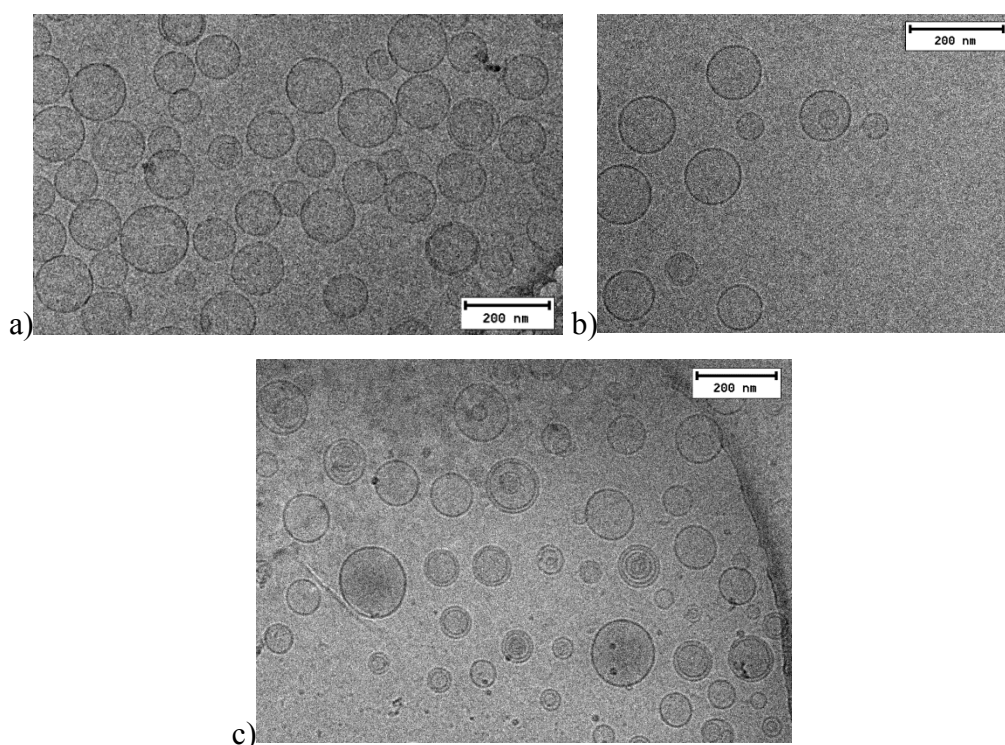


Figure 4.22. Cryo-TEM images of 10 mM LUVET₁₀₀ of POPC (a); 10 mM LUVET₁₀₀ POPC/POPG (b); LUVET₂₀₀ of POPC/POPG containing HRPC entrapped (c). The buffer used was MES pH = 5. Length of the bars = 200 nm.

As shown in *Figure 4.22*, there is a high percentage of unilamellar lipid vesicles of POPC and POPC/POPG, with uniform mean size around 110 nm. These results were confirmed by dynamic light scattering (DLS) measurements, which indicated a mean hydrodynamic diameter of 122 nm for POPC vesicles (mean polydispersity index = 0.08) and 108 nm for POPC/POPG vesicles (mean polydispersity index = 0.05). Each measurement (3 accumulations of 30 s) was repeated 3 times for reproducibility (See *Appendix-c*).

In contrast, enzyme containing vesicles have different size and lamellarity but I also see a lot of unilamellar vesicles with a size in the range of 200 nm.

4.5.1. Theoretical consideration

i. Number of enzyme per vesicle

By DLS measurements I measured enzyme containing POPC/POPG vesicle have an outer diameter of 148 nm (PDI = 0.092). The bilayer has a thickness of only about 3.7 nm [118] which corresponds, in first approximation, to about two times the length of an extended POPC molecule (I assumed the same length for POPC and POPG phospholipids). So I calculated the outer radius as $r_o = 74$ nm and the inner radius $r_i = 72$ nm.

Based on simple geometric considerations, one can calculate the approximate number of HRPC molecules present in the considered vesicles. The vesicles are considered as unilamellar phospholipids sphere, thus the internal volume for each vesicle is:

$$V = \frac{4}{3}\pi r_i^3 = \frac{4}{3}\pi 72^3 \text{ nm}^3 = 1562665 \text{ nm}^3 = 1.56 \times 10^{-18} \text{ L}$$

To prepare enzyme containing vesicles I used a HRPC solution 20 μM (20 $\mu\text{mol/L}$), therefore there are 12.04×10^{18} molecules of enzyme per liter. Assuming that the enzyme concentration is the same inside and outside the vesicles, I calculated the mean number of HRPC enzyme inside a vesicle with the following equation:

$$\text{HRPC num} = V_{\text{vesicle}} \cdot A \cdot [\text{HRPC}] \cong 19$$

Where A is the Avogadro number, $[\text{HRPC}]$ is the molar concentration of the enzyme, and V_{vesicle} is the average volume of the vesicles as obtained by DLS. Statistically, there is a defined number of enzymes per vesicles. Of course there will be vesicles with higher or lower number of enzyme entrapped, but the possibility to find empty vesicles should be low.

ii. Mean number of phospholipids molecules per vesicles

In the case of unilamellar vesicles with an outer diameter of 148 nm, it is possible to estimate the number of phospholipid molecules by simple geometrical consideration. I first need to calculate the total area of the vesicle including the inner layer area (inner radius $r_i = 72$ nm) and outer layer area (outer radius $r_o = 74$ nm), assuming a mean head group area of one POPC molecule of 0.72 nm^2 [119] and a bilayer thickness of 3.7 nm by the formula:

$$\text{Area total} = 4\pi r_i^2 + 4\pi r_o^2 = 134109 \text{ nm}^2$$

The number of phospholipids per vesicles is:

$$\text{number of lipids} = \frac{\text{Area total}}{\text{mean head group area}} = 1.86 \times 10^5 \text{ molecules}$$

This is certainly a rough estimation and the real situation in a curved bilayer is always asymmetric with different packing conditions (and mean surfactant head group areas) in the inner and outer layers [120].

Also, considering the low percentage of POPG in the vesicles and the similar structure of the two phospholipids, I approximated the mean head group area value of one POPC molecule to the same value for the POPG molecule [121].

iii. Number of vesicles in the pooled fractions

Considering 20 mM as initial phospholipids concentration and 2 mL as applied volume, I can roughly estimate the lipid concentration as 6.67 mM in the pooled fractions with a volume of 6 mL.

The approximated concentration of vesicles should be:

$$\text{Vesicles concentration} = \frac{\text{lipid concentration}}{\text{number of lipids}} = \frac{6.67 \text{ mM}}{1.86 \times 10^5} = 35.86 \text{ nM}$$

iv. Enzyme concentration

The theoretical concentration of enzyme in the pooled fractions is therefore:

$$\begin{aligned} [\text{HRPC}]_{\text{pooled fractions}} &= \text{vesicles concentration} \times \text{HRPC molecules per vesicle} \\ &= 35.86 \text{ nM} \times 19 \text{ molecules} = 681.34 \text{ nM} \end{aligned}$$

The theoretical considerations were made considering unilamellar vesicle of POPC with outer diameter of 148 nm. In conclusion, I assume that in the pooled fraction there is a lower possibility to find empty vesicles because the mean number of HRPC molecules per vesicle is around 19 molecules. Moreover, I expect that the maximum concentration of HRPC entrapped should be around 681 nM.

Enzyme release assays using Triton X-100 as detergent showed a concentration of entrapped enzyme around 400 nM. These experimental tests confirmed the accuracy and the applicability of the experimental method.

Chapter 5. Conclusion e discussion

The importance of AMPs in therapeutics is widely recognized. Understanding the role of the sequence of AMPs in their activity is important for their rational design as drugs. However, the most important chemical–physical features of a peptide that determine the antimicrobial activity are still not clear. The rapid increase in the number of AMPs demands a more efficient data registration and management method. The accuracy of prediction algorithms for AMPs heavily depends on the correctness and extent of information available in the training data sets used for the study.

For this reason, I collected structural properties and antimicrobial activity values, structural features and biological origin of antimicrobial peptides from published data. Moreover, the most relevant chemical physical properties have been calculated, like charge, hydrophobic moment, helicity, flexibility, isoelectric point, Boman and instability index, penetration capabilities, free energy of binding (ΔG) and the Molecular Lipophilicity Potential (MLP).

The outcome was YADAMP, a web database dedicated to antimicrobial peptides with detailed information. YADAMP is born to facilitate the access to important information on AMPs. I have given a particular attention to short α -helix peptides interacting with cell membranes. At the time of writing, the database contains 2525 manually annotated sequences extracted from other public databases and from scientific literature. YADAMP contains the highest number of active sequences with proven antimicrobial activity, permits a quick and easy search of peptides on the base of their activity (expressed as MIC against several bacterial strains) and of their structure to favor extensive QSAR analysis and the creation of activity models.

YADAMP is constantly updated by new sequences and new tools. Recently it has been improved with a BLAST tool that permits to find homologous

sequences, and with the 3-dimensional structures of peptides. Whereas possible the 3D structures have been retrieved from the protein databank. When the structure was not available, a guesstimate of the final folding was made by means of molecular dynamics.

A careful investigation of collected peptides permitted me to synthesize and insert modified amino acid into active AMP, maintaining the physical-chemical properties of AMP used as template. The modified amino acid named Fmoc-azoTyr was synthesized according to the classic scheme of diazocoupling reactions by adding azobenzene group as side chain of a tyrosine.

The preparation of azo-amino acids permitted to exploit the photochemical isomerization of the azobenzene moiety. This causes a photochemical change of the conformation of any peptide or protein having the modified amino acid inserted. In this way, this molecular switch could turn on or off antimicrobial activity of AMPs.

Our previous studies confirmed the antimicrobial and antifungal activity of azobenzene group. The modified peptide could have a broader spectrum of activity due at the azobenzene presence, and it could act as a prodrug, generating *in vivo* the antimicrobial azo compound.

Using YADAMP, I have selected an antimicrobial peptide as template for a new photoresponsive peptide. I have chosen a peptide, indicated as ALY. ALY is a short α -helix membrane active AMP with a tyrosine in the sequence to be replaced with Fmoc-azoTyr. ALY peptide and the modified peptide named azoALY have been synthesized with to the solid phase approach. The synthetic procedure performed was the same for both analogues, replacing tyrosine residue into active sequence by Fmoc-azoTyr.

To evaluate the difference in membrane permeability due to the introduction of the modified amino acid, I have performed studies of membrane permeability at the Swiss Federal Institute of Technology (ETH Zurich).

Calcein leakage assays showed that the modified amino acid introduced into active sequence increased the membrane permeability. At low concentrations (1 μM) during the first 15 min of exposure, the modified peptide azoALY causes a double release of calcein from a suspension of giant unilamellar vesicles formed by POPC/POPG (mixture 90:10 mol/mol) than the modified peptide at the same conditions. When high concentrations were used (50 μM), it was observed that azoALY had a faster effect on the membrane permeability than the natural peptide. This is a good motivation to continue, in the future, with the investigation of the azo-peptide membrane interaction using different kind of vesicles such as zwitterionic vesicles to understand the importance of the peptide charge and to clarify the influence of the azobenzene group.

To estimate the different interaction of unmodified and modified antimicrobial peptide, I have used a suspension of POPC/POPG (mixture 90:10 mol/mol) of large unilamellar vesicles.

Vesicles that contain HRP enzyme were prepared by mechanical extrusion and measurements of enzyme leakage were performed, after peptide interaction. In this assay the membrane permeability was associated with an increase in enzyme activity.

From theoretical analysis, I evaluated the accuracy and the reproducibility of the experimental method. I have calculated the theoretical and the experimental entrapment and release of the enzyme and I demonstrated the applicability of the method.

Preliminary results of enzyme leakage showed that using a suspension of large unilamellar vesicles with HRP entrapped, a solution of azoALY 4 μM caused a higher and time depending perturbation effect on LUVET₂₀₀ containing negatively charged lipids than the unmodified peptide.

In conclusion, the new photoresponsive peptide azoALY increased membrane permeability in GUVs as confirmed by calcein release assays and showed membrane perturbation with time-dependence enzyme leakage from LUVs.

More investigations are still needed to clarify the mechanism of pore formation.

Part II.

*Development of new antimicrobial and antifungal
compounds*

Chapter 6. Small azobenzene derivatives active against bacteria and fungi

6.1. Introduction

Antibacterial therapy is a powerful tool for the treatment of several diseases, and is a keystone of modern medicinal practice. Infections by pathogenic microorganisms are of great concern in many fields, particularly in medical devices, hospital surfaces, dental restoration and surgery equipment, health care products and hygienic applications, water purification systems, textiles, food packaging and storage. Generally, infections are combated with antimicrobial agents. However some bacteria, mutating their genes, have become resistant to common antibiotics and this makes difficult their elimination. For instance, *Pseudomonas aeruginosa* bacterium is a common opportunistic pathogen associated with a variety of infections including hospital-acquired pneumonia and is increasingly resistant to many antibiotics [122]. *Staphylococcus aureus* is a bacterium that commonly colonizes human skin and mucosa without causing severe problems. However, serious illnesses that range from mild to life-threatening can be developed if the bacteria enter the body such as abscesses infections, heart valves infections or endocarditis or bloodstream infection. Some of *S. aureus* are resistant to the antibiotic methicillin, methicillin-resistant *S. aureus*, and often require different types of antibiotic to treat them [123].

Fungal infections in humans can range from serious life-threatening diseases to common mild superficial infections such as athlete's foot and candidiasis or thrush (both vaginal and oral).

Therefore, the increased resistance of microorganisms to the currently used antimicrobials has led to the evaluation of other agents that might have antimicrobial activity.

Plants in their natural environment are challenged by many potential damaging organisms including viruses, nematodes, bacteria, fungi and insects. In many plant species one of the most efficient responses to combat attacking microbes is the rapid *de novo* synthesis of antimicrobial low molecular weight phytoalexins that accumulate rapidly in areas of pathogen infection.

Amongst these substances, stilbene phytoalexins (from the *Vitaceae* and other plant families) have been objects of extended investigations over the past decade, because they have been shown to possess biological activity against a wide range of plant and human pathogens.

Resveratrol (3,4',5-trihydroxystilbene) is a phytoalexin commonly found in grapes, grape products, wine, peanuts, cranberries, strawberry, and some other botanical sources (*Figure 6.1*).

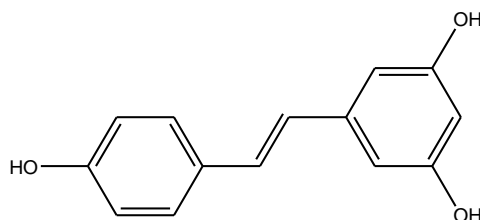


Figure 6.1. Structure of Resveratrol

Since the discovery of the resveratrol in 1940, several papers were published annually elucidating the benefits of this molecule on human health. Resveratrol can prevent or slow the progression of several diseases, including cardiovascular disease [124], carcinogenic [125] and neurodegenerative [126] prevent many aging processes and increase longevity as well [127]. Resveratrol moreover has anti-inflammatory [128], antioxidant [129] and antimicrobial properties [130].

The relationship between compound structure and antimicrobial activity has been investigated, those studies showed that the core with three hydroxyphenyl groups, found in many phytoalexins, might be important for antibacterial activity [131]. This indicated that the number of hydroxyl groups might be essential for antimicrobial activity of phenolic compounds.

Recent studies suggest a probable mechanism of action in which resveratrol and related polyphenols such as quercetin and piceatannol, inhibit the F1-ATPase portion from bovine heart mitochondria [132]. ATP synthase is the central enzyme in energy conversion in mitochondria, chloroplasts and bacteria and so it is essential for the living organism. The binding site is a hydrophobic pocket between the C-terminal tip of the γ -subunit and the β -subunit of the enzyme. The inhibitors probably prevent the enzymatic activity by blocking the rotation of the γ -subunit.

Stilbenes derivatives display only moderate antimicrobial effects, and they are usually toxic compounds. Nevertheless, stilbene-based compounds may be a useful lead structure for the chemical synthesis of new antimicrobial agents.

The goal of this work was to design molecules with similar structures to those stilbenes, but higher antimicrobial activity and low toxicity.

I considered the azobenzenes as a class of structural analogues of stilbenes having high structural similarity with stilbenes. Azo is the prefix indicating the group $-N=N-$ and in the azobenzene is a compound formed of two phenyl rings linked by azo solid bond. Though azobenzenes have been widely studied as dyes or photoresponsive materials, but very little is reported about their potential antimicrobial activity.

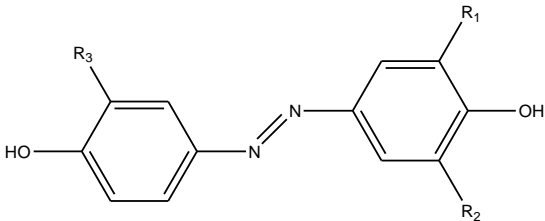
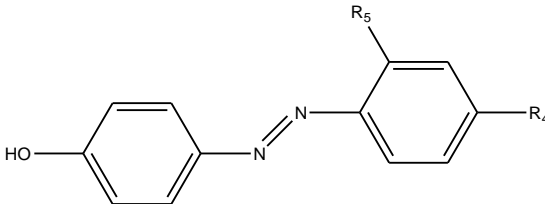
To design new azo compounds with potential antimicrobial activity, I carried out computational studies to predict the potential toxicity of a large set of azo molecules. I selected and then synthesized several molecules with lowest *in silico* toxicity values [86]. Synthesized molecules were thermal and optical characterized and finally microbiologically tested.

6.2. *In silico* screening

Using Accelrys Material Studio I built the library of azo compound analogues. I selected 18 substituents, chosen mainly for the ease of synthesis, to be linked to different positions on the subgroups AZO_A and AZO_B. The scaffold AZO_A allows three positions (R_1 , R_2 , and R_3) where the 18 substituents can be covalently linked and the possible combinations are $18^3 = 5832$. The scaffold AZO_B permits only two positions (R_4 and R_5) and in this case the possible combinations are $18^2 = 324$. The number of molecules that have been prepared for toxicity screening is, therefore, 6156. The 6156 considered azobenzenes are listed in *Table 6.1*.

I employed the *in silico* toxicity tool ADMET from Accelrys [133], to assess the potential toxicity of 6156 azo compounds within an organism. The ADMET protocols contain published models that you can use to compute and analyze Absorption, Distribution, Metabolism, Excretion, and Toxicity (ADMET) properties. For each molecule I calculated the aqueous solubility [134], the blood-brain penetration after oral administration [135], the cytochrome P450 2D6 inhibition [136], and the potential liver toxicity [137].

Table 6.1. Azobenzene compounds

<i>Base name</i>	<i>Scaffold</i>	<i>R₁, R₂, R₃, R₄, R₅</i>	<i>Number of molecules</i>
AZO_A		Br CH ₂ CH=CH ₂ CH ₂ CH ₂ CH ₃ CH ₂ CH ₃ CH ₂ OH CH ₂ SH	5832
AZO_B		CH ₃ Cl F H I N(CH ₂ CH ₃) ₂ N(CH ₃) ₂ NH ₂ OCH ₃ OH SCH ₃ SH	324

A total of 6156 different azobenzene analogues have been considered for ADMET parameter prediction. Column 3 shows the substituents taken into account. For the scaffold AZO_A, three positions, R₁, R₂, and R₃, are free to change; for the scaffold AZO_B there are only two positions, R₄ and R₅, free to change.

The aqueous solubility was estimated using the Cheng and Merz predictive model [134]. This model uses linear regression to predict the solubility of each compound in water at 25 °C. It was generated using a dataset containing 775 compounds (molecular weight between 50 and 800 g/mol⁻¹). The training set compounds cover numerous classes, including alkanes, alkenes, alkynes, halogens, amines, alcohols, *N*-containing compounds, ketones, aldehydes, organic acids, etc. At the end of the calculation, I chose molecules with solubility level between -5 and -3.5 that means a good solubility in water.

The BBB model (blood brain barrier) [135] predicts blood-brain penetration after oral administration; this model contains a quantitative linear regression model for the prediction of blood-brain penetration. The regression is based on 2D polar surface area (PSA_2D) and the solubility index AlogP98. The training set lies entirely within the 99% confidence ellipse. BBB values are the base 10 logarithm of the ratio (brain concentration)/(blood concentration). They were derived from over 800 compounds that are known to enter the CNS after oral administration. Therefore, I restricted the synthesis to the compounds with the lowest ratio.

The cytochrome P450 2D6 model predicts CYP2D6 enzyme inhibition using 2D chemical structure of 100 structurally diverse compounds with known CYP2D6 inhibition constants as input [136]. The CYP2D6 score is the sum of the predicted values (0 and 1) from all individual trees that comprise the ensemble recursive partitioning model, divided by the total number of trees in that model. The model classifies compounds as either 0 or 1 for non-inhibitor or inhibitor and provides an average-class-value estimate of confidence. I have restricted my attention to the molecules having smaller values.

The computational model for predicting potential liver toxicity of a compound was reported by Cheng and Dixon [137]; the model was developed from available literature data of 382 compounds known to exhibit liver toxicity (i.e., positive dose-dependent hepatocellular, cholestatic, neoplastic, etc.), or trigger

dose-related elevated aminotransferase levels in more than 10% of human population. The model generates hepatotoxicity values in the range (0, 1), and, almost all compounds exhibit the risk of toxicity. I limited the synthesis to the compounds having the lowest hepatotoxicity values.

The models were calculated for the 6156 molecules and the results were plotted in *Figure 6.2* in which the distribution of properties is evident using a multidimensional representation.

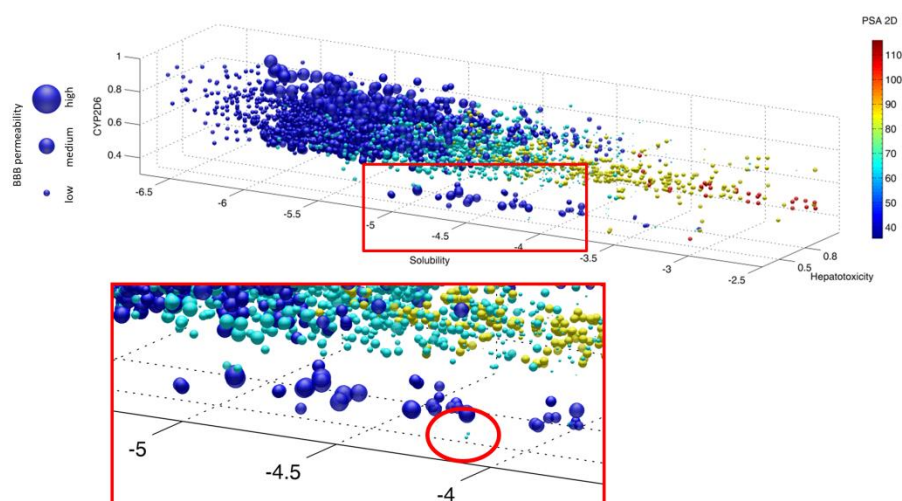


Figure 6.2. 5D plot of ADMET calculation. The solubility AlogP98, the inhibition of cytochrome D6 and the hepatotoxicity are represented on the orthogonal axes. The PSA 2D is color mapped onto the spheres and the probability to cross the blood-brain barrier is indicated with the size of the spheres. The square box represents the optimal subset of the 6156 molecules of *Table 6.2*. The best candidates are indicated within the small round box.

The subset that promised less toxicity effect is indicated within a large red box. The 7 best candidates listed in *Table 6.2* are all inside the red box. In particular, the two small cyan spheres (corresponding to A2 and A4 in *Table 6.2*) inside the red circle, exhibit the best overall indices. Unlike the remaining azobenzenes, that show extremely high probability of hepatotoxicity, the molecules of *Table 6.2* have probability of being nontoxic.

Table 6.2. ADMET parameters of the seven synthesized compounds

<i>Molecule</i>	<i>ID^a</i>	<i>Solubility^b</i>	<i>Hepatotoxicity</i>	<i>CYP2D6^c</i>	<i>PSA_2D^d</i>	<i>BBB^e</i>
A1	1144	-4.212	0.596	0.387	64.277	0.268
A2	496	-4.127	0.589	0.395	64.277	0.289
A3	820	-4.843	0.655	0.643	64.277	0.409
A4	1972	-5.001	0.655	0.712	64.277	0.439
A5	2062	-4.683	0.668	0.792	64.277	0.278
B10	6064	-3.899	0.556	0.861	67.631	0.190
B11	6046	-4.357	0.558	0.653	67.631	-0.026

a) molecule identification number; b) Solubility is the AlogP98; c) cytochrome P450 2D6 inhibition prediction; d) fast polar surface area; e) blood-brain barrier penetration coefficient. The values of hepatotoxicity and CYP2D6 fall in the range (0, 1). Values close to 0 correspond to low probability to cause dose-dependent toxicity against liver and cytochromes respectively. Values of BBB are the base 10 logarithm of the ratio (brain concentration)/(blood concentration).

6.3. Azo compounds synthesis

The majority of azobenzenes are obtained by coupling of diazonium salts with activated aromatic compounds. The methodology is based on the initial diazotization of an aromatic primary amine at low temperature, which then reacts with an electron rich aromatic nucleophile such as substituted arenes having electron donor groups like amine or hydroxyl, to give azobenzenes. Normally, such a substitution reaction takes place at the *para* position to the electron donor group on the activated aromatic ring, acting as a nucleophile. When this position is already occupied, the substitution occurs in the *ortho* position.

This reaction is very pH dependent. In accordance with the mechanism shown in *Figure 6.3*, for the formation of diazonium salt from a primary amine, acid is necessary to liberate *in situ* nitrous acid from NaNO₂. Further protonation and H₂O elimination provides the nitrosating agent (+N=O), whose reaction

with the amine leads to the *N*-nitroso derivative **5** a tautomer of the diazohydroxide **6**. A second protonation and H₂O elimination affords the diazonium salt **1** stabilized by resonance.

Regarding the reactivity of the starting materials, phenols have to react in the ionized form to undergo coupling because the neutral species are not sufficiently nucleophilic. In this case, moderately alkaline solutions are essential since the diazonium salt evolves into a diazohydroxide in the presence of a base, thus inhibiting the coupling. Therefore, the coupling of phenols has to be done in mild basic media at controlled pH, while the aromatic amines should react in weak acid medium to prevent *N*-coupling without reducing the nucleophilicity of the nitrogen that will be protonated in strong acid media.

After the diazonium salt is formed, an electrophilic aromatic substitution of the phenol with the electrophilic nitrogen of the diazonium salt.

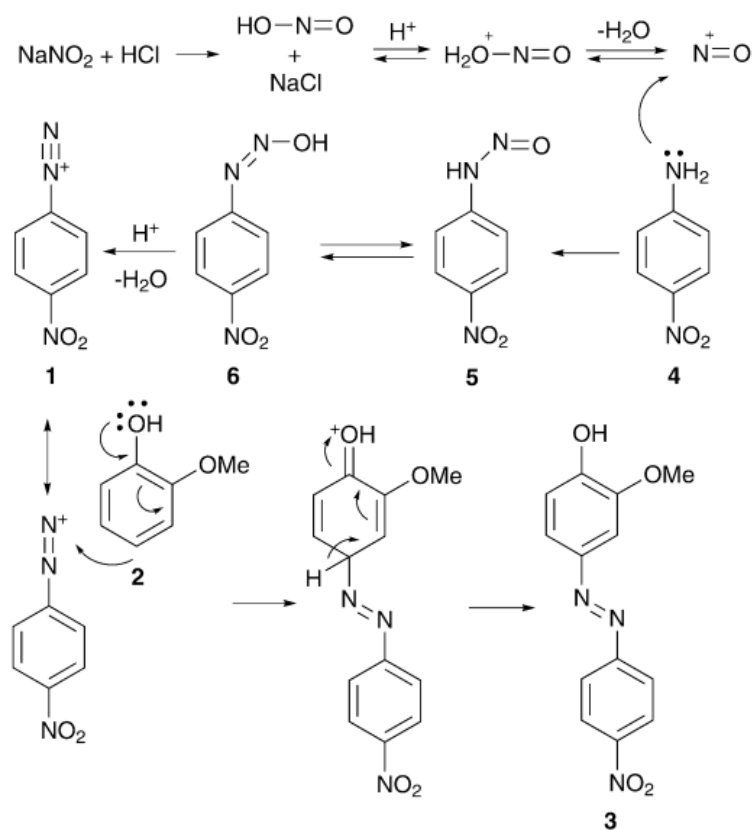
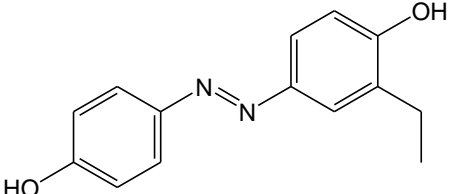
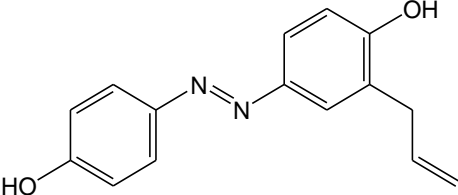
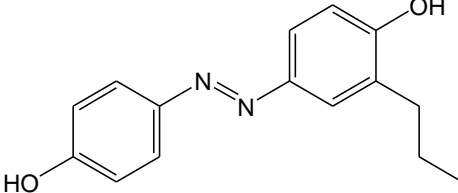
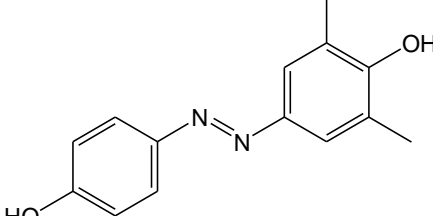
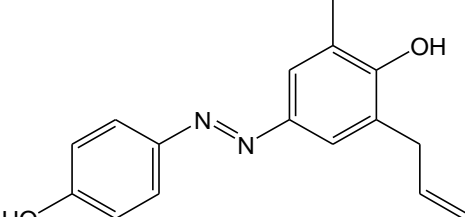
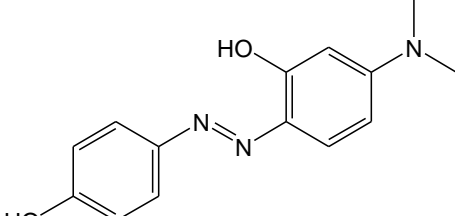
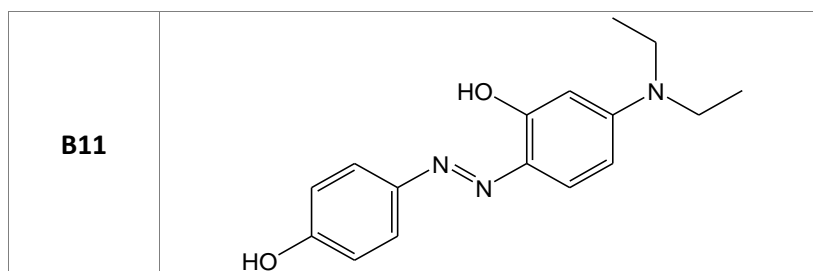


Figure 6.3. Scheme azo coupling reaction [138]

I have synthesized the molecules with the lowest *in silico* toxicity; their structure is given in Table 6.3.

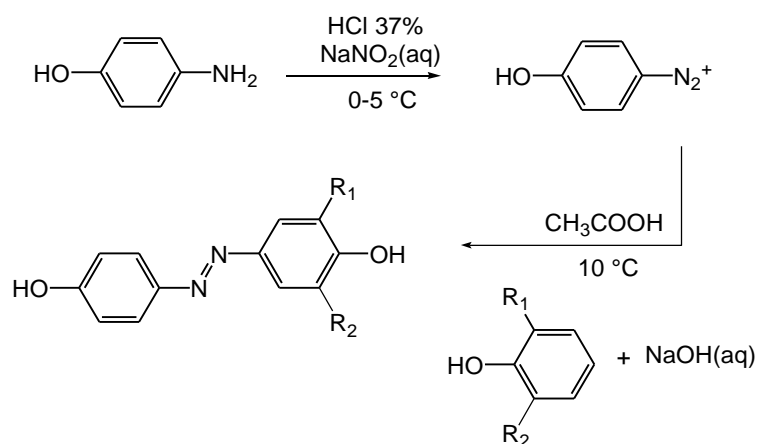
Table 6.3. Potential low toxic azo compounds synthesized

Name	Structure
A1	
A2	
A3	
A4	
A5	
B10	



6.3.1. Synthesis of A1-A5 molecules

Azo compounds A1-A5 were synthesized according to the classic scheme of diazocoupling reactions, as illustrated in *Figure 6.4*.



	R_1	R_2
A1	CH ₂ CH ₃	H
A2	CH ₂ CH=CH ₂	H
A3	CH ₂ CH ₂ CH ₃	H
A4	CH ₃	CH ₃
A5	CH ₃	CH ₂ CH=CH ₂

Figure 6.4. Synthesis scheme of azo compounds A1-A5

The procedure was the following: 2.00 g of 4-aminophenol (0.0183 mol) were suspended in a solution containing 16 mL of water and 4 mL of HCl 37%

(w/w). The solution was cooled at 0-5 °C in a water-ice bath. A solution of 1.39 g of sodium nitrite (0.0202 mol) dissolved in 4 mL of water was added drop-wise, obtaining a suspension of the diazonium salt (solution A). Separately, a solution containing 1.68 g of NaOH (0.0420 mol) in 16 mL of water with 0.0183 mol of the proper phenol (depending on A1-A5) was prepared (solution B).

Solution A was added drop-wise to solution B, under stirring at 12 °C. The system was left reacting for 20 min. Then the final solution was slowly added to 40 mL of an acid solution (50 mL of water and 4 mL of acetic acid), and then stirred for 30 min at 15 °C. A dark red precipitate of the azo compound formed. The crude precipitate was filtered and dried under vacuum. Yields ranged between 30 and 40%.

a. 4'-hydroxy-(4-hydroxy-3-ethyl)-azobenzene (A1)

4-aminophenol and 2-ethylphenol were used as starting reagents. The crude product was extracted, crystallized from boiling n-octane (500 mL) and dried under vacuum at 70 °C. Final crystallization from water/ethanol (10:1) gave pure A1 as gold yellow crystalline material.

¹H NMR (DMSO-d₆): δ (ppm) = 7.58 (m, 4H); 6.92 (t, 3H); 2.62 (m, 2H); 1.19 (t, 3H).

b. 4'-hydroxy-(4-hydroxy-3-allyl)-azobenzene (A2)

4-aminophenol and 2-allylphenol were used as starting reagents. The crude product was extracted and crystallized from boiling n-octane (500 mL) and dried. Final crystallization from water/ethanol (10:1) gave pure A2 as red-orange crystalline material.

¹H NMR (DMSO-d₆): δ (ppm) = 7.71 (d, 2H); 7.59 (s, 2H); 6.92 (m, 3H); 5.99 (m, 1H); 5.08 (t, 2H); 3.37 (m, 2H).

c. 4'-hydroxy-(4-hydroxy-3-propyl)-azobenzene (A3)

4-aminophenol and 2-propylphenol were used as starting reagents. The crude product was extracted and crystallized from boiling n-octane (100 mL) and dried. Final crystallization from boiling water/ethanol (3:1) gave pure A3 as gold yellow crystalline material.

^1H NMR (DMSO- d_6): δ (ppm) = 7.72 (d, 2H), 7.58 (m, 2H), 6.93 (t, 3H), 2.57 (m, 2H), 1.61 (m, 2H), 0.94 (t, 3H).

d. 4'-hydroxy-(4-hydroxy-3,5-dimethyl)-azobenzene (A4)

4-aminophenol and 2,6-dimethylphenol were used as starting reagents. The crude product was extracted and crystallized from boiling n-octane (100 mL) and dried. Final crystallization from boiling water/ethanol (3:1) gave pure A4 as orange crystalline material.

^1H NMR (DMSO- d_6): δ (ppm) = 7.72 (d, 2H), 7.48 (s, 2H), 6.91 (d, 2H), 2.26 (s, 6H).

e. 4'-hydroxy-(4-hydroxy-3-methyl-5-allyl)-azobenzene (A5)

4-aminophenol and 2-allyl-6-methylphenol were used as starting reagents. The crude product was extracted and crystallized from boiling n-octane (100 mL) and dried. After crystallization from boiling water/ethanol (3:1), final crystallization from boiling water gave pure A5 as red crystalline material.

^1H NMR (DMSO- d_6): δ (ppm) = δ 7.72 (d, 2H), 7.49 (d, 2H), 6.91 (d, 2H), 6.00 (t, 1H), 5.10 (t, 2H), 2.28 (s, 3H).

6.3.2. Synthesis of B10-B11 molecules

Azo compounds B10 and B11 were synthesized according to the classic scheme of diazocoupling reactions, as illustrated in *Figure 6.5*.

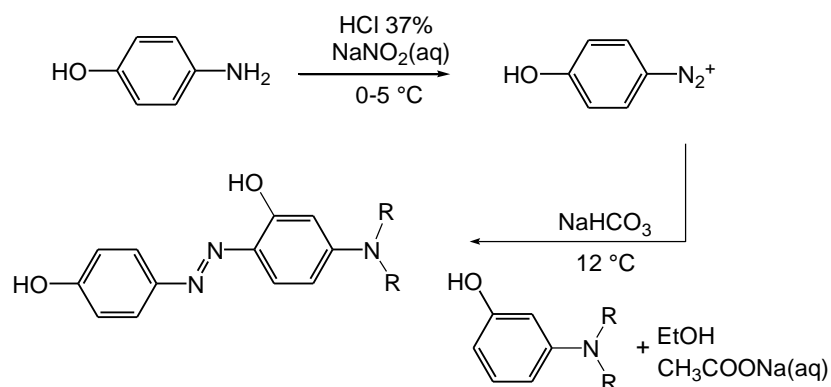


Figure 6.5. Synthesis scheme of azo compounds B10 and B11, with R as CH₃ for B10 and CH₂CH₃ for B11

The procedure was the following: 5.00 g of 4-aminophenol (0.0458 mol) were suspended in a solution containing 40 mL of water and 10 mL of HCl 37% (w/w). The solution was cooled at 0-5 °C in a water-ice bath. A solution of 3.49 g of sodium nitrite (0.0505 mol) dissolved in 10 mL of water was added drop-wise, obtaining a suspension of the diazonium salt (solution A). Separately, a solution B was prepared mixing a solution containing 7.5 g sodium acetate in 100 mL water (pH = 7) with a solution of 6.29 g 3-(dimethylamino)phenol (0.0459 mol) for B10 and 7.57 g 3-diethylaminophenol for B11 in 75 mL ethanol 96%. Solution A was added drop-wise to solution B, under stirring at 12 °C. The system was left reacting for 20 min. A basic solution of NaHCO₃ was added to reach pH = 6 and a dark brown precipitate of the azo compound was formed. The crude precipitate was filtered and dried under vacuum. Yields ranged between 50 and 60%.

a. *4'-hydroxy-(2-hydroxy-4-dimethylamino)-azobenzene (B10)*

4-aminophenol and 3-(dimethylamino)phenol were used as starting reagents. The crude product was solubilized in glacial acetic acid (few mL) and 1 L of a saturated sodium chloride solution was added. The system was left under stirring at 50 °C for 1 h (pH = 4). The crude precipitate was washed more time with water to eliminate salts residues and dried under vacuum.

¹H NMR (300 MHz, DMSO-d₆) δ = 7.65 (d, 2H), 7.55 (d, 1H), 6.88 (d, 2H), 6.48 (d, 1H), 6.12 (s, 1H), 3.05 (s, 6H).

b. *4'-hydroxy-(2-hydroxy-4-diethylamino)-azobenzene (B11)*

4-aminophenol and 3-(diethylamino)phenol were used as starting reagents. I used the same purification procedure used for B10.

¹H NMR (300 MHz, DMSO) δ = 7.63 (d, 2H), 7.53 (d, 1H), 6.89 (d, 2H), 6.44 (d, 1H), 6.09 (s, 1H), 3.44 (m, 4H), 1.15 (t, 6H).

After purification I obtained colored crystalline compounds. The proton resonance data for A1-A5 and B10-B11 were in agreement with the expected values; all spectra are reported in *Appendix-d* section. ¹H NMR spectra were recorded with a Bruker DRX/400 Spectrometer. Chemical shifts are reported relative to the residual solvent peak (dimethylsulfoxide-d₆: H = 2.50 ppm).

I performed polarized optical microscopy for all molecules using a Jenapol microscope fitted with a Linkam THMS 600 hot stage. The compounds A1, A2 and A3 showed the same needle crystalline habitus, in *Figure 6.6* is given A3 image as example. A4 and A5 compounds took on blade-like shape, slender and flattened; always in *Figure 6.6* is given A4 image as example. Instead B10 and B11 compounds looked as brown microcrystalline powder.

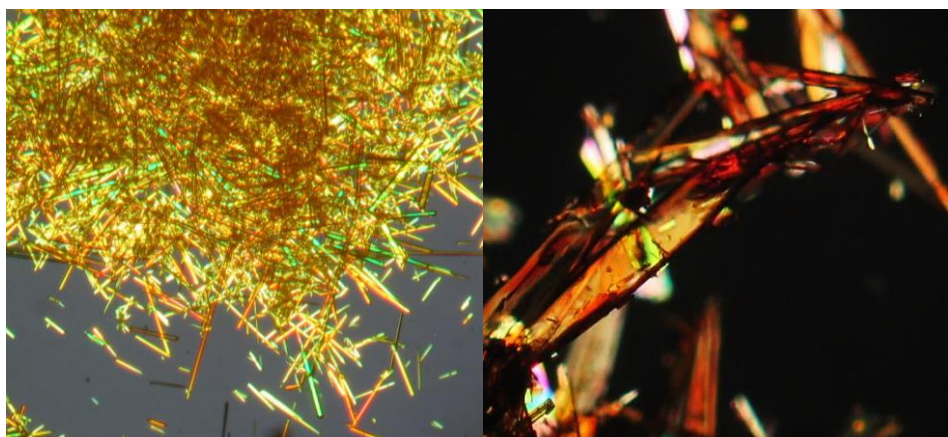


Figure 6.6. Polarized optical microscopy images 5x of A3 on the left and A4 on the right.

I used X-Ray powder diffraction on powders sample for structural characterization of materials. The measurements were recorded on a flat film camera Ni-filtered Cu-K α radiation. The Fujifilm MS 2025 imaging plate and a Fuji Bioimaging analyzer System, model BAS-1800, were used for digitizing the diffraction patterns. Ideally, every possible crystalline orientation is represented very equally in a powdered sample, when the scattered radiation is collected on a flat plate detector, the rotational averaging leads to smooth diffraction rings around the beam axis. According to X-Ray diffraction analysis azo compounds, as obtained from the synthesis after purification, are crystalline materials. In *Figure 6.7* are given the diffractograms of synthesized compounds. A1, A2 and A3 samples were composed of crystals with high dimension; in fact the resulting diffractograms were formed from many points that took a ring shape. Instead A4 and A5 powders were formed from many crystals with small dimension, in fact the diffractograms were formed from many rings with a continue lines. In the diffractograms of B10 and was possible to observe many reflections, index of the presence of a high number of small crystals.

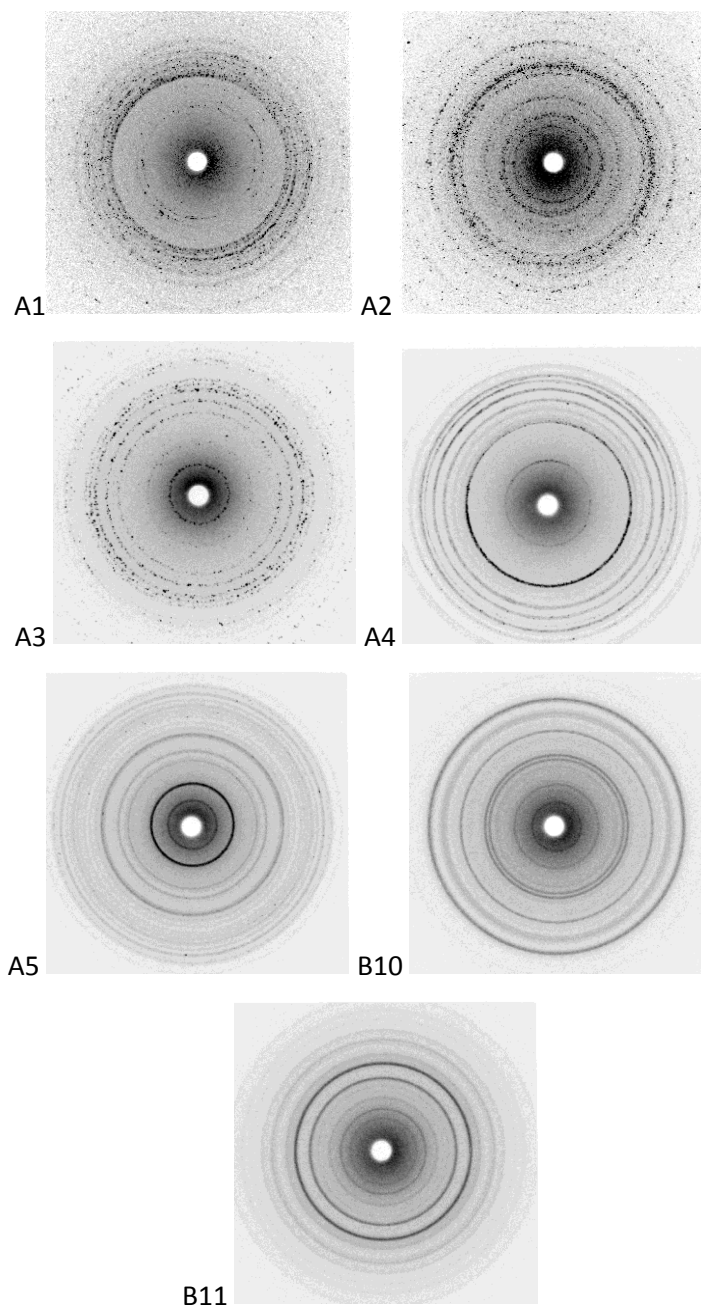


Figure 6.7. X-Ray diffractograms of synthesized compounds

6.4. Thermal and optical properties

Thermodynamic properties of synthesized azo compounds are given in *Table 6.4*.

The thermogravimetric analysis (TGA) showed that compounds presented initial decomposition temperatures expressed as T_d (5% weight loss) around 200 °C. This stability indicates the possibility to incorporate the azo compounds in a large number of commercial polymers matrices that undergo high temperature melt compounding processing, in order to obtain biomedical devices and food packaging films. The TGA thermograms are reported in *Appendix-e* section. Thermal measurements were performed by a DSC-7 Perkin Elmer calorimeter under nitrogen flow at 10 °C/min rate.

Table 6.4. Thermal characterization

Compounds	Thermal characterization				
	T_m (°C)	ΔH_m (J/g)	T_c (°C)	ΔH_c (J/g)	T_d (°C)
A1	156.3	139.0	100.3	89.6	200.3
A2	151.0	112.0	103.6	98.3	204.9
A3	173.3	97.9	135.9	88.7	198.3
A4	174.3	110.0	112.6	13.7	178.3
A5	105.3	82.5	-	-	203.4
B10	199.0	56.6	-	-	199.8
B11	158.3	26.4	-	-	199.9

T_m = melting temperature, from DSC analysis, 10 °C/min, nitrogen flow;

T_c = crystallization temperature, from DSC cooling run;

T_d = temperature of 5% of weight loss in the TGA trace, 10 °C/min, nitrogen flow.

Instrument error ± 0.5 °C.

$\Delta H_m/\Delta H_c$ = melting/crystallization enthalpy, evaluated by integration of the peak.

Experimental error $\pm 5\%$.

From DSC analysis I studied the thermal behavior of synthesized compounds; all thermograms are reported in *Appendix-f*.

A1, A2 and A4 showed a sharp melting peak in the first heating run and a crystallization peak in the cooling run. When heated in the second run, they showed the same melting peak as in the first run. In particular, A4 showed also a solid to solid transition in the first heating run at 110.3 °C ($\Delta_{k-k} = 109.8$ J/g) and, after cooling, it showed a second crystallization during the second heating run at 105.7 °C ($\Delta H_{c2} = 30.1$ J/g), as confirmed by polarized optical microscopy observation.

A3 had a different behavior: in the first heating run it showed a solid to solid transition, confirmed by the observation at the polarized optical microscope ($T_{k-k} = 151.6$ °C, $\Delta_{k-k} = 7.5$ J/g); this was followed by the melting of this new solid form at 173.3 °C (see *Table 6.4*). In the subsequent cooling run the molecule crystallized at 135.9 °C in a different crystalline form, which melts at 182.3 °C in the second heating run. This behavior was confirmed by polarized optical microscopy observation.

A5 showed only the first melting peak and it is not able to crystallize from the melt; this is probably due to its asymmetric structure, which comprises a short methyl group and a longer allyl group on the same ring.

B10 and B11 showed the first melting peak and immediately after their decomposition starts.

UV absorption spectra of the samples were recorded at 25 °C on a Perkin-Elmer Lambda 19 spectrophotometer. The spectral region 650-240 nm was investigated using cell path length of 1 cm. Azobenzene chromophore concentration of about 3.0×10^{-5} mol L⁻¹ was used.

The UV-visible spectra for A1-A5, made in acetonitrile solution, are qualitatively independent on the number and length of flexible aliphatic segments (methyl, ethyl, allyl) attached to the azobenzene core, and only depend on the active azo-containing unit, which is the same for all compounds. The UV absorption spectra of A1-A5 in *trans* configuration, in

the 240-650 nm region, showed two bands centered around 240 and 360 nm, related respectively to the $\pi \rightarrow \pi^*$ and $n \rightarrow \pi^*$ electronic transitions of the azobenzene chromophore [139]. The UV-visible spectra for B10-B11, made in ethanol solution, are qualitatively depending on the active azo-containing unit. The UV absorption spectra showed the typical absorption bands of the electronic transitions of the azobenzene chromophore. In particular B10 and B11 showed an absorption in the range 400-500 attributed to an extensive π electron delocalization due to amino group attached to the azobenzene core. This bathochromic effect causes a shift in absorption from 340 for A1-A5 analogues to 450 for B10 and B11 structures [140].

UV-Vis data are given in *Table 6.5* and all spectra are reported in *Appendix-g*.

Table 6.5. Optical characterization

Molecule	Optical characterization	
	λ_{\max} (nm)	ϵ_{\max} (L mol ⁻¹ cm ⁻¹)
A1	357	29500
A2	358	30300
A3	358	28700
A4	359	30500
A5	359	30100
B10	449	22100
B11	458	49100

λ_{\max} = wavelength at the principal absorption maximum,

ϵ_{\max} = molar extinction coefficient at absorption maximum.

6.5. Antimicrobial activity

6.5.1. Bacterial strains and minimum inhibitory concentrations (MICs)

The *in vitro* minimal inhibitory concentrations (MICs) of each compound was determined against *Candida albicans* SC5314 by the micro-broth dilution method in 96-well microtest plates according to the guidelines suggested by the Clinical and Laboratory Standards Institute (CLSI) [141] using three separate plates each containing the same batch of azo compounds.

Microtiter plates containing 100 μL of two-fold serial dilutions of azo compounds in RPMI 1640 medium were inoculated with 100 μL of cells containing 2.5×10^3 yeast/mL and incubated at 35 °C for 24 h. The resulting MICs were visually read as the lowest concentration of compound causing an absence of growth (optically clear) in comparison to the drug-free growth control.

For *S. aureus* A170 (kindly provided by Prof. R. Capparelli from the University of Naples, Italy), *L. monocytogenes*, *S. typhimurium*, *P. aeruginosa* ATCC-27853, MIC values of each compound were determined by the serial broth microdilution method as reported by Patton [142]. Therefore, flat-bottom polystyrene microtiter plates containing 100 μL of two-fold serial dilutions (six replicates per dilution) of azo compounds were inoculated with 100 μL of $\sim 5 \times 10^5$ CFU/mL of each bacterium grown in Mueller–Hinton broth 2. The controls were the wells contained broth only (negative control) and bacteria and broth (positive control).

Plates were incubated at 37 °C with shaking at 160 rpm for 24 h. Data were analyzed according to Patton et al. [142]. The optical density (OD) was determined just before the incubation (T_0) and again after 24 h incubation (T_{24}) at 600 nm. The OD for each replicate at T_0 was subtracted from the OD for each replicate at T_{24} . The adjusted OD of each control well was then

assigned a value of 100% growth. The MIC is reported as the lowest concentration of azo compounds which results in 100% inhibition of growth.

6.5.2. *Candida morphological analysis*

Hyphal growth of *Candida* treated cells was induced using RPMI 1640 medium. Stationary yeast cells were inoculated into a fresh pre-warmed medium at a density of 6×10^6 cells/mL in a flat-bottom 96 well microtiter plates. Different concentrations of azo compounds (ranging from 1 to 50 $\mu\text{g/mL}$), were added to each well. After incubation at 37 °C for 24 h, each microtiter plate was examined using an inverted microscope to monitor phenotypic modification and hyphae formation.

6.5.3. *Biofilms analysis*

C. albicans cells were grown for 24 h at 28 °C in YPD broth. These were washed twice with sterile and re-suspended in RPMI 1640 supplemented with MOPS buffer at 10^6 cells/mL. The cell suspension (200 μL) was seeded in pre-sterilized, polystyrene flat-bottom 96-well plates and incubated for 24 h at 37 °C. After biofilm formation, 20 $\mu\text{g/mL}$ of azo compounds were added to each well and incubated for 8 h at 37 °C. Afterwards, the medium was aspirated, and non-adherent cells were removed by washing biofilms 3 times with 200 μL of sterile PBS. Biofilms were quantified by the 2,3-bis (2-methoxy-4-nitro-5-sulfophenyl)-2H-tetrazolium-5-carboxanilide (XTT) reduction assay [143]. Briefly, XTT was dissolved in PBS at a final concentration of 1 mg/mL. The solution was filter-sterilized using a 0.22 μm -pore-size filter and stored at -70 °C until required. Menadione solution (0.4 mM) was also prepared and filtered. Before each assay, XTT solution was thawed and mixed with menadione solution at a volume ratio of 20:1. The XTT-menadione solution (250 μL) was then added to each well. The microtiter plates were then incubated in the dark for 1 h at 37 °C. Following incubation, 250 μL of the

XTT-menadione solution was recovered and centrifuged (to eliminate interference of cells with colorimetric readings); 100 μL of the solution was transferred to new wells, and the color change resulting from XTT reduction was measured at 490 nm with a microtiter plate reader (LAB system multiscan EX). Each assay was performed 3 times.

A similar protocol has been used for the inhibition of *Candida* biofilm by the azo compounds [144]. Briefly, following the adhesion phase of 100 μL of 2×10^6 cells/mL of *C. albicans* on flat-bottom polystyrene microtiter plates, wells were washed twice with 150 μL of PBS to remove loosely adherent cells. The biofilms were allowed to develop up to 24 h at 37 °C in the presence of different concentrations of azo compounds (ranging from 8 to 60 $\mu\text{g/mL}$). For the photographs, non-adherent cells were removed by washing, and adherent cells were stained with crystal violet (CV) 0.3% solution.

In order to assess the *S. aureus* biofilm formation, bacteria were grown overnight in MHB medium. Cultures were then diluted to approximately 10^7 CFU/mL in fresh MHB medium, and 200 μL was used to inoculate flat-bottom 96-well polystyrene microtiter plates containing different concentrations of azo compounds (from 8 to 60 $\mu\text{g/mL}$). After incubation for 24 h at 37 °C without shaking, the plate wells were washed twice with phosphate-buffered saline (pH 7.2) to remove non-adherent bacteria and dried in an inverted position. Finally, the adherent cells were stained with CV 0.3%.

Similarly, *S. aureus* (200 μL of 10^4 CFU/mL) was inoculated in microtiter plate and incubated for 18 to 24 h at 35 °C to allow biofilm formation. Afterwards, serial diluted solutions of azo compounds (20, 25, 30 and 50 $\mu\text{g/mL}$) were added on each well and incubated 8 h at 37 °C. For crystal violet staining, wells were rinsed with water to remove loosely adherent cells and then stained for 1 min with 200 μL of Gram's crystal violet. Wells were rinsed with water and dried. The amount of biofilm mass was obtained by destaining

the wells with 200 μ L of 33% acetic acid and then measuring the absorbance of the CV solution in a microplate spectrophotometer set at 595 nm.

6.5.4. Results

Antimicrobial tests were made by Prof. Amalia Porta at the University of Salerno (DIFARMA).

The MICs (minimum inhibitory concentrations) of the synthesized compounds for bacterial strains and *C. albicans* SC5314, determined by the microbroth dilution are shown in Table 6.6. In this table I also reported the MIC₀ values along with the data on resveratrol published by Weber [145] and Paulo [130].

Table 6.6. Antimicrobial and antifungal activity

Molecule	MIC ₀ (μ g/mL) after 24 h				
	<i>S. aureus</i>	<i>L. monocytogenes</i>	<i>S. typhimurium</i>	<i>P. aeruginosa</i>	<i>C. albicans</i>
Resveratrol	100 [§]	-	>400 [§]	>400 [§]	>128 [*]
A1	30	50	>60	>60	30
A2	20	25	>60	>60	20
A3	20	25	>60	>60	20
A4	20	25	>60	>60	17
A5	25	>60	>60	>60	15
B10	>60	>60	>60	>60	>60
B11	>60	>60	>60	>60	>60

[§] data from [130]; ^{*}data from [145]

MIC₀: Minimum Inhibitory Concentration required to inhibit the growth of 100% of organisms. The values are the geometric mean of at least three determinations.

Compared to the reference molecule, resveratrol, azo compounds A1-A5 show a higher antibacterial and antifungal activity. In particular, compounds A4 and A5, exhibit MIC₀ values 4-6 times smaller than those of resveratrol. Instead B10 and B11 do not show antibacterial and antifungal activity. Interesting is that there is antibacterial activity only against Gram-positive bacteria.

Probably the outer membrane in the Gram-negative prevents the entry of the azo compound into bacterial cell and so its antimicrobial action.

Figure 6.8 shows the effect of azo compounds (A3) on hyphae formation of *C. albicans*. In the absence of azo compounds (A1-A5), an extensive hyphae formation was observed, whereas when azo compounds were present, hyphae formation was severely hampered in a concentration-dependent manner. Here, I observed a total inhibition of germination above 10 $\mu\text{g/mL}$ of A3.

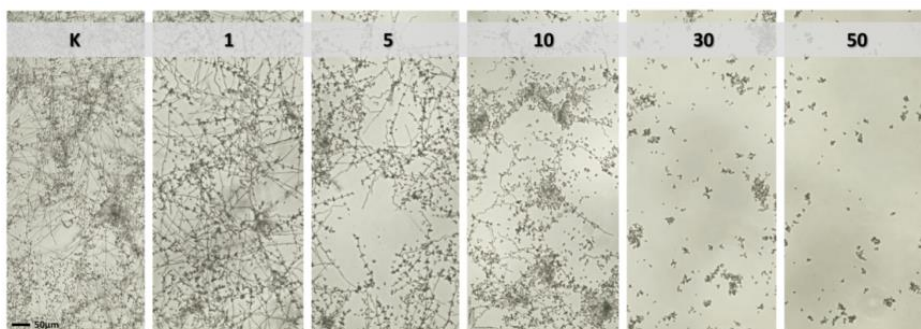


Figure 6.8. Inhibition of hyphae formation in *Candida albicans* at different concentrations of A3

The same analysis made on A4 and A5 are reported in Figure 6.9 and Figure 6.10.

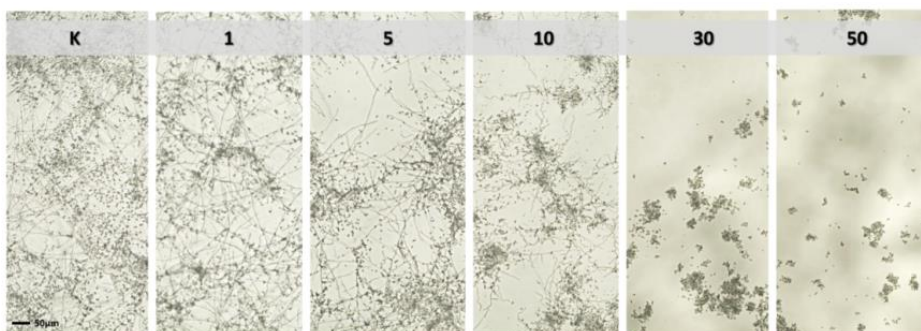


Figure 6.9. Inhibition of hyphae formation in *Candida albicans* at different concentrations of A4

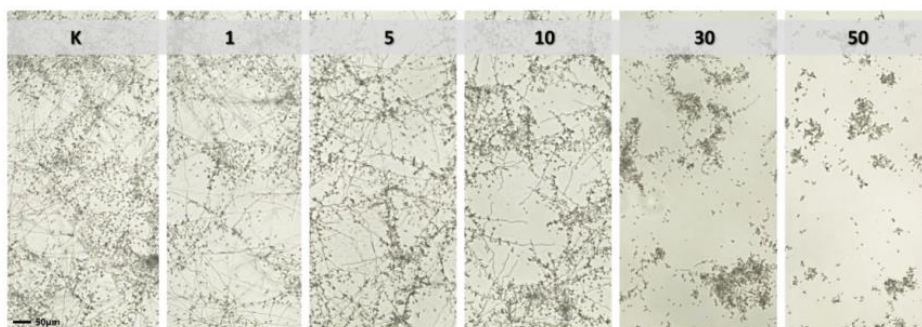


Figure 6.10. Inhibition of hyphae formation in *Candida albicans* at different concentrations of A5

To determine the inhibition of biofilms formation we performed a semi-quantitative colorimetric assay that does not differentiate between live and dead cells, using different concentrations of azo compounds (8, 10, 15, 20, 25, 30, 50 and 60 $\mu\text{g}/\text{mL}$), followed by staining with CV (crystal violet).

As shown in Figure 6.11, *Candida* treated with different concentrations of azo compounds displayed a severe defect in biofilm formation compared to the control.

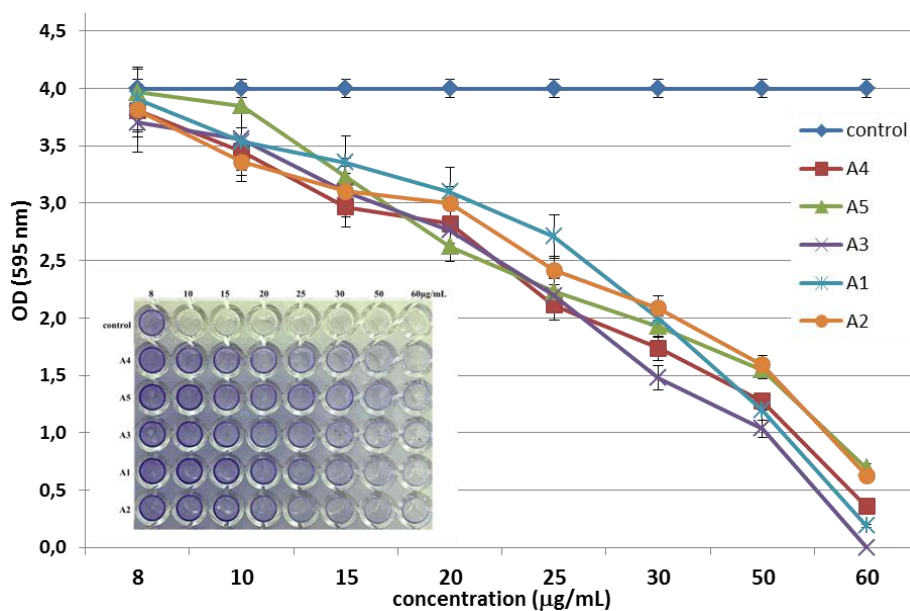


Figure 6.11. Inhibition of *C. albicans* biofilm formation. Equal numbers of *Candida* cells incubated in 96-well plates for 24 h at 37 °C. Adherent cells were stained with CV.

These results were confirmed by the effects of 20 $\mu\text{g}/\text{mL}$ of azo compounds on *Candida* biofilms degradation using an XTT assay, which characterizes living biomass (Figure 6.12).

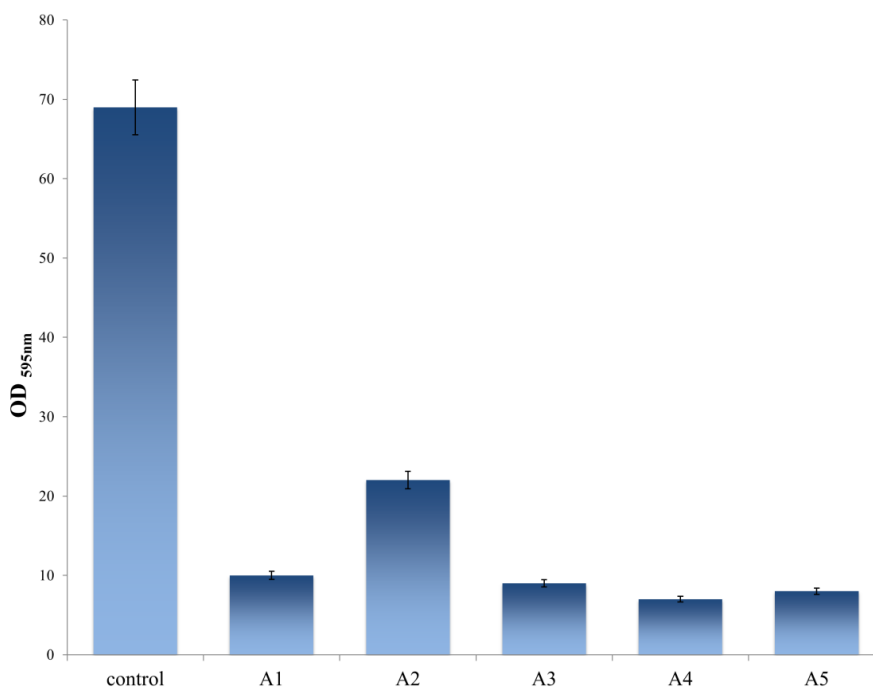


Figure 6.12. XTT assay. Metabolic activity of *Candida* biofilms treated with 20 $\mu\text{g}/\text{mL}$ of azo compounds, compared to control (biofilm treated with vehicle only). Each value is the mean \pm S.D. of 3 independent experiments.

S. aureus forms biofilms that can be detected by staining the adhered cells with CV. We analyzed the ability of different concentrations of azo compounds (8, 10, 15, 20, 25, 30, 50 and 60 $\mu\text{g}/\text{mL}$) to inhibit biofilm formation. As shown in the graph of *Figure 6.13.*, while A4 prevents biofilms formation when used at 30 $\mu\text{g}/\text{mL}$, the other azo compounds had the same effect already at 25 $\mu\text{g}/\text{mL}$.

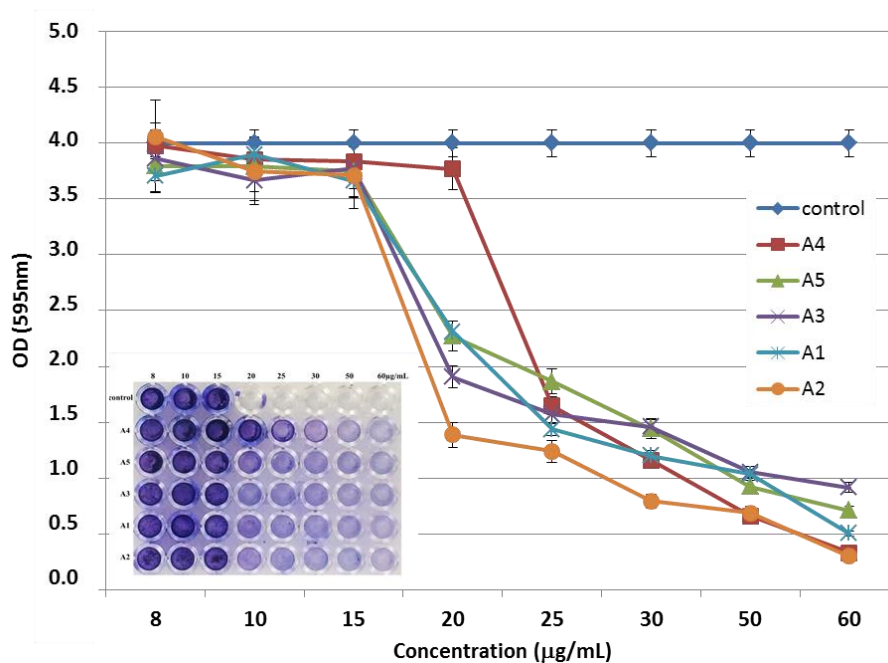


Figure 6.13. Inhibition of *S. aureus* biofilm formation. *Staphylococcus* (0.2×10^7 cells/mL) was incubated in 96-well plates for 24 h at 37 °C. Biofilm was stained with CV and each assay was performed 3 times.

To verify that the inhibitory effect on biofilm formation was not a result of growth inhibition, different concentrations of azo compounds (20, 25, 30 and 50 $\mu\text{g/mL}$) were added to a preformed *S. aureus* biofilm. Results in *Figure 6.14* confirmed that 30 $\mu\text{g/mL}$ of A1, A2, A3 and A5 were able to degrade more than 60% of preformed biofilm. As expected, 30 $\mu\text{g/mL}$ of A4 degraded only the 40% of *S. aureus* biofilm. Complete biofilm degradation required 50 $\mu\text{g/mL}$ of azo compounds.

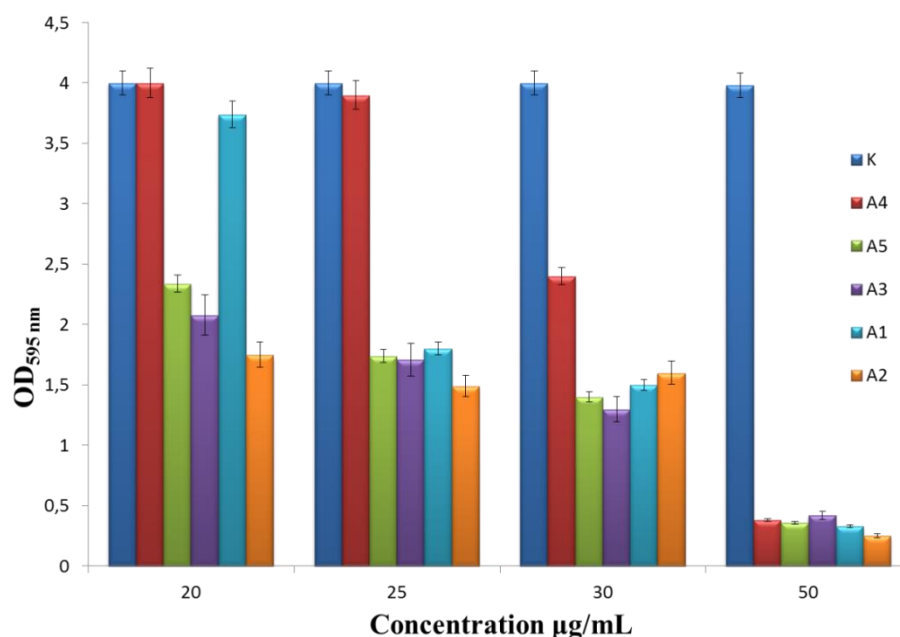


Figure 6.14. Staphylococcus biofilm degradation. Preformed biofilms were treated for 8 h with different concentrations of azo compounds. The histogram shows the levels of treated biofilm (biofilm treated with vehicle only) as determined by CV staining. Each value is the mean \pm S.D. of 3 independent experiments.

Chapter 7. Structure modifications using A4 as lead compound

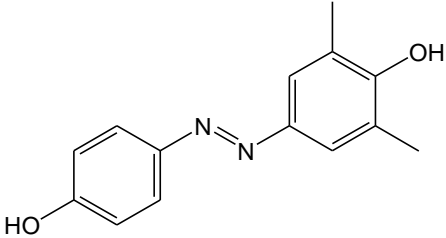
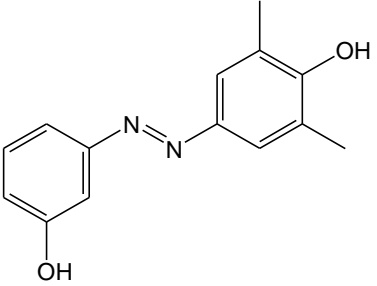
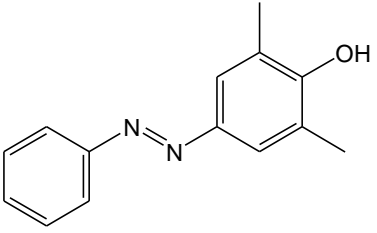
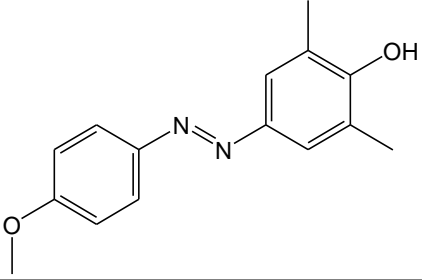
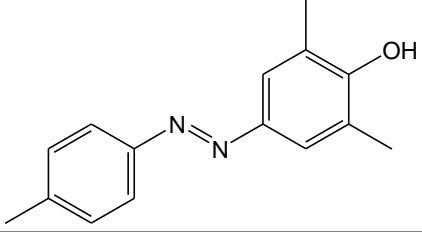
7.1. Introduction

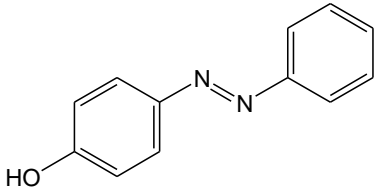
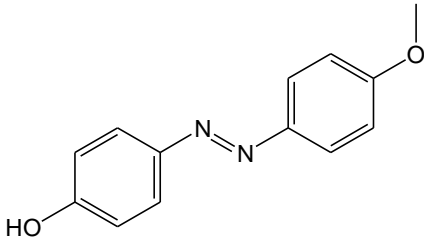
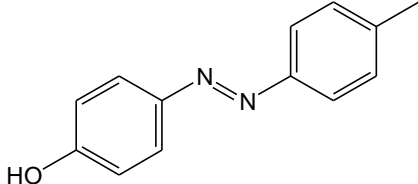
Despite a high chemical similarity, structural analogues are not necessarily functional analogues and can have very different biological activity.

Since the different antibacterial activities of synthesized azo compounds I decided to introduce some structure modifications to enhance the biological activity and in particular to evaluate the change in activity related to different types of substituents linked on the azobenzene structure.

I chose A4, the best antibacterial azo compound, as lead compound to synthesize several analogues (see *Table 7.1*). I conserved the basic scaffold and I introduced simple molecular modifications on the first and on the second azobenzene ring, in particular, to evaluate the role of the phenolic hydroxyl group in the mechanism of action. The modifications involved moving of the phenolic hydroxyl group from *para*- to *meta*- position, or removing of the phenolic hydroxyl group, and also replacing of the phenolic hydroxyl group by the methoxy and the methyl group.

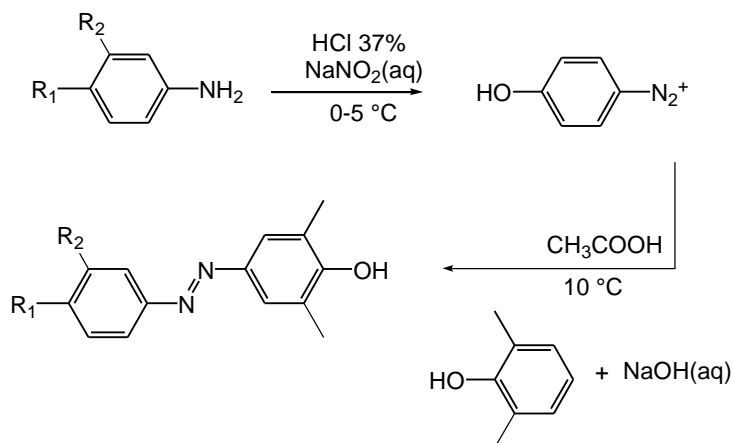
Table 7.1 Structures of A4 analogues compounds

Name	Structure	Modification description
A4		Lead compound
Modifications on the second ring		
m-A4		Moving phenolic hydroxyl group position
an-A4		Removing phenolic hydroxyl group
ani-A4		Replacing phenolic hydroxyl group by the methoxy group
t-A4		Replacing phenolic hydroxyl group by the methyl group

Modifications on the first ring		
an-A0		Removing phenolic hydroxyl group
ani-A0		Replacing phenolic hydroxyl group by the methoxy group
t-A0		Replacing phenolic hydroxyl group by the methyl group

7.2. Synthesis of A4 analogues with modified second ring

A4 analogues compounds were synthesized according to the classic scheme of diazocoupling reactions, as illustrated in *Figure 7.1*.



	R_1	R_2
m-A4	H	OH
an-A4	H	H
ani-A4	OCH_3	H
t-A4	CH_3	H

Figure 7.1. Synthesis scheme of A4 analogues with modified second ring

The procedure was the following: 0.0183 mol of the proper aromatic amine (depending on A4 analogue) were suspended in a solution containing 38 mL of water and 4 mL of HCl 37% (w/w). The solution was cooled at $0-5\text{ }^\circ\text{C}$ in a water-ice bath. A solution of 1.39 g of sodium nitrite (0.0202 mol) dissolved in 8 mL of water was added drop-wise, obtaining a suspension of the diazonium salt (solution A). Separately, a solution containing 0.7 g of NaOH (0.0175 mol) in 50 mL of water with 2.23 g of 2,6-dimethylphenol (0.0183 mol) was prepared (solution B). Solution A was added drop-wise to solution B, under stirring at $12\text{ }^\circ\text{C}$. The system was left reacting for 30 min,

maintaining the pH = 10-11. Then the final solution was slowly added to 103 mL of an acid solution (100 mL of water and 3 mL of acetic acid), and then stirred for 30 min at 15 °C. A dark red precipitate of the azo compound was formed. The crude precipitate was filtered and dried under vacuum. Yields ranged between 30 and 40%.

a. 3'-hydroxy-(4-hydroxy-3,5-dimethyl)-azobenzene (m-A4)

3-aminophenol and 2,6-dimethylphenol were used as starting reagents. The crude product was extracted and crystallized from boiling n-octane (100 mL) and dried. Final crystallization from boiling water/ethanol (3:1) gave pure m-A4. Polarized optical microscopy and X-Ray powder diffraction on powders sample were performed. m-A4 showed the needle crystalline habitus. The crystals were orange colored and in big size.

^1H NMR (DMSO- d_6): δ (ppm) = 7.55 (s, 2H), 7.34 (m, 2H), 7.19 (d, 1H), 6.90 (d, 1H), 2.27 (s, 6H).

b. 4-hydroxy-3,5-dimethyl-azobenzene (an-A4)

Aniline and 2,6-dimethylphenol were used as starting reagents. The crude product was extracted and crystallized from boiling water/ethanol (3:1) and dried. Final pure an-A4 was amber crystalline material. Polarized optical microscopy and X-Ray powder diffraction on powders sample were performed. an-A4 showed the needle crystalline habitus. The crystals were yellow colored and in small size.

^1H NMR (DMSO- d_6): δ (ppm) = 7.82 (d, 2H), 7.55 (m, 5H), 2.27 (s, 6H).

c. 4'-methoxy-(4-hydroxy-3,5-dimethyl)-azobenzene (ani-A4)

p-anisidine and 2,6-dimethylphenol were used as starting reagents. The extraction and crystallization of the crude product from boiling water/ethanol (3:1) gave the pure ani-A4 as yellow crystalline material. Polarized optical

microscopy and X-Ray powder diffraction on powders sample were performed. ani-A4 showed the needle crystalline habitus. The crystals were yellow colored and in big size.

^1H NMR (DMSO- d_6): δ (ppm) = 7.81 (d, 2H), 7.51 (s, 2H), 7.11 (d, 2H), 3.85 (s, 3H), 2.26 (s, 6H).

d. 4'-methyl-(4-hydroxy-3,5-dimethyl)-azobenzene (t-A4)

p-toluidine and 2,6-dimethylphenol were used as starting reagents. The extraction and crystallization of the crude product from boiling water/ethanol (3:1) gave the pure t-A4 as orange crystalline material. Polarized optical microscopy and X-Ray powder diffraction on powders sample were performed. t-A4 took on the blade crystalline habitus. The crystals were dark yellow colored.

^1H NMR (DMSO- d_6): δ (ppm) = 7.72 (d, 2H), 7.54 (s, 2H), 7.36 (d, 2H), 2.39 (s, 3H), 2.27 (s, 6H).

7.3. Synthesis of A4 analogues with modified first ring

A4 analogues compounds were synthesized according to the classic scheme of diazocoupling reactions, as illustrated in *Figure 7.2*.

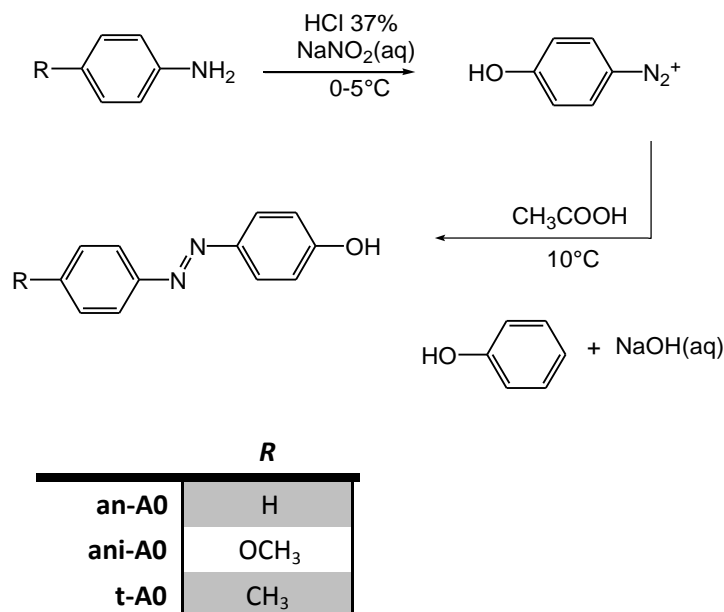


Figure 7.2. Synthesis scheme of A4 analogues with modified first ring

To synthesize these A4 analogues I used the same procedure described for the other azo compounds. Solution A was prepared suspending 0.0183 mol of the proper aromatic amine (depending on A4 analogue) in a solution containing 38 mL of water and 4 mL of HCl 37% (w/w). The solution was cooled at 0-5 °C in a water-ice bath. A solution of 1.39 g of sodium nitrite (0.0202 mol) dissolved in 8 mL of water was added drop-wise, obtaining a suspension of the diazonium salt (solution A). Separately, a solution containing 0.7 g of NaOH (0.0175 mol) in 100 mL of water (pH = 14) with 1.72 g of phenol (0.0183 mol) was prepared (solution B). Solution A was added drop-wise to solution B, under stirring at 12 °C. The system was left reacting for 30 min, maintaining the pH = 11. The final solution was slowly added to 300 mL of an aqueous solution of acetic acid (pH = 5) and then stirred for 30 min at 15 °C.

In this step, to facilitate the precipitation of the azo compound I added 0.5 g of sodium acetate powder and stirred for 20 min in water-ice bath. A dark precipitate of the azo compound was formed and it was filtered and dried under vacuum. Yields ranged between 50 and 60%.

a. 4'-hydroxy-azobenzene (an-A0)

Aniline and phenol were used as starting reagents. The crude product was extracted and crystallized from boiling n-octane (100 mL) and dried. Final crystallization from boiling water gave pure an-A0. Polarized optical microscopy and X-Ray powder diffraction on powders sample were performed to observe the needle crystalline habitus of the azo compound. The crystals were orange/yellow colored and in very small size.

$^1\text{H NMR}$ (DMSO- d_6): δ (ppm) = 7.81 (t, 4H), 7.54 (m, 3H), 6.96 (d, 2H).

b. 4'-hydroxy-4-methoxy-azobenzene (ani-A0)

p-anisidine and phenol were used as starting reagents. The crude product was extracted and crystallized from boiling n-octane (100 mL) and dried. Final crystallization from boiling water/ethanol (3:1) gave pure ani-A0. Polarized optical microscopy and X-Ray powder diffraction on powders sample were performed to observe the blade crystalline habitus of the azo compound. The crystals were bronze colored.

$^1\text{H NMR}$ (DMSO- d_6): δ (ppm) = 7.80 (dd, 4H), 7.51 (s, 2H), 7.11 (d, 2H), 6.93 (d, 2H), 3.86 (s, 3H).

c. 4'-hydroxy-4-methyl-azobenzene (t-A0)

p-toluidine and phenol were used as starting reagents. The crude product was extracted and crystallized from boiling n-octane (100 mL) and dried. Final crystallization from boiling water/ethanol (3:1) gave pure t-A0. Polarized optical microscopy and X-Ray powder diffraction on powders sample were

performed to observe the needle crystalline habitus of the azo compound. The crystals were brilliant yellow colored.

^1H NMR (DMSO- d_6): δ (ppm) = 7.75 (dd, 4H), 7.54 (s, 2H), 7.35 (d, 2H), 6.93 (d, 2H), 2.39 (s, 3H).

The proton resonance data were in agreement with the expected values; all spectra are reported in *Appendix-d* section.

7.4. Thermal and optical properties of A4 analogues compounds

From DSC analysis I studied the thermal behavior of synthesized compounds (see *Table 7.2*).

The analogues compounds with modified second ring such as m-A4, an-A4 and T-A4 showed only a melting peak in the first heating run and they were not able to crystallize from the melt, in particular m-A4 melts at 114.4 °C, an-A4 at 87.7 °C and t-A4 at 89.3 °C.

ani-A4 showed a sharp melting peak in the first heating run at 128.3 °C and a crystallization peak at 94.6 °C in the cooling run. When heated in the second run, it showed the same melting peak as in the first run.

The analogues compounds with modified first ring such as an-A0 showed only a melting peak at 162.0 °C in the first heating run and it was not able to crystallize from the melt.

ani-A0 showed a sharp melting peak in the first heating run at 147.3 °C and a crystallization peak at 110.6 °C in the cooling run. When heated in the second run, it showed the same melting peak as in the first run.

t-A0 showed a sharp melting peak in the first heating run at 158.7 °C and a crystallization peak at 90.7 °C in the cooling run. When heated in the second run, it showed the same melting peak as in the first run. All spectra are reported in *Appendix-f*.

Table 7.2. Thermal characterization of A4 analogues

Compounds	Thermal characterization			
	T_m (°C)	ΔH_m (J/g)	T_c (°C)	ΔH_c (J/g)
m-A4	114.4	5.7	-	-
an-A4	87.7	78.0	-	-
ani-A4	128.3	98.1	94.6	92.1
t-A4	89.3	86.1	-	-
an-A0	162.0	149.8	-	-
ani-A0	147.3	123.3	110.6	104.5
t-A0	158.7	139.4	90.7	83.7

T_m = melting temperature, from DSC analysis, 10 °C/min, nitrogen flow;

T_c = crystallization temperature, from DSC cooling run; Instrument error ± 0.5 °C.

$\Delta H_m/\Delta H_c$ = melting/crystallization enthalpy, evaluated by integration of the peak.

Experimental error $\pm 5\%$.

UV absorption spectra of the samples were recorded at 25 °C on a Perkin-Elmer Lambda 19 spectrophotometer. The spectral region 650-240 nm was investigated by using cell path length of 1 cm and a concentration of about 3.0×10^{-5} mol L⁻¹ of azobenzene.

UV-Vis data are given in *Table 7.3* and all spectra are reported in *Appendix-g*.

Table 7.3. Optical characterization of A4 analogues

Molecule	Optical characterization	
	λ_{max} (nm)	ϵ_{max} (L mol ⁻¹ cm ⁻¹)
m-A4	358	9333
an-A4	344	18333
ani-A4	360	14000
t-A4	354	11428
an-A0	344	14473
ani-A0	355	14193
t-A0	358	14356

λ_{max} = wavelength at the principal absorption maximum,

ϵ_{max} = molar extinction coefficient at absorption maximum.

The UV-visible spectra for A4 analogues, made in acetonitrile solution, are qualitatively only depend on the active azo-containing unit, which is the same for all compounds. The UV absorption spectra of A4 analogues in *trans* configuration, showed the typical absorption bands of the electronic transitions of the azobenzene chromophore.

7.5. Antimicrobial activity of A4 analogues compounds

Synthesized analogues were microbiological testes by Prof. Amalia Porta at the University of Salerno (DIFARMA) using the same procedure described in the *paragraph 6.5*.

The MICs (*Table 7.4.*) of the synthesized compounds were determined by the microbroth dilution for *S. aureus* A170, *P. aeruginosa* ATCC-27853 strains and *C albicans* SC5314.

Table 7.4. Antimicrobial and antifungal activity of A4 analogues

<i>Molecule</i>	MIC ₅₀ (µg/mL) after 24 h		
	<i>S.aureus</i>	<i>C.albicans</i>	<i>P. aeruginosa</i>
A4	15	15	>35
m-A4	30	25	>35
an-A4	MIC ₀ 10	10	>35
ani-A4	>35	>35	>35
t-A4	>35	>35	>35
an-A0	25	20	>35
ani-A0	25	25	>35
t-A0	7	3	>35

The values are the geometric mean of at least three determinations. MIC₅₀: Minimum Inhibitory Concentration required to inhibit the growth of 50% of organisms. MIC₀: Minimum Inhibitory Concentration required to inhibit the growth of 100% of organisms. The values are the geometric mean of at least three determinations.

an-A4 is the most antimicrobial analogue active exhibiting activity at a concentration lower than the lead compound concentration. Moreover, it is the only analogue able to inhibit the growth of 100% of *S. aureus*, indeed for other compounds is reported only the MIC₅₀ values (Table 7.4).

t-A0 is the most antifungal analogue active showing activity against *C. albicans* already at 3 µg/mL.

Compared to the reference molecule, other analogues such as m-A4, an-A0 and ani-A0 show low activities. Anyway they still possess antimicrobial and antifungal activity at concentrations greater than A4.

ani-A4 and t-A4 compounds lose antibacterial and antifungal activity and all analogues do not exhibit antimicrobial activity against *P. aeruginosa*, as already observed for A1-A5 (Table 6.6).

Figure 7.3 shows the total inhibition of germination and hyphae formation of azo compounds (t-A0) on of *C. albicans* at 3 µg/mL of t-A0.

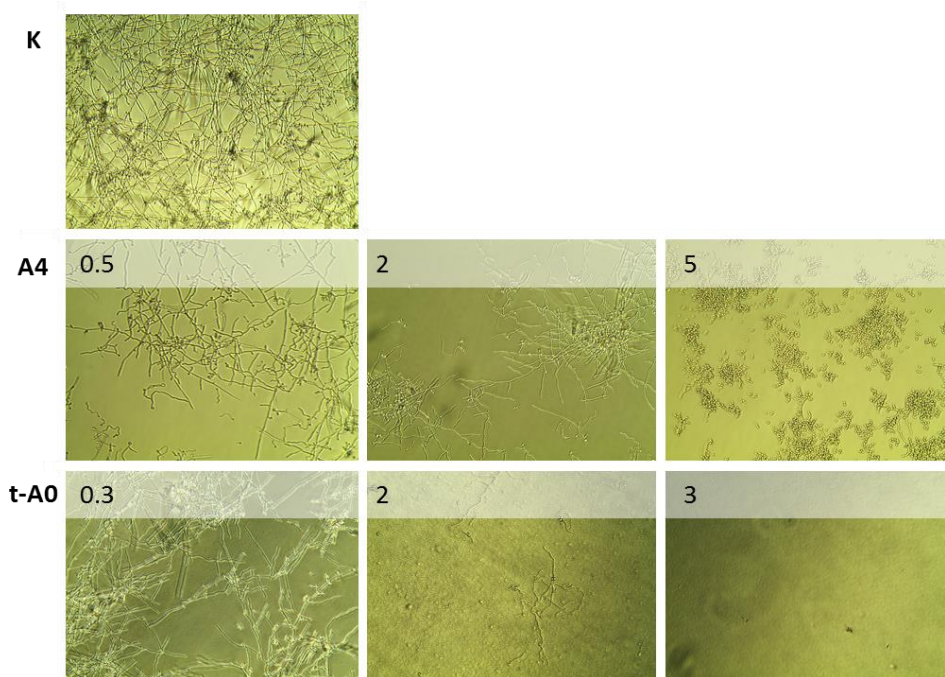


Figure 7.3. Inhibition of hyphae formation in *Candida albicans* at different concentrations (µg/mL) of A4 and t-A0 (20x optical zoom).

Chapter 8. Conclusions and outlook

Infections by pathogenic microorganisms are of great concern in many fields, and the emergence of strains resistant to the most common antimicrobials renders the evaluation of new drugs a dramatic quest.

Phytoalexin derivatives are antimicrobial substances synthesized *de novo* by plants that accumulate rapidly on areas of pathogen infection. I have used the phytoalexin resveratrol as template to design a new class of active compounds with azobenzene structure. I selected the best candidates by preliminary *in silico* test of ADMET properties and then I synthesized the azo compounds with lowest *in silico* toxicity values (A1, A2, A3, A4, A5, B10 and B11) according to the classic scheme of diazocoupling reaction. The antimicrobial activity and the thermal stability of each compound were evaluated. The majority of synthesized compounds exhibited high antibacterial activity against *S. aureus* and antifungal activity against *C. albicans*, but they were inactive against Gram-negative bacteria such as *P. aeruginosa* and *S. Typhimurium*. The different antibacterial activities of synthesized azo compounds suggest that these molecules interact with protein receptors and that the interaction with membranes is of minor importance. This hypothesis is supported by studies of inhibition of ATP synthase after binding with resveratrol and related polyphenols. It is well known that numerous stilbenes are capable to interact and inhibit ATP synthase, binding at the interface between α and γ subunits of ATP synthase. I propose that the activity and selectivity of antimicrobial azo compounds having structural similarity with stilbenes are influenced by ATP synthase binding. To validate this hypothesis I have performed molecular docking on different F1-ATPase of all synthesized azo compounds (data unreported).

Supported by modeling analysis, I carried out structural modifications of azo compounds to enhance their biological activity. I have used the best antimicrobial azo compounds named A4 (4'-hydroxy-(4-hydroxy-3,5-dimethyl)-azobenzene) as lead compound to synthesize several analogues having modifications on the first and on the second azobenzene ring. This include the moving of the phenolic hydroxyl group from *para*- to *meta*-position, the removal of the phenolic hydroxyl group, and the replacement of the phenolic hydroxyl group by the methoxy or the methyl group. The best results were obtained for *an-A4* (4-hydroxy-3,5-dimethyl-azobenzene): this molecule showed antibacterial activity against *S. aureus* higher than lead compound. The best antifungal activity was obtained for *t-A0* (4'-hydroxy-4-methyl-azobenzene) that is able to inhibit the growth of 50% of *C. albicans* at a concentration three times lower than the lead compound.

These preliminary results of antibacterial activity of A4 analogues compounds confirm the enzyme interaction. However, a larger combinatorial library of these compounds is required to define precisely the interaction with ATP synthases.

The antimicrobial activities of these azo compounds and their thermal stability are very promising and indicate that these molecules may have interesting and therapeutically significant applications. In the third part of this thesis, I show an example of possible applications: the insertion of azo compounds into polymeric matrices to produce potential active thin films.

Part III.

*Development of new antimicrobial and antifungal
polymer films*

Chapter 9. Novel antimicrobial polymer films active against bacteria and fungi

9.1. Introduction

The use of biomaterial implants and medical devices such as catheters, heart valves, stents, shunts, ophthalmic delivery systems, arthroprosthesis and fracture fixation devices is an increasingly common and often life-saving procedure [146]. However, bacteria frequently attach to medical devices by forming multicellular communities known as biofilms, which can be the source of persistent infections that are recalcitrant systemic antibiotic therapy. Biofilms are surface-associated bacterial communities within which bacteria have up to 1000 times higher resistance to antimicrobials and host defenses compared with their planktonic counterparts [147]. Healthcare-associated infection is widely recognized as the most frequent adverse event in hospitals. It has been estimated that 80% of the infections acquired in hospitals involve biofilms. As a result, a number of technologies have been developed to prevent or reduce the biofilm formation.

Most strategies for reducing biofilm-associated infections focus on the modification of existing materials that are used to manufacture indwelling medical devices by the incorporation of antibiotics or other antimicrobials into polymers. The most common antimicrobial agents used in polymer films are triclosan, chlorhexidine, tetracycline and derivatives, benzophenon, and rifampicin. Most of the work to obtain antimicrobial polymers was done on polystyrene, polyvinylchloride, poly lactic acid or poly (lactide-co-glycolic acid), chitosan, and cellulose. Occasionally, cyclodextrin inclusion compounds were added to stabilize the antimicrobial agents at high polymer-processing temperature [148].

Contamination by microorganisms is of great concern in a variety of areas, such as water purification systems, hospitals, dental office equipment, food packaging, food storage, and so on. In wake of this there has been a growing interest in developing antibacterial polymeric materials.

The post-processing contamination is one of the major causes of foodborne illness, a major public health issue and an economic burden for the food industry. Therefore, post-processing antimicrobial interventions are gaining significance in order to control the growth of bacteria that contaminate the food product after the primary lethal treatment. Traditional methods of preserving foods from the effect of microbial growth include thermal processing, drying, freezing, refrigeration, irradiation, modified atmosphere packaging, and adding antimicrobial agents or salts. Unfortunately, some of these techniques cannot be applied to some food products, such as fresh meats and ready-to-eat products. Packaging of foods is one of the final steps in food processing before storage and consumption and therefore is a critical step for incorporating antimicrobial mechanisms especially to control the post-processing contamination. Antimicrobial packaging is a promising form of active food packaging, in particular for meat products [149]. When antimicrobial agents are incorporated into polymer, the material limits or prevent microbial growth to provide higher safety and quality products.

The use of potent and/or specific antimicrobial systems will help to mitigate, combat and/or eradicate microbial infections, which means an improvement in the state of well-being. In this sense, polymers due to their intrinsic properties are extensively and efficiently employed in all of these fields. Polymers can act as matrix of the materials holding the antimicrobial agents. In this case the characteristics of the polymer such as its hydrophobicity or its molecular weight have a great influence on the final antimicrobial activity concerning aspects from the rate of biocide release to even conferring synergistic activities. The development of polymers with antimicrobial activity

themselves is also an important area of research focused on solve the problem of contamination by microorganisms.

As the most types of the commonly applied polymers have no antibacterial action, they have to be modified to obtain polymer materials with the desired properties. There are different approaches to incorporate antimicrobial activity into polymers. Keeping in mind the multitude of existing systems, a generic classification [148] of the different synthetic materials is carried out:

- (a) polymers that exhibit antimicrobial activity by themselves such as antimicrobial peptides already described in the first chapter;
- (b) polymers whose biocide activity is conferred through their chemical modification;
- (c) polymers that incorporate antimicrobial organic compounds with either low or high molecular weight;
- (d) materials that involve the addition of active inorganic systems.

I synthesized a new class of azo compounds, which exhibited very high activity against Gram-positive bacteria and fungi (Part II of this thesis).

Our strategy was to insert these molecules into commercially polymeric matrices, in order to produce composites having low cost of production, processability, antimicrobial potential, and low cytotoxicity. This was the first time in which a novel azobenzene based antimicrobial compound has been added into polymer films.

The final material can be used in all those applications where an intrinsic antimicrobial ability of the material is required, like biomedical tools, antibacterial surfaces, and films for food packaging.

Plastics are ideal for many applications such as in packaging, building materials and commodities, as well as in hygiene products. So the first my choice were the polyolefins, which permit the preparation of novel materials by a simple mold-casting technique. However, traditional petroleum-derived

plastics are not readily biodegradable as these materials and because of their resistance to microbial degradation, they accumulate in the environment.

In wake of this I focused on biodegradable polymers and in particular biodegradable biopolymers [150]. Depending on their origin, biodegradable polymers can be divided into three broad categories:

- (1) natural biopolymers, available in large quantities from renewable sources, such as carbohydrates, proteins, and lipids, obtained from plants or animals;
- (2) renewable-resource-based biopolymers, such as aliphatic polyesters and chemically synthesized biopolymers such as poly-(vinyl alcohol), and polylactides (PLA);
- (3) blends or composites of these biopolymers.

Renewable biodegradable polymers represent a valid alternative to traditional oil-derived polymers in many applications, to reduce environmental impact and to develop eco-sustainable cost-competitive products. When disposed in bioactive environments, biopolymers are degraded. Biodegradation takes place through the action of enzymes and/or chemical deterioration associated with living organisms. This event occurs in two steps. The first one is the fragmentation of the polymers into lower molecular mass species by means of either abiotic reactions (i.e. oxidation, photodegradation or hydrolysis), or biotic reactions (i.e. degradations by microorganisms). This is followed by bioassimilation of the polymer fragments by microorganisms and their mineralization. Biodegradability depends not only on the origin of the polymer but also on its chemical structure and the environmental degrading conditions [151].

9.2. Thin film preparation techniques

I used two different methods to realize thin antimicrobial films by introducing different percentages of azo compounds in different polymer matrices.

9.2.1. Mold-casting method

In collaboration with Prof. Loredana Incarnato and Prof. Roberto Pantani at the Department of Industrial Engineering, University of Salerno, I used mold-casting technique to prepare thin films.

The procedure consists of two steps. First I prepared the blended materials by mixing of commercially matrices and synthesized azo compounds. Briefly, pellets of the polymers, together with powder of azo compounds, are mixed in the hopper at 180 °C for a few minutes. The material is then conveyed forward by a feeding screw. Heating elements, placed over the barrel, soften and melt the mix. In this step I used two different extruders the Brabender Do-Corder E 330 and the Thermo Scientific Haake Minilab II for the biodegradable films. Both extruders work in the same way, but the second is a micro extruder and it works with small quantities of sample (about 5 g), in contrast to the first one that needs at least a sample amount of 30 g.

The temperature of the material is controlled by thermocouples and by measuring the torque of the drive motor and the pressure in the backflow channel; the reaction process can be monitored effectively. At the end of the barrel, the melt is extruded through a thin slot, cooled and collected as a solid piece.

In the second step, the extruded materials are placed between two sterilized sheets of Teflon and mold casted under pressure at 180 °C in a Carver Model C Laboratory Press to obtain thin films.

9.2.2. Solvent casting method

Solvent casting technique is a very easy way to prepare thin polymer films. The first step requires the dissolution of polymer matrix and the azo compound into a volatile solvent, to form a homogeneous solution. The

solution is then casted in a glass or Teflon support and after solvent removal (usually at room temperature) a homogeneous film is peeled from the support. Compared to the thermic extrusion, this method allows working with unstable molecules, because it avoids the high temperature of the extruder, but it produces thicker films, depending on the solution concentration.

9.3. Material used

9.3.1. Polypropylene (PP)

I used polypropylene random copolymer. Commercial name of this polyolefin is Moplen, grade RP241H. It is commonly used for sheet extrusion, blow molding, and thermoforming processes. This polymer exhibits high transparency and good impact strength, and it is suitable for food contact.

The selection was made by choosing polyolefin that can be processed at temperature lower than the degradation temperature of the azo compound and that can be addressed to both rigid and flexible packaging.

9.3.2. Linear low-density polyethylene (LLDPE)

I used linear low-density polyethylene with a commercial trade Luflexen, grade 18 TFA. Based on metallocene catalyst synthesis, Luflexen is used extensively in film applications.

9.3.3. Poly(lactic acid) (PLA)

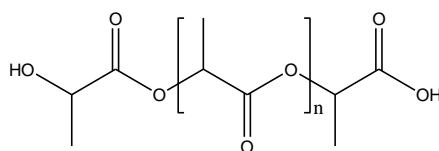


Figure 9.1. Structure of Poly (lactic acid)

Among the aliphatic polyesters, poly(lactic acid) (PLA) (*Figure 9.1*) is one of the most promising because it is thermoplastic, biodegradable, and biocompatible and has high strength, high modulus, and good processability. PLA is synthesized from lactic acid, which is derived from renewable resources, such as corn or sugar beets [152]. Due to its environment friendly nature, PLA can be used for food contact surfaces and is generally recognized as safe. Because PLA is known to be soluble in a variety of solvents such as tetrahydrofuran, benzene, chloroform, and dioxane, the solvent casting method has been commonly used for the preparation of biopolymer films. However PLA films can also be made by extrusion or mold casting.

In this study I prepared PLA films with two different methods: mold casting and solvent casting, and I used two different PLA matrices: 4032D and 4060D. PLA Polymer 4042D from NatureWorks® LLC is formed by 98.5% of L-isomer and 1.5% of D-isomer. This polymer shows glass transition temperature of 52 °C and melting point of 135 °C. Films formed with PLA have excellent optical properties, good machinability and exceptional twist and fold. These properties make PLA 4042D film an ideal candidate for packaging applications. Additional properties include advantageous barrier to flavor and grease and superior oil resistance.

PLA 4060D from NatureWorks® LLC is formed by 88% of L-isomer and 12% of D-isomer. It can be coextruded with other PLA resins to form a sealant layer for biaxially oriented PLA film. It shows glass transition at 58 °C and seal initiation at 80 °C. This polymer has excellent heat seal and hot tack performance and its films show high gloss and transparency, aroma and grease barrier.

9.3.4. Poly(vinyl alcohol) (PVA)

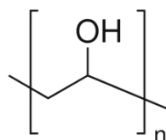


Figure 9.2. Structure of poly(vinyl alcohol)

Poly(vinyl alcohol) (PVA) (Figure 9.2) is one of the synthetic, biodegradable, biocompatible, water-soluble polymers utilized in medical applications such as wound dressings, artificial skin, coatings, transdermal patches, cardiovascular devices, and drug delivery systems. Moreover, it has good barrier properties against scents, oils, and fats. The physical characteristics of PVA depend on its method of preparation by hydrolysis or partial hydrolysis of poly(vinyl acetate). The value of glass transition temperature is 85 °C and the melting temperature is 190 °C.

9.3.5. Mater-Bi[®]

Among biopolymers, starch is one of the most widely investigated, as it is widely available and easily modified to get a thermoplastic polymer; nevertheless, due to the hydrophilic nature responsible for fast degradation via hydrolysis, thermoplastic starch applications are limited. To overcome this experimental drawback, starch is generally modified by blending with synthetic polymers, such as polyesters or vinyl alcohol copolymers. This approach has been adopted by Novamont under the Mater-Bi[®] trademark [153]. The company today produces four classes (Z, Y, V and A) of biodegradable materials, all based on starch and differing in synthetic components. In this work I used a Mater-Bi CF03A of class Z. They are biodegradable and compostable resins, mainly for films and sheets. They contain thermoplastic starch and poly-ε-caprolactone. Target markets of Mater-Bi include packaging materials, disposable cutlery, consumer goods and

agricultural tools. Mater-Bi resins are extremely versatile, and meet demanding end-use requirements. This includes important properties like elongation, tear resistance, tensile strength and water vapor permeability.

9.3.6. Plasticizers in biopolymer films

In recent years, much research has been focused on the replacement of petroleum-based commodity plastics with biodegradable materials offering competitive mechanical properties. Biopolymers have been considered the most promising materials for this purpose. However, they generally present poor mechanical properties in terms of processability and end-use application. Plasticizers are generally added to provide the necessary workability of biopolymers.

The council of the IUPAC (International Union of Pure and Applied Chemistry) defined a plasticizer as ‘a substance or material incorporated in a material (usually a plastic or elastomer) to increase its flexibility, workability, or distensibility’. These substances reduce the tension of deformation, hardness, density, viscosity and electrostatic charge of a polymer, at the same time as increasing the polymer chain flexibility, resistance to fracture and dielectric constant [154]. Other properties are also affected, such as degree of crystallinity, optical clarity, electric conductivity, fire behavior and resistance to biological degradation, amongst other physical properties [155].

In order to observe any improvements of the mechanical properties I used two different plasticizers: PEG 400 and Tween 80.

a. Polyethylene glycol

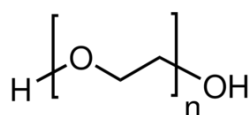


Figure 9.3. PEG structure

Polyethylen glycol 400 (*Figure 9.3*) is a low molecular weight grade of polyethylene glycol. It has been used to change mechanical properties of PVA films. The additive is a clear, colorless, viscous liquid. It has the potential ability to increase strength and flexibility as well as increase coating permeability to water vapor and gases. PEG is generally used as a coating, a binding and plasticizing agent, and/or a lubricant in food tablets.

b. Tween 80

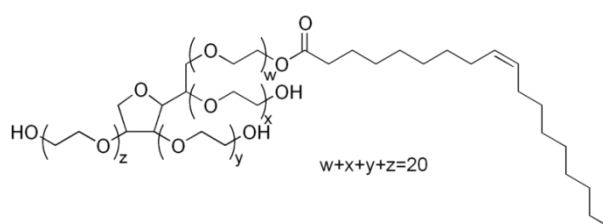


Figure 9.4. Tween 80 structure

Molecules named Tween[®] belong to the polysorbate family. Tween 80 (*Figure 9.4*) is a nonionic surfactant and emulsifier derived from polyethoxylated sorbitan and oleic acid, and is often used in foods. Polysorbate 80 is a viscous, water-soluble yellow liquid. The hydrophilic groups in this compound are polyethers also known as polyoxyethylene groups which are polymers of ethylene oxide. In the nomenclature of polysorbates, the numeric designation following polysorbate refers to the lipophilic group, in this case the oleic acid.

9.4. Experimental part: film preparation

9.4.1. Mold-casting method

a. Preparation of PP (MoplenRP241H) films adding A1 and A2

The first film realized by mold casting technique was prepared using A1 azo compound and PP polymer. The two components were mixed in bulk at 180 °C in a Brabender Do-Corder E 330, for 5 min at 50 rpm [156]. I prepared two matrices containing 1% and 5% of antimicrobial agent as given in *Table 9.1*, also I prepared the blank extruding only PP.

Table 9.1. Composition of prepared films in PP and A1

Film	PP	A1
Blank	30 g	-
1%	29.7 g	0.3 g
5%	28.5 g	1.5 g

Extruded matrices looked homogeneous and very colorful (in particular the matrix with 5% of A1) (*Figure 9.5*).



Figure 9.5. Blended matrices of PP blank (a), A1 1% (b) and A1 5% (c)

Small portion of extruded matrices were placed between two Teflon sheets and mold casted under pressure at 180 °C to obtain thin films.

A problem arose during the extrusion of the matrix with 5% of A1: the mixing was difficult and slow. This affected the thermal decomposition of the active principle, as confirmed by the poor antimicrobial activity measured in the antimicrobial tests. So I reduced the percentage of azo compound to 0.01%, 0.1%, 0.5 and 1% of A1 and A2 (see *Table 9.2*).

Table 9.2. Composition of thin films of PP/ A1 and A2

Film	PP	azo compound
Blank	30.20 g	-
0.01%	28.80 g	3.20 mg
0.1%	31.47 g	31.50 mg
0.5%	29.85 g	0.15 g
1%	29.70 g	0.30 g

Extruded matrices looked homogeneous and colorful as clear yellow (*Figure 9.6*).



Figure 9.6. Blended matrices of PP with A1 0.01%

b. Preparation of LLDPE (Luflexen18 TFA) films adding A1

LLDPE films with A1 were prepared in the same way reported for PP films. I extruded LLDPE polymer adding 1% (w/w) of A1 (*see Table 9.3*), also I prepared the blank extruding only LLDPE [157].

Table 9.3. Composition of LLDPE/A1 films

Film	PP	azo compound
Blank	30.0 g	-
1%	29.7 g	0.3 g

c. *Preparation of PLA4032D films adding A3, A4 and A5*

In wake of good antimicrobial results (Paragraph 9.6) using low percentages of A1 in PP matrix, I chose to prepare biodegradable active films reducing the percentages of antimicrobial agents into polymer matrices (from 0.01% to 0.1%).

PLA was first dried in vacuum at 35 °C for one week before of the extrusion. This step is necessary to avoid the matrix degradation during the hot mixing. I prepared three matrices containing 0.01%, 0.05% and 0.1% of antimicrobial agent in PLA4032D as given in *Table 9.4*. I also extruded the polymer without the azo compound to use as blank.

Table 9.4. Composition of PLA 4032D films

Film	PLA 4032D	azo compound
blank	5.0 g	-
0.01%	20.0 g	2.0 mg
0.05%	7.0 g	3.5 mg
0.1%	7.0 g	7.0 mg

Weighed materials were mixed in the hopper Haake Minilab II extruder (Thermo Scientific) and mixed at 180 °C for 5 min at 60 rpm. *Figure 9.7* shows the extrusion step of the matrix formed by PLA4032D and A4 0.1%.



Figure 9.7. Extrusion of the matrix formed by PLA4032D and A4 0.1% using Thermo Scientific Haake Minilab II extruder

Blended materials were cooled and collected as a solid piece; they looked perfectly transparent and without bubble air inside, as showed in *Figure 9.8*.

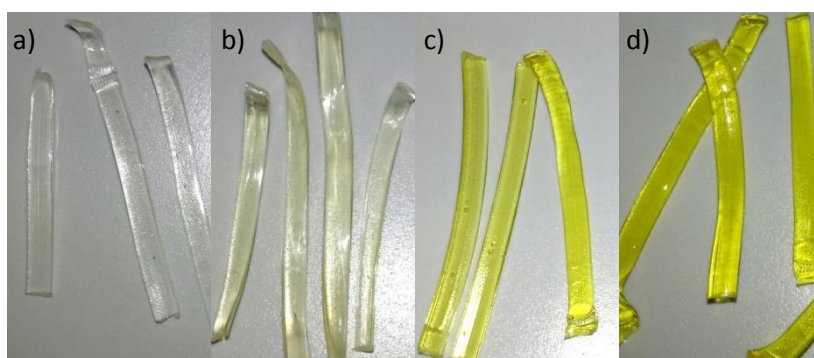


Figure 9.8. Blended matrix formed by PLA4032D after cooling used as blank (a), with A3 0.01% (b), A3 0.05% (c) and A3 0.1% (d)

After a few days under vacuum, the drier matrices were placed between two sheets of sterilized Teflon and mold casted under pressure at 180 °C to obtain thin films (*Figure 9.9*).



Figure 9.9. Thin film mold casted of PLA4032D blank (a); with A3 0.01% (b), A3 0.05% (c) and A3 0.1% (d)

d. Preparation of Mater-Bi CF03A films adding A3, A4 and A5

By mold casting method, I prepared Mater-Bi CF03A containing 0.01%, 0.05% and 0.1% of A3, A4 and A5 azo compounds (see *Table 9.5*).

Table 9.5 Composition of Mater-Bi films

Film	Mater-Bi CF03A	azo compound
Blank	7.0 g	-
0.01%	20.0 g	2.0 mg
0.05%	7.0 g	3.5 mg
0.1%	7.0 g	7.0 mg

I followed the same procedure used to prepare PLA4032D films. In *Figure 9.10* (a) and (b) the extruded matrices of pure Mater-Bi (used as blank) and Mater-Bi plus 0.01% of A3, are reported as example. *Figure 9.10* (c) shows the mold casted thin film mold casted of Mater-Bi with A3 0.01%. The realized films were homogenous and opaque.

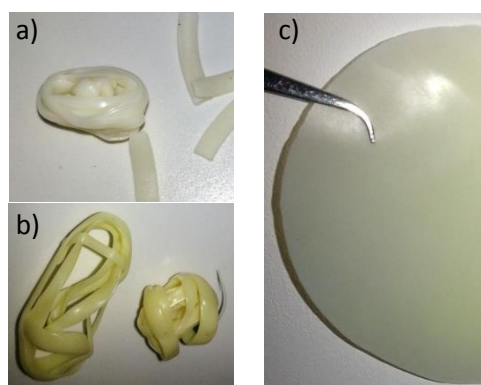


Figure 9.10. On the left the blended matrices of Mater-Bi blank (a) and with A3 0.01% (b). On the right the thin film mold casted of Mater-Bi with A3 0.01%.

9.4.2. Solvent casting method

a. Preparation of PLA films adding A3, A4 and A5

By solvent casting method, I realized two kinds of PLA films, in which the total amount of the matrix formed by plasticizer and polymeric pellets was 0.5 g. In the first film I used 0.45 g PLA4060D as matrix and in the second one a mixture of 0.25 g PLA4060D and 0.20 g PLA 4032D. In both cases I added 10% (w/w) of Tween 80 as plasticizer.

For the preparation of the solvent casted films, weighted amount of polymeric matrix and Tween 80 were dissolved in 10 mL of chloroform with vigorous mixing at room temperature for 5 h.

Separately I prepared three different stock solutions by dissolving 1 mg of A3, A4 and A5 azo compounds in 1 mL of acetone.

I split the matrix in different beakers, adding in each the exact volume to reach the final concentration of 0.01%, 0.05% e lo 0.1% (w/w) of antimicrobial agent. After gentle mixing at room temperature for a few minutes, the viscous solutions were poured onto different glass Petri dishes, and left for 24 h at room temperature. After solvent evaporation the films were peeled intact from the casting surface. Homogeneous and elastic films were obtained, approximately 700 μm thick (*Figure 9.11*).

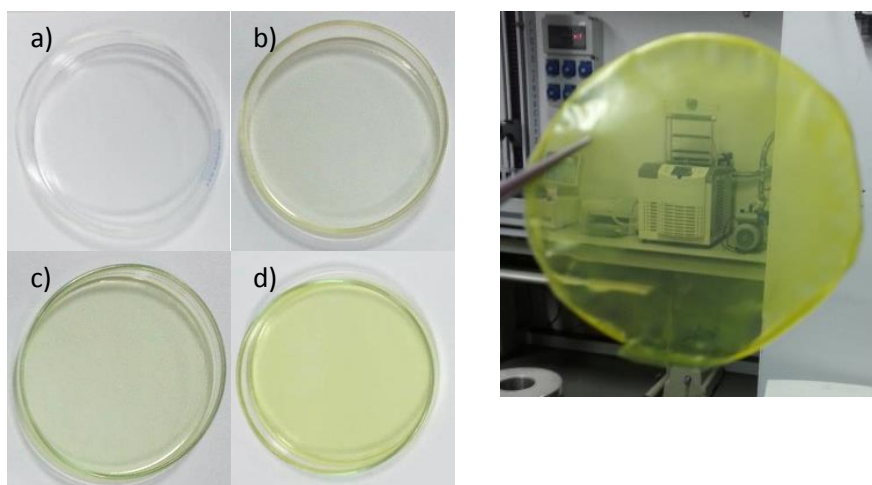


Figure 9.11. Casted matrix in Petri dishes of (a) PLA4060D and Tween 80 used as blank, (b) with A4 0.01%, (c) 0.05% and (d) 0.1% w/w. On the right: peeled A4 0.1% film.

I could not prepare film formed from only PLA4032D, because I observed matrix crystallization during peeling step. Using a mixture of polymers I overcame that problem obtaining homogenous and amorphous polymers.

b. Preparation of PVA films adding A3, A4 and A5

PVA-based films with different concentrations of azo compounds were prepared by solvent casting technique in the following way [158].

I prepared an aqueous polymer solution (1 g PVA in 9 mL distilled water) by dissolving polymer pellets in water. In addition, to increase the film elasticity, 0.1 g of PEG 400 was added, and the system was left at 80 °C for 20 min, under continuous stirring. Separately I prepared three different stock solutions by dissolving 2 mg of A3, A4 and A5 azo compounds in 1 mL of acetone. After dissolving the PVA, I split the matrix in four different beakers and I added the specific amount of azo compounds to the polymer solution, stirring for a few minutes. Then solutions were poured into different glass Petri dishes and left for 24 h at room temperature. After solvent evaporation the materials were peeled intact from the casting surface, obtaining homogeneous and elastic films, approximately 600 µm thick (*Figure 9.12*).



Figure 9.12. Film of PVA used as blank realized by solvent casting procedure

c. Preparation of Mater-Bi films

The optimized procedure for these preparations was: I suspended 1.5 g Mater-Bi and 0.15 g PEG 400 in 10 mL CHCl_3 stirring for 20 min until complete dissolution. I prepared three stock solutions solubilizing 3 mg of azo compound in 1.5 mL of acetone and I realized the thin films as described

previously for PLA. I obtained flexible and opaque films as shown in *Figure 9.13*.



Figure 9.13. 1Dried films in Petri dishes of Mater-Bi and PEG 400 used as blank (a) and Mater-Bi and PEG 400 with 0.01%, 0.05% and 0.1% of A4 (b-c-d respectively)

9.5. Thermal characterization of the films

All films were characterized by thermal gravimetric analysis (TGA) and differential scanning calorimetry (DSC). Here I focus the attention on the more interesting biodegradable materials. Dried films were observed under polarized light, using an optical microscope, in order to confirm the amorphous nature of the material and to exclude the presence of crystallized azo compound in the matrix; these aspects were then confirmed by X-Ray analysis. Moreover, I performed TGA and DSC to analyze the thermal behavior of prepared films and to evaluate the changes made by azo compounds on the polymers. As representative examples, here I report the results of the analyses made on the blank matrices and on films containing the highest percentage of A4 azo compound. All spectra are reported in section *Appendix-h*.

a. PLA4060D with Tween 80 film prepared by solvent casting method

As confirmed by X-Ray analysis, PLA4060D films are amorphous. *Figure 9.14* shows the diffractograms of films of PLA4060D/Tween 80 (a), PLA4060D/Tween 80 with 0.1% of A4 (b) and A4 crystals (c). For both films

the RX show only the amorphous halo, in contrast to a crystalline pattern visible for A4 (on the right).

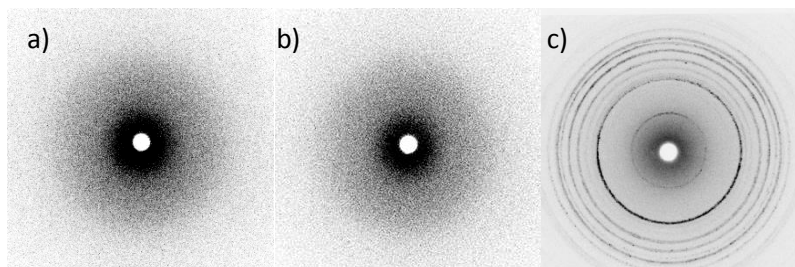


Figure 9.14. X-Ray diffractograms (a) PLA4060D with Tween 80 film, (b) PLA4060D and Tween 80 with 0.1% of A4 and (c) A4 powder

The thermogravimetric analysis (TGA) showed that both films (blank and PLA4060D/Tween 80 with 0.1% of A4) undergo an initial decomposition (5% weight loss) around 108 °C. The spectra were completely overlapping, showing that the presence of A4 compound did not influence the thermal behavior of the film.

The glass transition temperature (T_g) of PLA4060D is 60 °C. From DSC analysis, the blank matrix showed $T_g = 33.9$ °C: I attributed this decrease to the plasticizer introduced. PLA4060D/Tween 80 with 0.1% showed $T_g = 33.9$ °C, so I concluded that the presence of A4 in the matrix did not influence the thermal behavior of the material.

b. PLA4060/4032D with Tween 80 film prepared by solvent casting method

As confirmed by X-Ray analysis, PLA mixture films showed amorphous aspect (Figure 9.15). The film used as blank (PLA4060/4032D with Tween 80) and the same film with 0.1% of A4 had the amorphous nature in contrast to a crystalline pattern showed from the powder of A4 on the right.

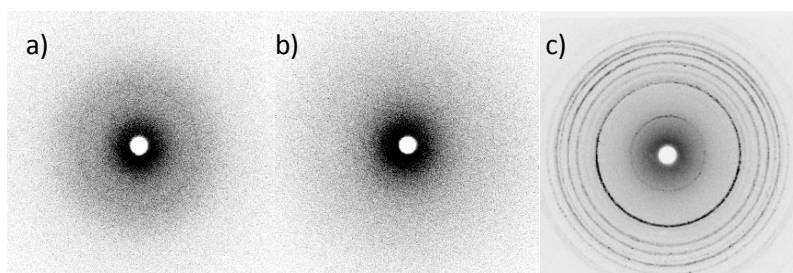


Figure 9.15. X-Ray diffractograms (a) PLA4060D/4032D with Tween 80 film, (b) PLA4060D/4032D and Tween 80 with 0.1% of A4 and (c) A4 powder

The thermogravimetric analysis (TGA) of the blank and PLA4060D/4032D with Tween 80 and 0.1% of A4 films showed initial decomposition (5% weight loss) around 100 °C. The thermograms of both films were completely overlapping, so the presence of A4 compound did not influence the thermal behavior of the film.

From DSC analysis the glass transition temperature (T_g) for the PLA4060D/4032D film is 70.7 °C and for the film with azo compound was 65.1 °C. As observed for the other PLA films the presence of A4 in the matrix did not influence the thermal behavior of the system.

c. PLA4032D film prepared by mold casting method

X-Ray analysis confirmed the amorphous nature of PLA films obtained by mold casting method. As shown in *Figure 9.16* there are no crystals of A4 in the matrix: this suggests that A4 is homogeneously dispersed in the polymer.

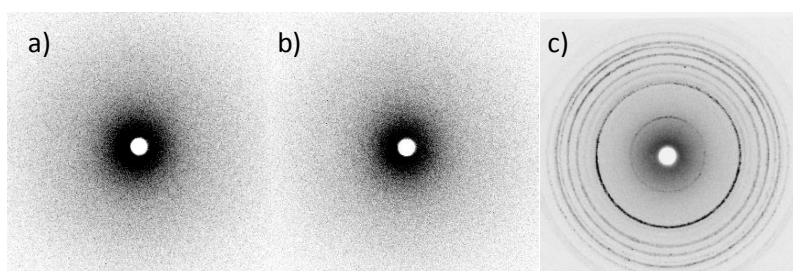


Figure 9.16 X-Ray diffractograms (a) PLA4032D, (b) PLA4032D with 0.1% of A4 and (c) A4 powder

I performed thermogravimetric analysis for the film without and with 0.1% A4. An initial decomposition (5% weight loss) was observed at 318.5 °C. The spectra were completely overlapping, so the presence of A4 compound did not influence the thermal behavior of the film. The DSC analysis of the blank and of the PLA4032D with 0.1% of A4 showed that the presence of azo compound did not change the glass transition temperature. The T_g was 60.9 °C for the blank and 59.6 °C for the film with A4.

9.5.2. PVA films

X-Ray analysis confirmed the amorphous aspect of PVA films prepared by solvent casting method. Analyzing the diffractogram of the film with 0.1% of A4, I observed a very light crystalline ring, but I did not attribute this ring to the precipitation of azo compound because I observed the same in the X-Ray diffractogram of film without A4 (*Figure 9.17*).

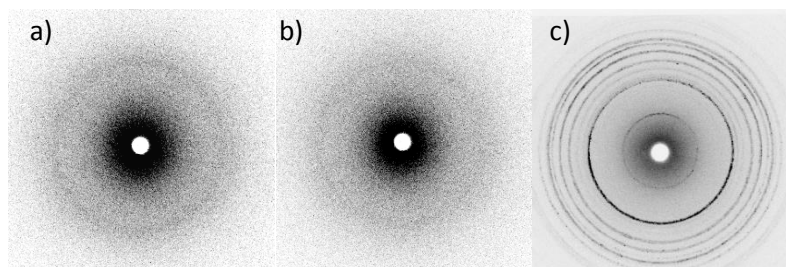


Figure 9.17 X-Ray diffractograms (a) PVA with PEG 400, (b) PVA with PEG 400 and 0.1% of A4 and (c) A4 powder

The thermogravimetric analysis (TGA) of the blank and PVA with PEG 400 adding 0.1% of A4 films showed initial decomposition (5% weight loss) around 82.4 °C. The thermograms of both films were completely overlapping, so the presence of A4 compound did not influence the thermal behavior of the film.

The DSC analysis of the blank showed the $T_g = 50.2\text{ }^\circ\text{C}$, and for the film with 0.1% of A4 the T_g was $55.2\text{ }^\circ\text{C}$.

9.5.3. Mater-Bi films

a. Mater-Bi CF03A with PEG 400 film prepared by solvent casting method

I performed X-Ray analysis to establish the amorphous nature of Mater-Bi. The results are shown in *Figure 9.18*.

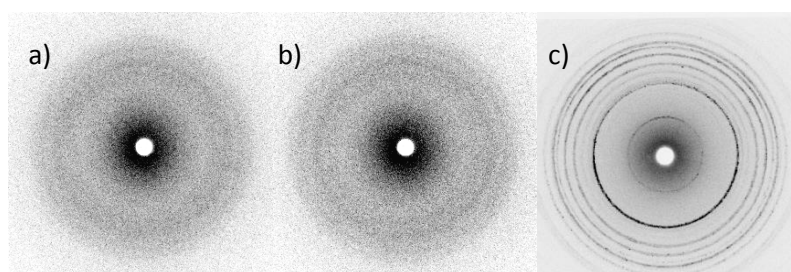


Figure 9.18. X-Ray diffractograms of solvent casting (a) Mater-Bi CF03A with PEG 400, (b) Mater-Bi CF03A with PEG 400 and 0.1% of A4 and (c) A4 powder

Analyzing the diffractogram of the film with 0.1% of A4, I observed a few light rings, I attributed these signals to the matrix, because I observed them also in the X-Ray diffractogram of film without A4.

The thermogravimetric analysis (TGA) of the blank and the film with 0.1% of A4 films showed initial decomposition (5% weight loss) around $181\text{ }^\circ\text{C}$. The thermograms of both films were completely overlapping, so the presence of A4 compound did not influence the thermal behavior of the film. I performed the DSC analysis but I could not individuate the glass transition temperature for the blank film and the film with 0.1% of A4.

b. Mater-Bi CF03A film prepared by mold casting method

As made for films prepared by solvent casting technique, I performed X-Ray analysis to establish the amorphous nature of the films prepared by mold casting. The results are shown in *Figure 9.19*.

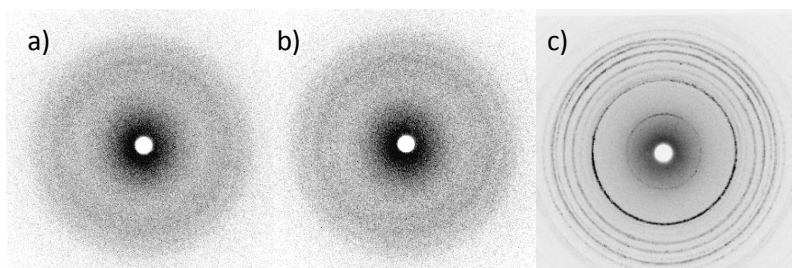


Figure 9.19. X-Ray diffractograms of mold casted (a) Mater-Bi CF03A with PEG 400, (b) Mater-Bi CF03A with PEG 400 and 0.1% of A4 and (c) A4 powder

As observed in the X-Ray diffractograms for Mater-Bi film prepared by solvent casting method, also in these cases I could see a few light rings.

The thermogravimetric analysis (TGA) of the blank and of the film with 0.1% of A4 films showed the same initial decomposition temperature (5% weight loss) around 239.7 °C. The thermograms of both films were completely overlapping, so the presence of A4 compound did not influence the thermal behavior of the film. I performed the DSC analysis, but as observed for the same films by solvent casting I could not individuate the glass transition temperature for the blank film and the same film with 0.1% of A4.

9.6. Summary of films characteristics

In *Table 9.6* is given a summary of the thermal characterizations described in the previous paragraphs. All spectra are inserted in *Appendix-h*.

Table 9.6 Thermal characteristics of the films

Film	T _g (°C)	T _d (°C)	Method of preparation
PLA4060D with Tween 80 with 0.1% of A4	33.9	305 [§]	SC
Blank	33.9	305 [§]	
PLA4060/4032D with Tween 80 with 0.1% of A4	65.1	309 [§]	SC
Blank	70.7	309 [§]	
PLA4032D with A4 0.1%	59.6	318	MC
Blank	60.9	318	
PVA with A4 0.1 %	55.2	82	SC
Blank	50.2	82	
Mater-Bi CF03A with PEG 400 with A4 0.1 %	-*	181	SC
Blank	-*	181	
Mater-Bi CF03A with A4 0.1 %	-*	240	MC
Blank	-*	240	

Blank = polymeric matrices without azo compounds.

T_g = glass transition temperature; *T_d* = 5% degradation temperature; *SC* = solvent casting; *MC* = mold casting. * = not detectable from DSC. § = extrapolated data.

Thermal characterizations indicated that the presence of 0.1% of A4 in the matrix does not influence the thermal behavior of the material. Thermogravimetric spectra of the blank and the azo-film were completely overlapping giving the same *T_d*. Changes in glass transition temperature were very limited, only in the case of PVA-based films I observed that A4 presence reduced the *T_g* of 5 °C. As expected, the thermal properties were strongly altered from the presence of plasticizers: the presence of plasticizers decreases the *T_g* values of the pure polymer matrices.

Interesting were the changes due to the preparation method. The thermal stability for the films prepared by mold casting was different from the results obtained for the films prepared by solvent casting. The PLA-based films prepared by mold casting showed T_d value 200 °C higher than the T_d of PLA-based films prepared by solvent casting method. Correspondingly the Mater-Bi film prepared by mold casting showed the T_d value 50 °C higher of than the correspondent films by solvent casting. For PLA polymers, it was clear that the initial weight loss for the solvent casted films could be attributed to the loss of adsorbed water. As an example, I reported in *Figure 9.20* a comparison between two films of PLA obtained from solvent casting (a) and mold casting (b). The film obtained by solvent casting method (a) shows a weight loss at about 100°C: this could be attributed to the loss of water from the raw polymer mixture. The film obtained by mold casting (b) has been extensively dried before the process, so its weight loss is due only to the decomposition of the material. If you consider that this weight loss does not belong to the polymer, the extrapolated T_d values are the ones reported in *Table 9.6*.

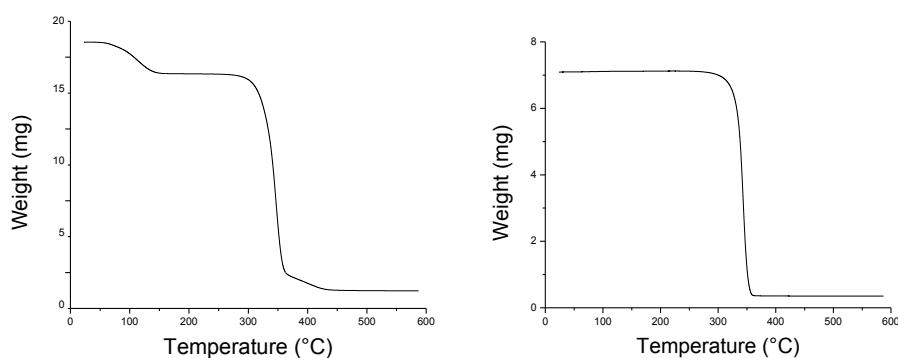


Figure 9.20. Comparison between TGA thermograms of (a) PLA 4060D/4032D with Tween 80 and 0.1% of A4 prepared by solvent casting; (b) PLA4032D + 0.1% A4 prepared by mold casting.

9.7. Microbiological Characterization

Realized films were tested *in vitro* against a Gram-positive bacterium and a fungus to establish the antimicrobial and antifungal activity of the azo compounds dissolved into polymeric films. Microbiological tests were performed by Prof. Amalia Porta at the Department of Pharmacy, University of Salerno.

9.7.1. Antimicrobial results on PP/azo and LLDPE/azo films

The antimicrobial effect of the PP-based films was tested analyzing the degradation of preformed biofilms of *Staphylococcus* and *Candida* on the active films, by staining with crystal violet.

S. aureus cells ($\sim 10^4 - 10^5$ CFU/mL) were grown in a 24-well plate at 37 °C. Portions of the PP-films (1 cm²) were added to each well and incubated for 48 h at 37 °C. Films were moved in a new 24-well plate and washed to remove non-adherent cells and afterward stained with crystal violet solution 0.3% (w/v). After rinsing with water and drying, the films were photographed to allow a qualitative comparison between tested films.

The same protocol was used for the *C. albicans* biofilm degradation. *Candida albicans* cells were suspended in 200 µL RPMI Medium 1640 at 10⁶ cells/mL, seeded in a flat-bottom 24-well plate for 48 h at 37 °C. After, portions of films (1 cm²) were added to each well and incubated 48 h at 37 °C. Films were moved in a new 24-well plate and washed to remove non-adherent cells and afterward stained with crystal violet solution 0.3% (w/v). After rinsing with water and drying, the films were photographed to allow a qualitative comparison between tested films.

The formation of biofilms is indicated by violet coloration. In *Figure 9.21* is reported a section of tested photographed films. It shows that at concentrations of A1 and A2 higher than 0.01% in PP films there is a complete inhibition of

biofilms, whereas for the films with 0.01% (w/w) both biofilms are only partially formed.

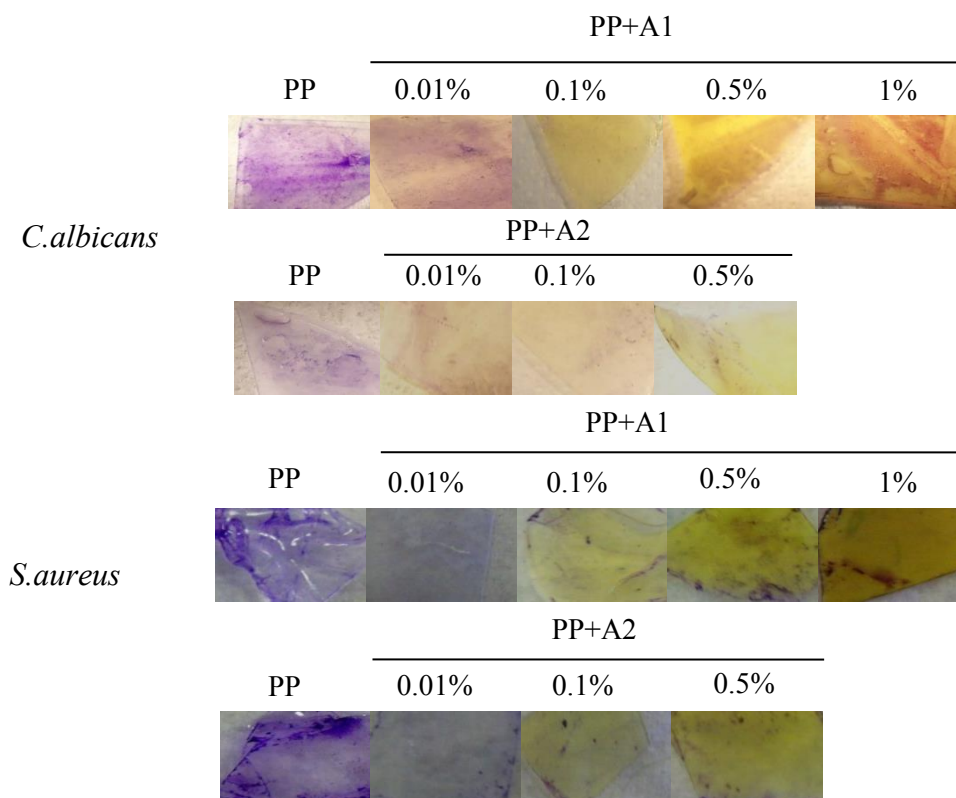


Figure 9.21. Biofilms formation on PP/A1 and PP/A2 films

Antimicrobial activity of LLDPE-based films was tested against *S. aureus*. In particular, after biofilm formation films were washed, dried, and the weight compared to the pure matrix (Figure 9.22). These preliminary tests showed that in the case of PP films with 1% of A1, the formation of *S. aureus* colonies on the polymer surface was completely inhibited.

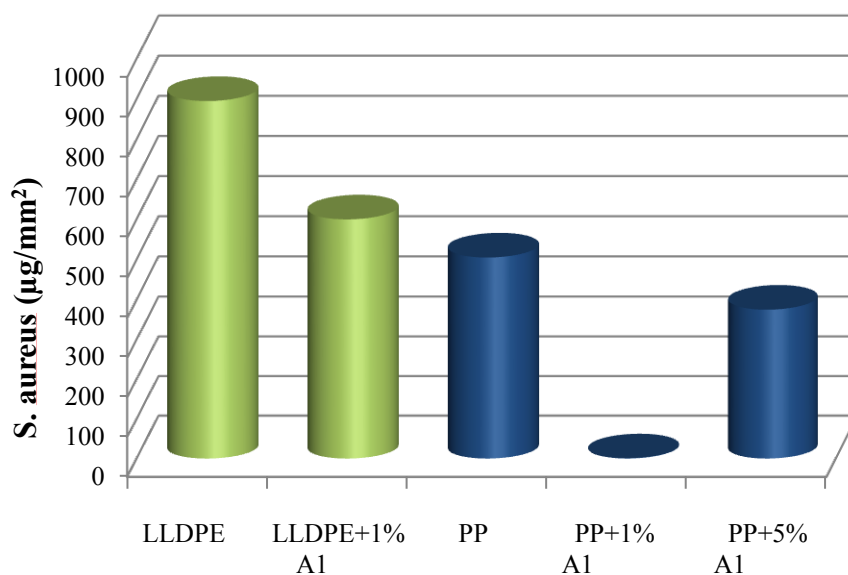


Figure 9.22. Antimicrobial activity of PP/A1 and LLDPE/A1 films against *S. aureus*

PP films at 5% of A1 showed a lower activity than the PP films at 1% of azo compound. This reduction in activity was probably due to the decomposition of the active system, as was evident from the dark color of the produced films (as described in section 9.4.1). For LLDPE matrix, the film surface was quite rough, which could explain the different behavior of this material during the microbiological tests. Similarly to the PP system, the active LLDPE film with 5% of A1 also shows degradation; therefore, it was not microbiological tested.

9.7.2. Antimicrobial results for azo/biodegradable films

We analyzed the inhibition of *Staphylococcus* or *Candida* biofilms formation on biodegradable films by staining with crystal violet.

For PVA and Mater-Bi it was not possible to proceed with standard antimicrobial tests, because the films are water soluble.

Analyzed films were:

- PLA4060D with 10% Tween 80 by solvent casting
- PLA4060D/4032D with 10% Tween 80 by solvent casting

- PLA4032D by mold casting.

We tested films with 0.01%, 0.05% and 0.1% of A3, A4 and A5 and we used as blank the polymeric films without azo compound. The protocol was the same used for PP-based films.

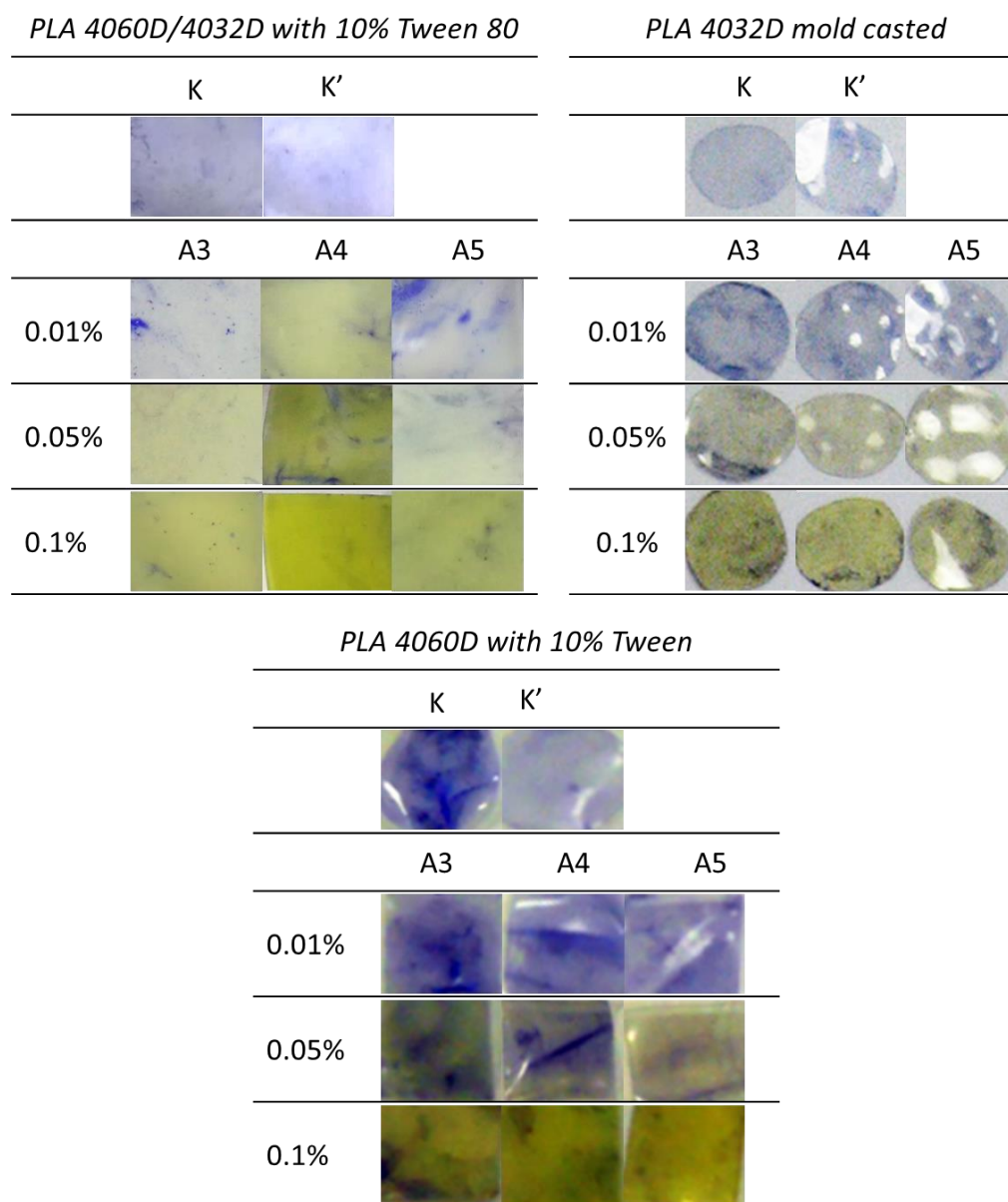


Figure 9.23. *S. aureus* biofilms formation on PLA film
K = positive control, *K'* = negative control

Figure 9.23 shows that the formation of *S. aureus* colonies on the polymer surface with 0.1% of azo compounds was completely inhibited; this is evident by the complete discoloration of these films.

In particular, the best antimicrobial agent was A4 into PLA4060D/4032D matrix, which showed complete inhibition of *S. aureus* biofilm formation even at 0.01%. For PLA4032D matrices it was very hard to discern the best antibacterial agent, all azo compounds showed partial inhibition of biofilm formation at 0.01%.

Finally, into PLA4060D matrix, A5 was the most active, showing inhibition of *S. aureus* biofilm formation at 0.05%.

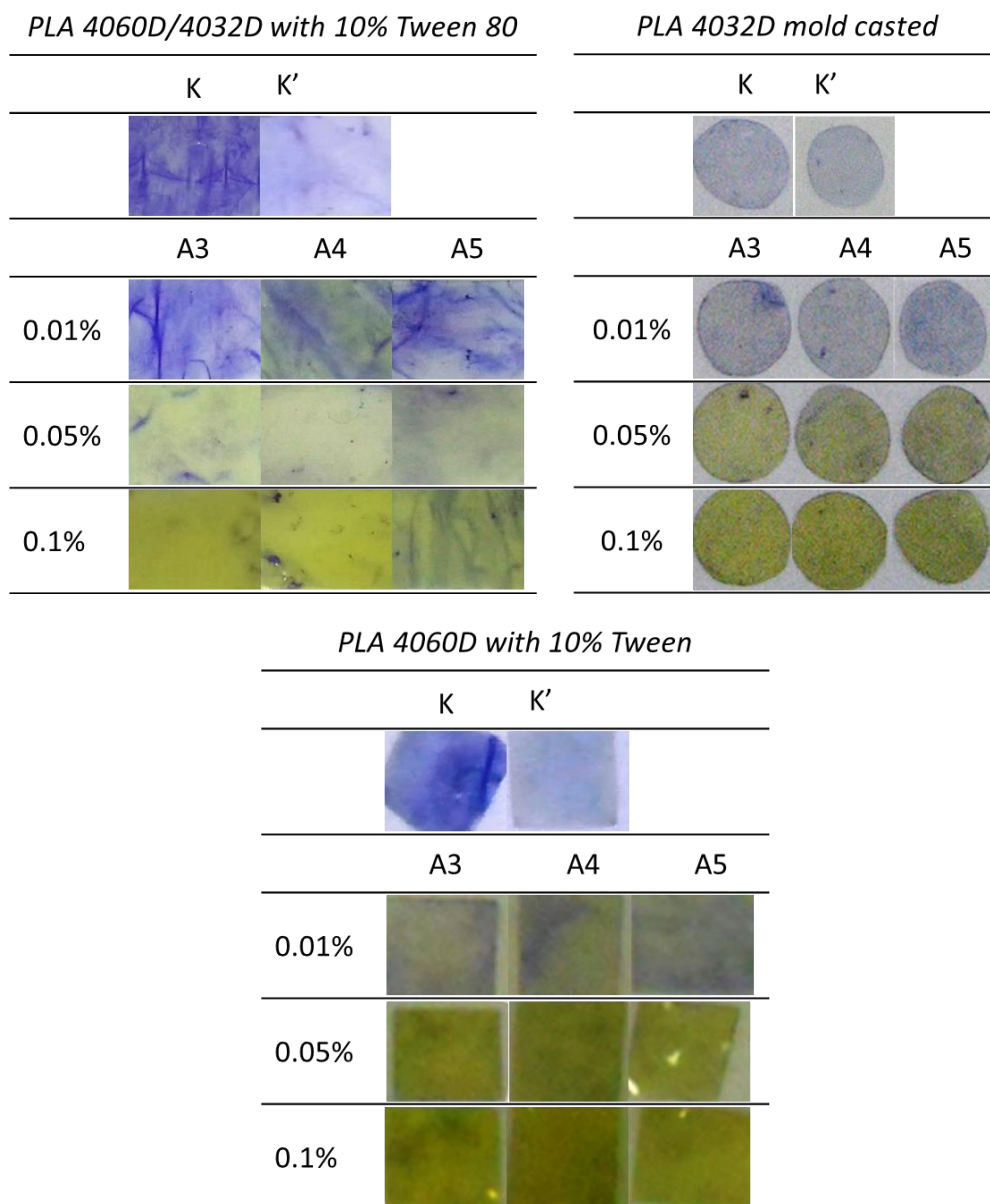


Figure 9.24 *C. albicans* biofilms formation on PLA films

K = positive control, K' = negative control

Figure 9.24 shows the results of inhibition of *C. albicans* biofilm formation on the surface of PLA-based films. For each azo compound, a good activity was observed starting from 0.05% of azo compounds.

In particular, into PLA4060D/4032D matrix, A4 showed antifungal activity even at 0.01%. Into PLA4060D matrix all azo compounds showed partially inhibition of biofilm formation at 0.01%.

9.8. Conclusions and outlook

Infections by pathogenic microorganisms are of great concern in many fields, principally in medical devices, drugs and food packaging. The overuse of conventional antibiotics has led to the development of microorganisms resistant to the most common drugs. Therefore, it is essential to develop new materials with antimicrobial activity to solve the problem of contamination by microorganisms.

I have synthesized a new class of active compounds with azobenzene structure. The compounds having the strongest bactericidal activity against Gram+ and fungi and the ability to inhibit the biofilm formation have been selected for incorporation into commercially polymeric matrices, in order to produce composites with low production cost, good processability, and antimicrobial potential. This is the first time that a novel azobenzene based antimicrobial compound has been added into polymer films.

In the beginning I have realized active antimicrobial and antifungal films using polypropylene and linear low-density polyethylene, by introducing different percentages of two antimicrobial azo dyes (A1 and A2) in polymer matrices. The polymeric materials were mold-casted and the films were tested in vitro against *S. aureus* and *C. albicans*. The films exhibited antimicrobial activity and the capability to inhibit biofilms formation of *S. aureus* and *C. albicans*. Concentration of 0.01% (w/w) permitted the preparation of active, uncolored and transparent polymers with potential applications for food packaging.

However, the same properties which make polyolefins ideal for many applications, can lead to waste disposal problems, because these materials are

not readily biodegradable. I then focused my attention to biodegradable polymers and in particular to prepare antimicrobial biodegradable biopolymers. Using solvent casting and mold casting methods, biodegradable antimicrobial materials were realized by introducing different percentages of azo compounds in poly(lactic acid), poly(vinyl alcohol) and Mater-Bi polymer matrices. In order to observe any improvements of the mechanical properties I used some plasticizers such as Tween 80 and PEG 400. The polymers have been loaded with low percentages of A3, A4 and A5 azo compounds (from 0.01% to 0.1%). The obtained thin films retained the proprieties of the pure matrices without azo compounds such as thermal proprieties, flexibility and shine; also I prepared transparent amorphous films, as confirmed by X-Ray analysis.

Antimicrobial tests were not performed on PVA films, since the aqueous solubility of the polymer makes them difficult, and tests on Mater-Bi films are currently under study. The PLA prepared films exhibited biocide activity. Preliminary tests of *S. aureus* biofilm formation on PLA films was analyzed by staining with crystal violet, showing a complete discoloration at a concentration of 0.1% of azo compounds. The best antimicrobial agent was A4 that showed a complete inhibition of *S. aureus* biofilm formation at 0.01% in PLA4060D with 10% Tween 80 prepared by solvent casting. *C. albicans* biofilm formation on PLA films was analyzed by staining with crystal violet showing a complete discoloration at a concentration of 0.05% of azo compounds.

These preliminary tests confirmed that the new materials realized in this thesis are promising for future applications in the field where an intrinsic antimicrobial ability of the material is required, like biomedical tools, antibacterial surfaces, and films for food packaging. Finally I am currently studying the azo compounds release from the polymer matrices by

spectrophotometric methods, in order to establish the stability of the prepared materials.

Appendix-a MatLab Scripts

Calculate_Charge.m

```
% This script computes the charge at three different pH 5,
7, 9 using pKa values taken from Lehninger Principles of
Biochemistry.
load pKa_value.mat
fid = fopen('AMP.txt', 'r');
fid2 = fopen('AMP_Charge.txt', 'w');
fprintf(fid2, 'Calculation of charge at pH5,7 and 9\n');
fprintf(fid2, 'sequence           pH5           pH7
pH9\n');
string = fgetl(fid)
while string ~= -1
    val5=0;
    val7=0;
    val9=0;
    peptide_length = length(string);
    for j = 1:peptide_length
        switch string(j)
            case ('K')
                val5=val5 + 10.^10.5/(10.^10.5+ 10^5);
                val7=val7 + 10.^10.5/(10.^10.5+ 10^7);
                val9=val9 + 10.^10.5/(10.^10.5+ 10^9);
            case ('R')
                val5=val5 + 10.^12.4/(10.^12.4+ 10^5);
                val7=val7 + 10.^12.4/(10.^12.4+ 10^7);
                val9=val9 + 10.^12.4/(10.^12.4+ 10^9);
            case ('H')
                val5=val5 + 10.^6/ (10.^6+ 10^5);
                val7=val7 + 10.^6/ (10.^6+ 10^7);
                val9=val9 + 10.^6/ (10.^6+ 10^9);
            case ('Y')
                val5=val5 - 10.^5/(10.^10+ 10^5);
                val7=val7 - 10.^7/(10.^10+ 10^7);
                val9=val9 - 10.^9/(10.^10+ 10^9);
            case ('D')
                val5=val5 - 10.^5/(10.^3.86+ 10^5);
                val7=val7 - 10.^7/(10.^3.86+ 10^7);
                val9=val9 - 10.^9/(10.^3.86+ 10^9);
            case ('E')
                val5=val5 - 10.^5/(10.^4.25+ 10^5);
                val7=val7 - 10.^7/(10.^4.25+ 10^7);
                val9=val9 - 10.^9/(10.^4.25+ 10^9);
```

```
        case ('C')
            val5=val5 - 10.^5/(10.^8.33+ 10^5);
            val7=val7 - 10.^7/(10.^8.33+ 10^7);
            val9=val9 - 10.^9/(10.^8.33+ 10^9);
        end;
    end;
    val5 = val5 + 10.^9.69/(10.^9.69 + 10^5)-
    10.^5/(10.^2.34+ 10^5)
    val7 = val7 + 10.^9.69/(10.^9.69 + 10^7)-
    10.^7/(10.^2.34+ 10^7);
    val9 = val9 + 10.^9.69/(10.^9.69 + 10^9)-
    10.^9/(10.^2.34+ 10^9);
    fprintf(fid2, '%s\t\t\t%f\t%f\t%f\n', string, val5,
    val7, val9);
    string = fgetl(fid);

end;

fclose('all');
```

Calculate_Boman_index.m

```
% This script computes the Boman index in accordingly
with Journal of Internal Medicine 2003; 254: 197-215
fid = fopen('AMP.txt', 'r');
fid2 = fopen('AMP_BomanIndex.txt', 'w');
fprintf(fid2, 'Boman index of alpha AMPs\n\n');
string = fgetl(fid);
while string ~= -1

    peptide_lenght = length(string);
    temp = 0;
    bindex=0;
    for j = 1: peptide_lenght
        %         mono = 1;

            first = char(string(j));
            switch first
                case ('W')
                    aminoacidA = 2.33;
                case ('C')
                    aminoacidA = 1.28;
                case ('M')
                    aminoacidA = 2.35;
                case ('H')
                    aminoacidA = -4.66;
                case ('Y')
                    aminoacidA = -0.14;
                case ('F')
                    aminoacidA = 2.98;
                case ('Q')
                    aminoacidA = -5.54;
                case ('N')
                    aminoacidA = -6.64;
                case ('I')
                    aminoacidA = 4.92;
                case ('R')
                    aminoacidA = -14.92;
                case ('D')
                    aminoacidA = -8.72;
                case ('P')
                    aminoacidA = 0;
                case ('T')
                    aminoacidA = -2.57;
                case ('K')
                    aminoacidA = -5.55;
                case ('E')
                    aminoacidA = -6.81;
```

```
        case ('V')
            aminoacidA = 4.04;
        case ('S')
            aminoacidA = -3.40;
        case ('G')
            aminoacidA = 0.94;
        case ('A')
            aminoacidA = 1.81;
        case ('L')
            aminoacidA = 4.92;
    end;
    temp = temp + aminoacidA;

end;

bindex = -temp/ peptide_lenght;
fprintf(fid2, '%f\t%s\n', bindex, string);
string = fgetl(fid);

end;

fclose('all');
```

Calculate_HydrophobicityMoment_Flexibility.m

```
% This script computes the mean hydrophobicity and the
hydrophobic moment in accordingly with Faraday Symp. Chem.
Soc., 1982, 17, 109-120.
% In addition it computes the Flexibility value in
accordingly with Angew. Chem. Int. Ed. 2003, 42, 2269 -
2272.
load string_Hydrophobicity
fid = fopen('AMP.txt', 'r');
fid2 = fopen('AMP_HydrophobicMoment.txt', 'w');
fid3 = fopen('AMP_Flexibility.txt', 'w');
fprintf(fid2, 'Hydrophobic moments of alpha AMPs\n');
fprintf(fid2, 'length      h_mom_a      mean_hm_a
h_mom_b      mean_hm_b      h_mom_c      mean_hm_c\n');
fprintf(fid3, 'Flexibility of alpha AMPs\n');

string = fgetl(fid);
while string ~= -1
    hxa=0;
    hxb=0;
    hxc=0;
    hya=0;
    hyb=0;
    hyc=0;
    flex=0;
    peptide_length = length(string);
    for j = 1:peptide_length
        s = sin(1.7453*j);
        c = cos(1.7453*j);
        switch string(j)
            case ('A')
                hxa=hxa+c*values(1,1);
                hya=hya+s*values(1,1);
                hxb=hxb+c*values(1,2);
                hyb=hyb+s*values(1,2);
                hxc=hxc+c*values(1,3);
                hyc=hyc+s*values(1,3);
                flex= flex+18;
            case ('R')
                hxa=hxa+c*values(2,1);
                hya=hya+s*values(2,1);
                hxb=hxb+c*values(2,2);
                hyb=hyb+s*values(2,2);
                hxc=hxc+c*values(2,3);
                hyc=hyc+s*values(2,3);
                flex= flex+4.6;
            case ('N')
```

```
hxa=hxa+c*values(3,1);
hya=hya+s*values(3,1);
hxb=hxb+c*values(3,2);
hyb=hyb+s*values(3,2);
hxc=hxc+c*values(3,3);
hyc=hyc+s*values(3,3);
flex= flex+20;
case ('D')
hxa=hxa+c*values(4,1);
hya=hya+s*values(4,1);
hxb=hxb+c*values(4,2);
hyb=hyb+s*values(4,2);
hxc=hxc+c*values(4,3);
hyc=hyc+s*values(4,3);
flex= flex+20;
case ('C')
hxa=hxa+c*values(5,1);
hya=hya+s*values(5,1);
hxb=hxb+c*values(5,2);
hyb=hyb+s*values(5,2);
hxc=hxc+c*values(5,3);
hyc=hyc+s*values(5,3);
flex= flex+20;    % estimated by
comparison with Ser
case ('Q')
hxa=hxa+c*values(6,1);
hya=hya+s*values(6,1);
hxb=hxb+c*values(6,2);
hyb=hyb+s*values(6,2);
hxc=hxc+c*values(6,3);
hyc=hyc+s*values(6,3);
flex= flex+7.2;
case ('E')
hxa=hxa+c*values(7,1);
hya=hya+s*values(7,1);
hxb=hxb+c*values(7,2);
hyb=hyb+s*values(7,2);
hxc=hxc+c*values(7,3);
hyc=hyc+s*values(7,3);
flex= flex+8.2;
case ('G')
hxa=hxa+c*values(8,1);
hya=hya+s*values(8,1);
hxb=hxb+c*values(8,2);
hyb=hyb+s*values(8,2);
hxc=hxc+c*values(8,3);
hyc=hyc+s*values(8,3);
flex= flex+39;
```



```
case ('H')
    hxa=hxa+c*values(9,1);
    hya=hya+s*values(9,1);
    hxb=hxb+c*values(9,2);
    hyb=hyb+s*values(9,2);
    hxc=hxc+c*values(9,3);
    hyc=hyc+s*values(9,3);
    flex= flex+4.8;
case ('I')
    hxa=hxa+c*values(10,1);
    hya=hya+s*values(10,1);
    hxb=hxb+c*values(10,2);
    hyb=hyb+s*values(10,2);
    hxc=hxc+c*values(10,3);
    hyc=hyc+s*values(10,3);
    flex= flex+2.3;
case ('L')
    hxa=hxa+c*values(11,1);
    hya=hya+s*values(11,1);
    hxb=hxb+c*values(11,2);
    hyb=hyb+s*values(11,2);
    hxc=hxc+c*values(11,3);
    hyc=hyc+s*values(11,3);
    flex= flex+10;
case ('K')
    hxa=hxa+c*values(12,1);
    hya=hya+s*values(12,1);
    hxb=hxb+c*values(12,2);
    hyb=hyb+s*values(12,2);
    hxc=hxc+c*values(12,3);
    hyc=hyc+s*values(12,3);
    flex= flex+3.4;
case ('M')
    hxa=hxa+c*values(13,1);
    hya=hya+s*values(13,1);
    hxb=hxb+c*values(13,2);
    hyb=hyb+s*values(13,2);
    hxc=hxc+c*values(13,3);
    hyc=hyc+s*values(13,3);
    flex = flex+ 7; % intermediate value
between L and K
case ('F')
    hxa=hxa+c*values(14,1);
    hya=hya+s*values(14,1);
    hxb=hxb+c*values(14,2);
    hyb=hyb+s*values(14,2);
    hxc=hxc+c*values(14,3);
    hyc=hyc+s*values(14,3);
```

```

flex= flex+7.6;
case ('P')
  hxa=hxa+c*values(15,1);
  hya=hya+s*values(15,1);
  hxb=hxb+c*values(15,2);
  hyb=hyb+s*values(15,2);
  hxc=hxc+c*values(15,3);
  hyc=hyc+s*values(15,3);
  flex= flex+0.1;
case ('S')
  hxa=hxa+c*values(16,1);
  hya=hya+s*values(16,1);
  hxb=hxb+c*values(16,2);
  hyb=hyb+s*values(16,2);
  hxc=hxc+c*values(16,3);
  hyc=hyc+s*values(16,3);
  flex= flex+25;
case ('T')
  hxa=hxa+c*values(17,1);
  hya=hya+s*values(17,1);
  hxb=hxb+c*values(17,2);
  hyb=hyb+s*values(17,2);
  hxc=hxc+c*values(17,3);
  hyc=hyc+s*values(17,3);
  flex= flex+11;
case ('W')
  hxa=hxa+c*values(18,1);
  hya=hya+s*values(18,1);
  hxb=hxb+c*values(18,2);
  hyb=hyb+s*values(18,2);
  hxc=hxc+c*values(18,3);
  hyc=hyc+s*values(18,3);
  flex = flex+8; % estimated by comparison
with Phe
case ('Y')
  hxa=hxa+c*values(19,1);
  hya=hya+s*values(19,1);
  hxb=hxb+c*values(19,2);
  hyb=hyb+s*values(19,2);
  hxc=hxc+c*values(19,3);
  hyc=hyc+s*values(19,3);
  flex = flex+8; % estimated by comparison
with Phe
case ('V')
  hxa=hxa+c*values(20,1);
  hya=hya+s*values(20,1);
  hxb=hxb+c*values(20,2);
  hyb=hyb+s*values(20,2);

```

```
        hxc=hxc+c*values(20,3);
        hyc=hyc+s*values(20,3);
        flex= flex+3;
    end;
end;
flex = flex/peptide_lenght;
hydro_moment_a = sqrt(hxa*hxa + hya*hya);
mean_hydro_moment_a = hydro_moment_a/peptide_lenght;
hydro_moment_b = sqrt(hxb*hxb + hyb*hyb);
mean_hydro_moment_b = hydro_moment_b/peptide_lenght;
hydro_moment_c = sqrt(hxc*hxc + hyc*hyc);
mean_hydro_moment_c = hydro_moment_c/peptide_lenght;
fprintf(fid2,
'%d\t\t\t%f\t%f\t%f\t%f\t%f\t%s\n',peptide_lenght,
hydro_moment_a, mean_hydro_moment_a, hydro_moment_b,
mean_hydro_moment_b, hydro_moment_c, mean_hydro_moment_c,
string);
    fprintf(fid3, '%f\n', flex);
    string = fgetl(fid);

end;

fclose('all');
```

Parsing_Helicity_prediction.m

```
% This script produces the Helicity prediction values
after computing by DSC algorithm presents in Discovery
Studio from Accelrys.
fid = fopen('yadamp-DscPrediction.txt', 'r');
fid2 = fopen('AMP_Helicitiy.txt','w');
fprintf(fid2, 'Helicity prediction\n\n');
string = fgetl(fid);
number = 0;
j=1;
flag = 0;
tot = 0;
while string ~= -1
    string = fgetl(fid);
    peptide_lenght = 0;
    if string
        if string(1) == 'D'
            string = fgetl(fid);
            for i= 14:67
                number = double(string(i));
                if number <= 32
                    flag =0;

                else
                    peptide_lenght = peptide_lenght +1;
                    tot = tot + number-48;
                    flag = 0;
                end
            end
            tot = tot/ (peptide_lenght);
            fprintf(fid2, '%f\t%s\n', tot, string);
            tot =0;
            flag = 0;
        end
    end
end
fclose('all');
```

Calculate_InstabilityIndex.m

```
% This script computes the Instability index in
accordingly with Protein Engineering vol.4 no.2 pp.155-
161. 1990.
load aminoacids_instability.mat
load instability_matrix.mat
fid = fopen('AMP.txt', 'r');
fid2 = fopen('AMP_InstabilityIndex.txt', 'w');
fprintf(fid2, 'Instability index of alpha AMPs\n\n');
string = fgetl(fid);

while string ~= -1
    iindex=0;
    temp=0;

    peptide_lenght = length(string);

    dimers = nmercount(string, 2);
    dimers_number = length(dimers);

    for j = 1:dimers_number

        dimer = sscanf(char(dimers(j)), '%c');
        first = char(dimer(1));
        switch first
            case ('W')
                aminoacidA = 1;
            case ('C')
                aminoacidA = 2;
            case ('M')
                aminoacidA = 3;
            case ('H')
                aminoacidA = 4;
            case ('Y')
                aminoacidA = 5;
            case ('F')
                aminoacidA = 6;
            case ('Q')
                aminoacidA = 7;
            case ('N')
                aminoacidA = 8;
            case ('I')
                aminoacidA = 9;
            case ('R')
                aminoacidA = 10;
            case ('D')
                aminoacidA = 11;
```

```
case ('P')
    aminoacidA = 12;
case ('T')
    aminoacidA = 13;
case ('K')
    aminoacidA = 14;
case ('E')
    aminoacidA = 15;
case ('V')
    aminoacidA = 16;
case ('S')
    aminoacidA = 17;
case ('G')
    aminoacidA = 18;
case ('A')
    aminoacidA = 19;
case ('L')
    aminoacidA = 20;
end;
temp(1) = aminoacidA;
second = char(dimer(2));
switch second
case ('W')
    aminoacidA = 1;
case ('C')
    aminoacidA = 2;
case ('M')
    aminoacidA = 3;
case ('H')
    aminoacidA = 4;
case ('Y')
    aminoacidA = 5;
case ('F')
    aminoacidA = 6;
case ('Q')
    aminoacidA = 7;
case ('N')
    aminoacidA = 8;
case ('I')
    aminoacidA = 9;
case ('R')
    aminoacidA = 10;
case ('D')
    aminoacidA = 11;
case ('P')
    aminoacidA = 12;
case ('T')
    aminoacidA = 13;
```

```
        case ('K')
            aminoacidA = 14;
        case ('E')
            aminoacidA = 15;
        case ('V')
            aminoacidA = 16;
        case ('S')
            aminoacidA = 17;
        case ('G')
            aminoacidA = 18;
        case ('A')
            aminoacidA = 19;
        case ('L')
            aminoacidA = 20;
    end;
    temp(2) = aminoacidA;
    iindex = iindex + INSTMATRIX(temp(1),temp(2));
end;
iindex = 10/peptide_lenght*iindex;

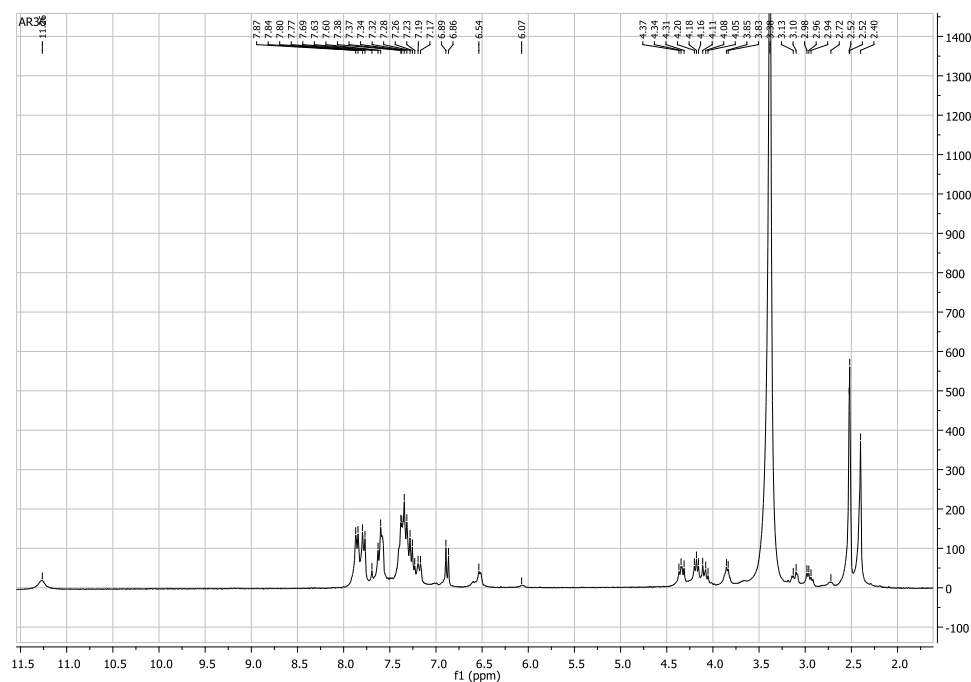
fprintf(fid2, '%f\t%s\n', iindex, string);
string = fgetl(fid);

end;

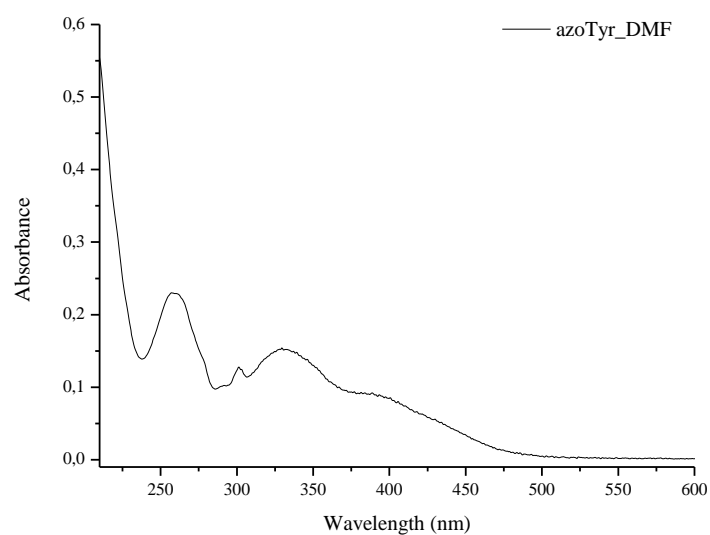
fclose('all');
```


Appendix-b Fmoc-azoTyr characterization

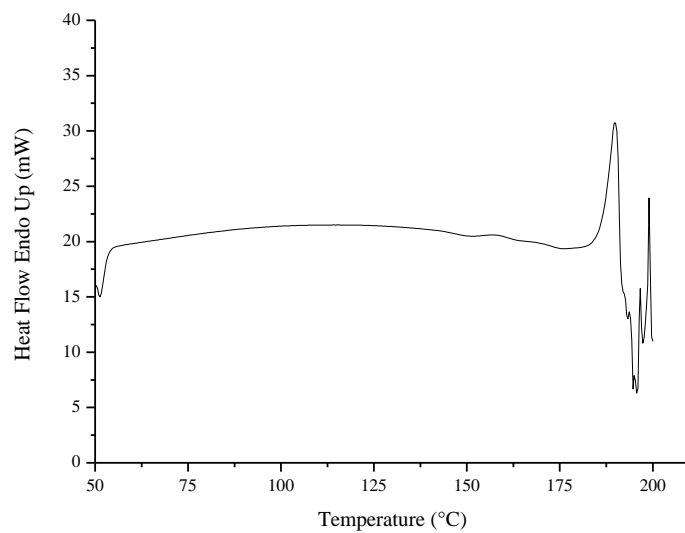
^1H NMR of Azo-amino acid 3-(p-tolyldiazenyl)-N-Fmoc-tyrosine in DMSO-d_6



UV-Vis spectrum of Fmoc-azoTyr in DMF



Thermal behavior of Fmoc-azoTyr, from DSC analysis, 10 °C/min, nitrogen flow



Appendix-c Dynamic light scattering results

Dynamic light scattering results for POPC/POPG (90:10) vesicles 0.1 mM. Measurements were repeated on the same sample for one month to estimate vesicles stability.

Sample Name	Measurements day	Z-Ave (d.nm)	Average	St. Dev.	PdI	Average
POPC/POPG_ MES pH = 5 0.1mM_1	1st day	110.2	107.5	2.570	0.059	0.0537
POPC/POPG_ MES pH = 5 0.1mM_2		107.1			0.053	
POPC/POPG_ MES pH = 5 0.1mM_3		105.1			0.049	
POPC/POPG_ MES pH = 5 0.1mM_1	2nd day	109.5	108.1	1.692	0.075	0.0493
POPC/POPG_ MES pH = 5 0.1mM_2		108.5			0.024	
POPC/POPG_ MES pH = 5 0.1mM_3		106.2			0.049	

Sample Name	Measurements day	Z-Ave (d.nm)	Average	St. Dev.	PdI	Average
POPC/POPG_ MES pH = 5 0.1mM_1	5th day	107.3	107.1	0.153	0.033	0.0423
POPC/POPG_ MES pH = 5 0.1mM_2		107			0.049	
POPC/POPG_ MES pH = 5 0.1mM_3		107.1			0.045	
POPC/POPG_ MES pH = 5 0.1mM_1	8th day	109.4	108.0	1.290	0.041	0.0340
POPC/POPG_ MES pH = 5 0.1mM_2		107.6			0.026	
POPC/POPG_ MES pH = 5 0.1mM_3		106.9			0.035	
POPC/POPG_ MES pH = 5 0.1mM_1	11th day	106.3	107.3	0.954	0.056	0.0437
POPC/POPG_ MES pH = 5 0.1mM_2		107.4			0.042	
POPC/POPG_ MES pH = 5 0.1mM_3		108.2			0.033	

Sample Name	Measurements day	Z-Ave (d.nm)	Average	St. Dev.	PdI	Average
POPC/POPG_ MES pH = 5 0.1mM_1	14th day	110.5	108.8	1.609	0.045	0.0353
POPC/POPG_ MES pH = 5 0.1mM_2		107.3			0.029	
POPC/POPG_ MES pH = 5 0.1mM_3		108.6			0.032	
POPC/POPG_ MES pH = 5 0.1mM_1	21th day	106.5	108.2	1.553	0.061	0.0517
POPC/POPG_ MES pH = 5 0.1mM_2		108.7			0.054	
POPC/POPG_ MES pH = 5 0.1mM_3		109.5			0.04	

Sample Name	Measurements day	Z-Ave (d.nm)	Average	St. Dev.	Pdl	Average
POPC/POPG_ MES pH = 5 0.1mM_1	25th day	108.4	107.0	1.721	0.036	0.0463
POPC/POPG_ MES pH = 5 0.1mM_2		107.6			0.061	
POPC/POPG_ MES pH = 5 0.1mM_3		105.1			0.042	
POPC/POPG_ MES pH = 5 0.1mM_1	30th day	111.2	108.6	2.957	0.054	0.0713
POPC/POPG_ MES pH = 5 0.1mM_2		109.3			0.089	
POPC/POPG_ MES pH = 5 0.1mM_3		105.4			0.071	

Dynamic light scattering results for POPC (9:1) vesicles 0.1 mM.

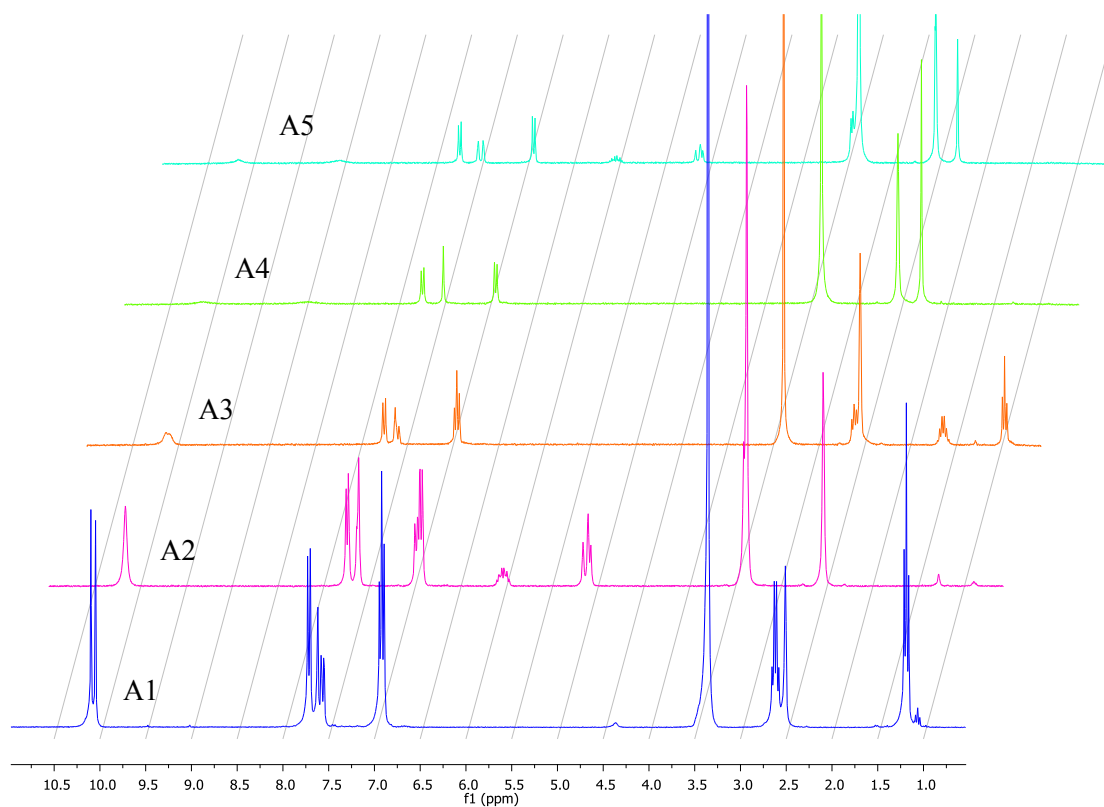
Measurements were repeated on the same sample for one month to estimate vesicles stability.

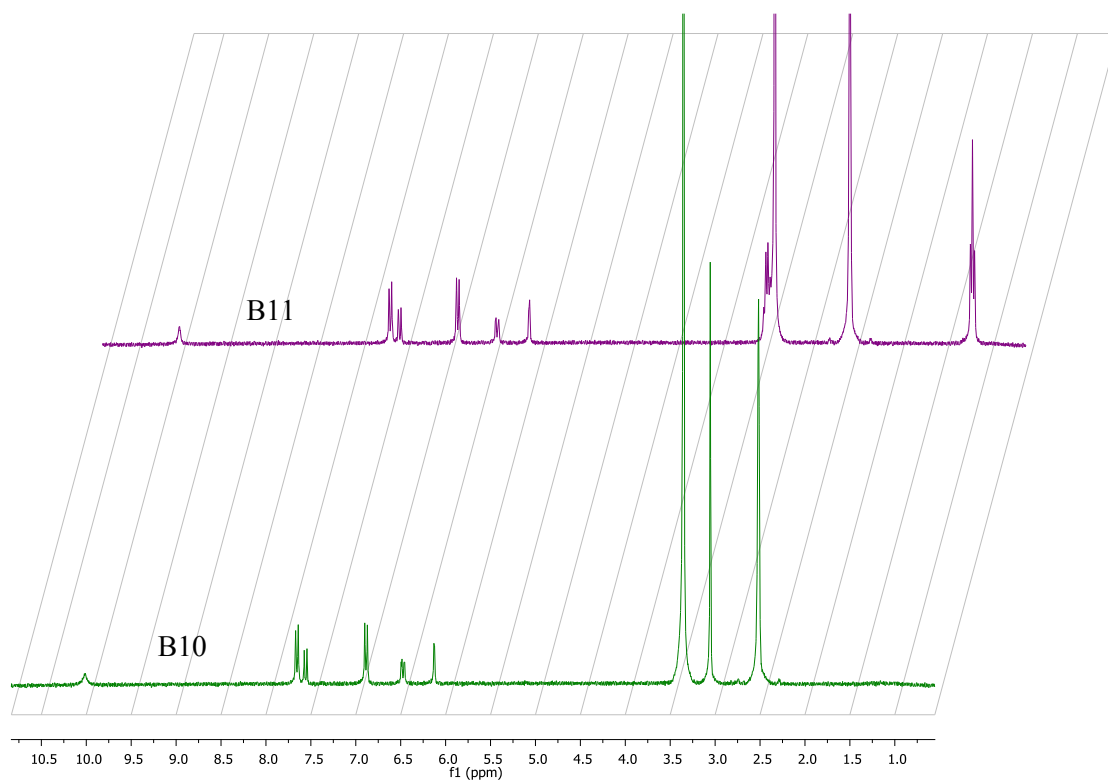
Sample Name	Measurements day	Z-Ave (d.nm)	Average	St. Dev.	PdI	Average
MESpH5_POP C 0.1mM_1	1st Day	124.2	122.4	1.626	0.088	0.077
MESpH5_POP C 0.1mM_2		121.8			0.103	
MESpH5_POP C 0.1mM_3		121.1			0.04	
MESpH5_POP C 0.1mM_1	4th Day	117.2	116.1	1.007	0.076	0.085
MESpH5_POP C 0.1mM_2		116			0.099	
MESpH5_POP C 0.1mM_3		115.2			0.079	
MESpH5_POP C 0.1mM_1	6th Day	117.3	115.6	1.513	0.084	0.077
MESpH5_POP C 0.1mM_2		114.4			0.086	
MESpH5_POP C 0.1mM_3		115.1			0.061	
MESpH5_POP C 0.1mM_1	11th Day	118	116.0	1.758	0.07	0.069
MESpH5_POP C 0.1mM_2		115.3			0.067	
MESpH5_POP C 0.1mM_3		114.7			0.07	

Sample Name	Measurements day	Z-Ave (d.nm)	Average	St. Dev.	PdI	Average
MESpH5_POP C 0.1mM_1	14th Day	114.7	113.5	1.124	0.096	0.080
MESpH5_POP C 0.1mM_2		113.2			0.076	
MESpH5_POP C 0.1mM_3		112.5			0.068	
MESpH5_POP C 0.1mM_1	21th day	115.6	117.3	1.493	0.056	0.067
MESpH5_POP C 0.1mM_2		118.4			0.078	
MESpH5_POP C 0.1mM_3		117.9			0.068	
MESpH5_POP C 0.1mM_1	25th day	115.6	114.9	2.274	0.047	0.069
MESpH5_POP C 0.1mM_2		112.4			0.084	
MESpH5_POP C 0.1mM_3		116.8			0.076	
MESpH5_POP C 0.1mM_1	30th day	114.6	115.7	1.345	0.041	0.044
MESpH5_POP C 0.1mM_2		117.2			0.058	
MESpH5_POP C 0.1mM_3		115.3			0.033	

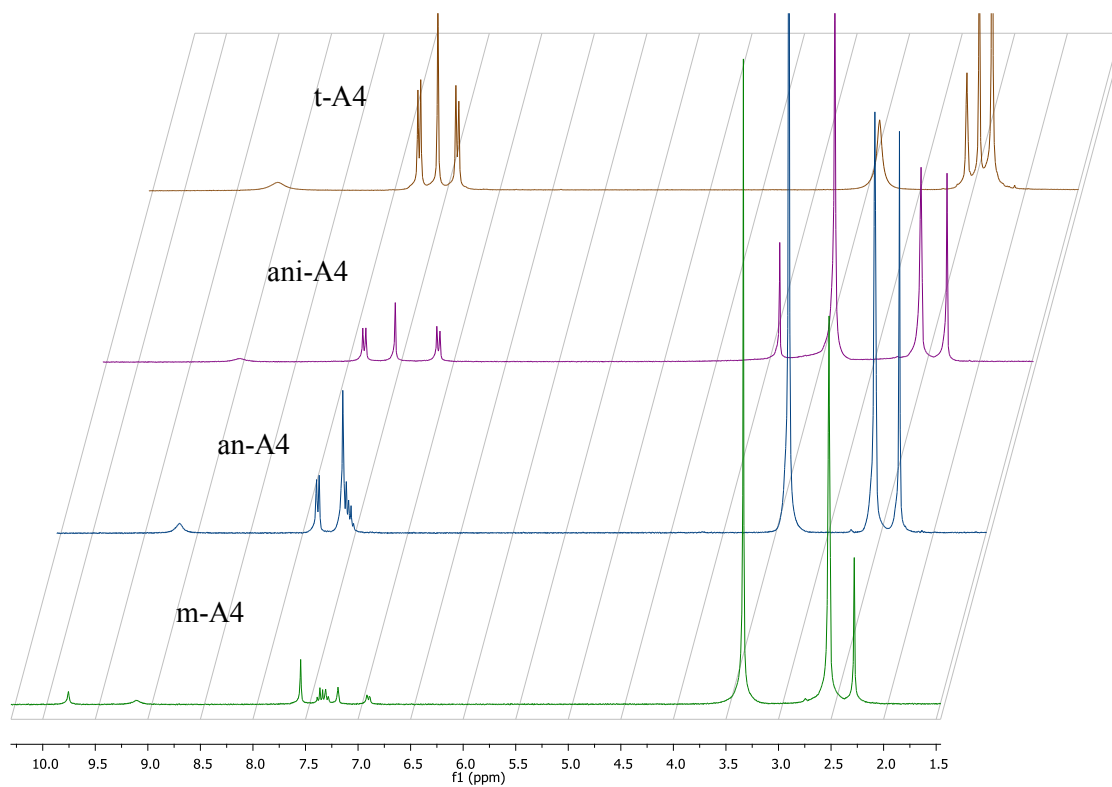
Appendix-d ^1H NMR spectra of azo compounds

^1H NMR of A1, A2, A3, A4, A5 in DMSO-d_6

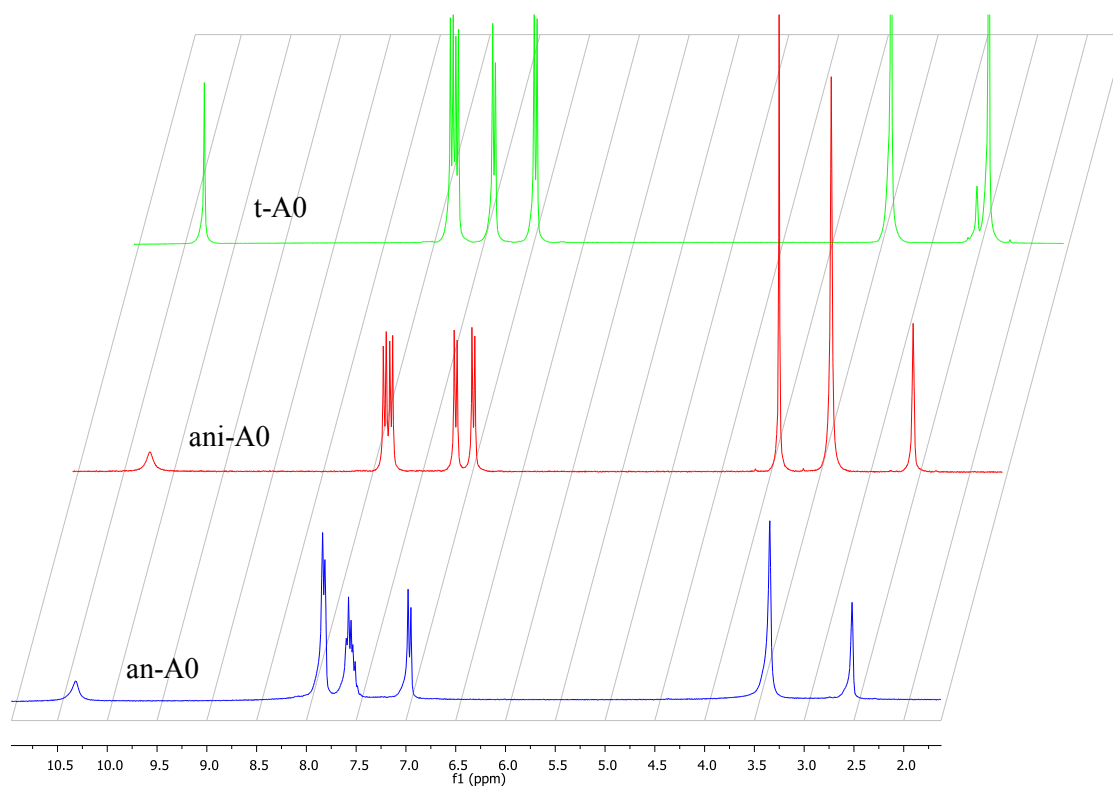


^1H NMR of B10 and B11 in DMSO- d_6 

^1H NMR of m-A4, an-A4, ani-A4, t-A4 in DMSO-d_6

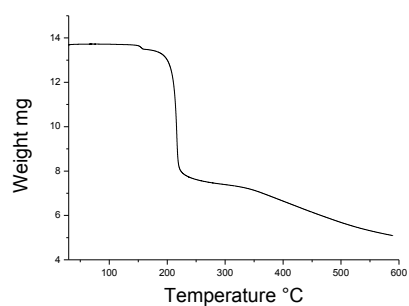


^1H NMR of an-A0, ani-A0, t-A0 in DMSO-d_6

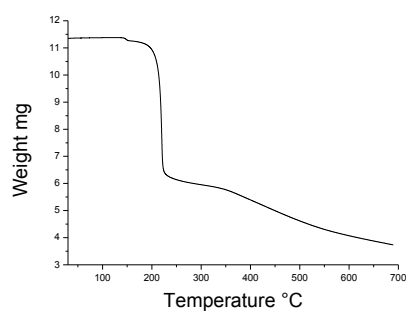


Appendix-e Thermogravimetric characterization of azo compounds

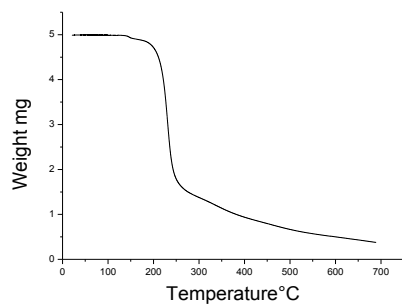
TGA thermogram A1



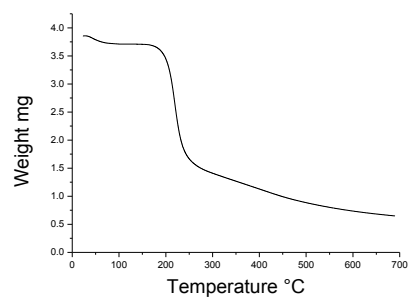
TGA thermogram A2



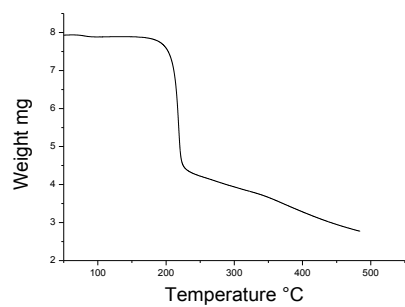
TGA thermogram A3



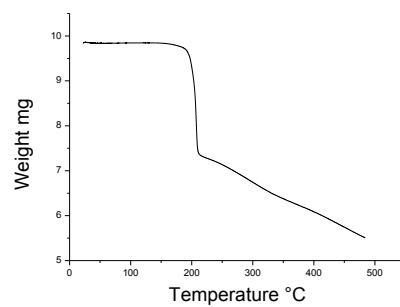
TGA thermogram A4



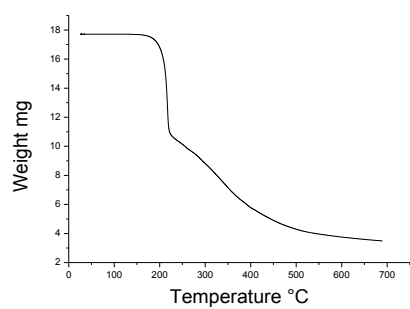
TGA thermogram A5



TGA thermogram B10

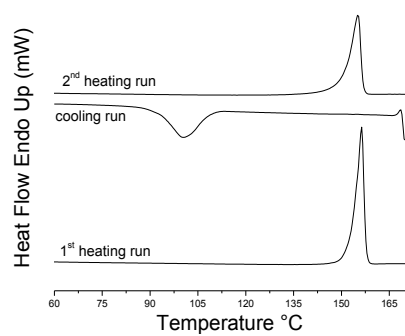


TGA thermogram B11

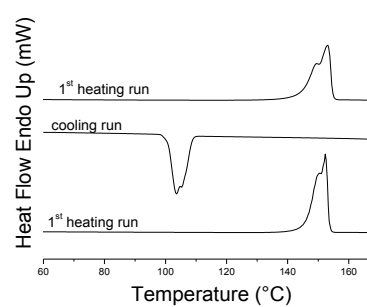


Appendix-f Thermal characterization of azo compounds

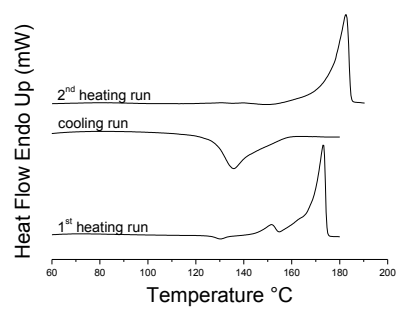
DSC thermogram of A1



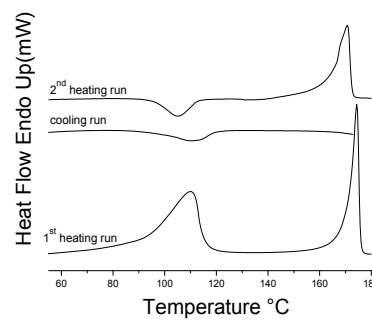
DSC thermogram of A2



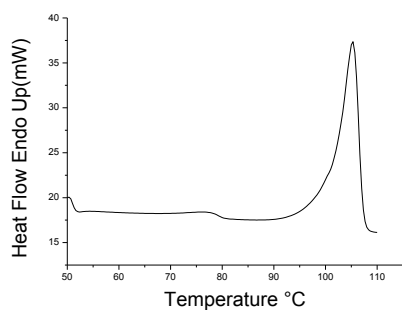
DSC thermogram of A3



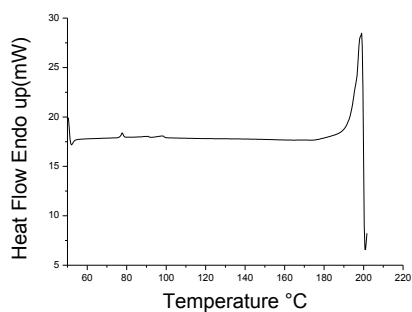
DSC thermogram of A4



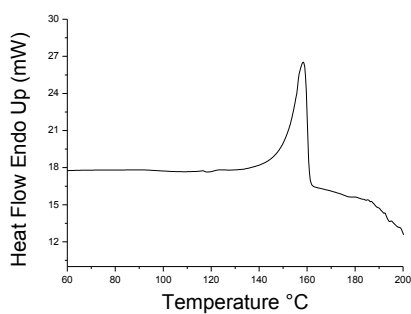
DSC thermogram of A5



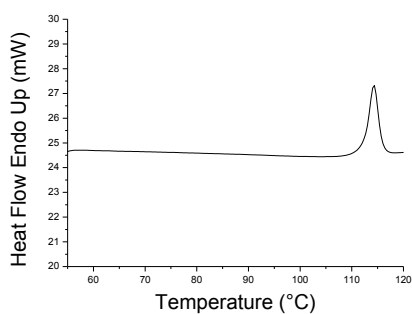
DSC thermogram of B10



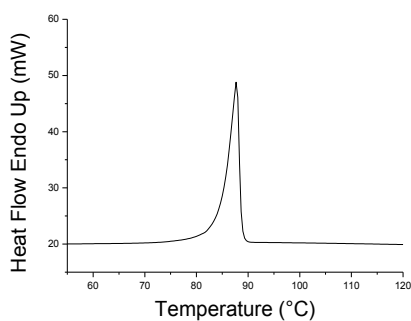
DSC thermogram of B11



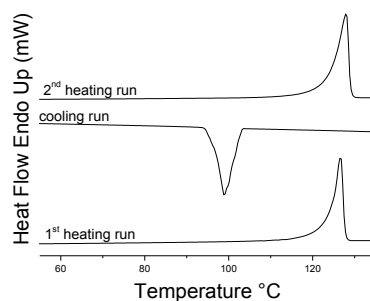
DSC thermogram of m-A4



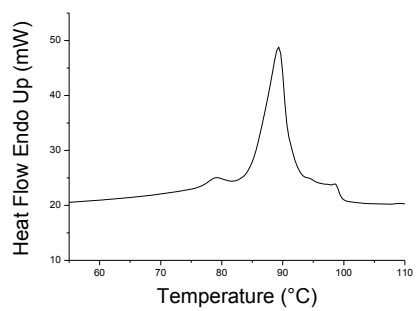
DSC thermogram of an-A4



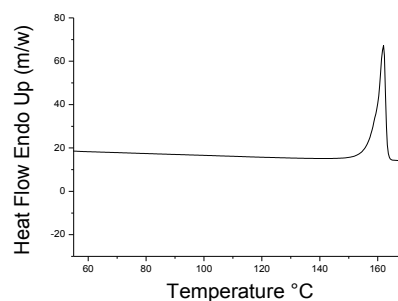
DSC thermograms of ani-A4



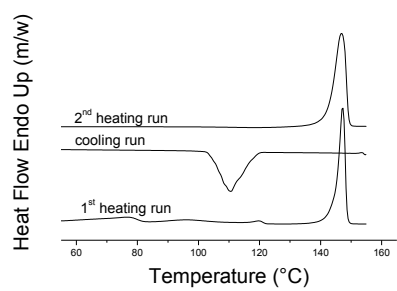
DSC thermogram of t-A4



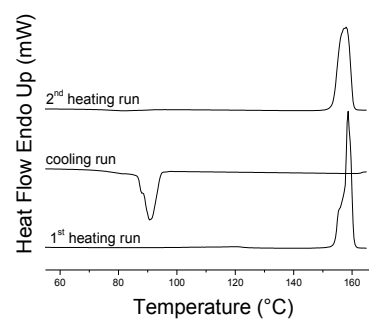
DSC thermograms of an-A0



DSC thermograms of ani-A0

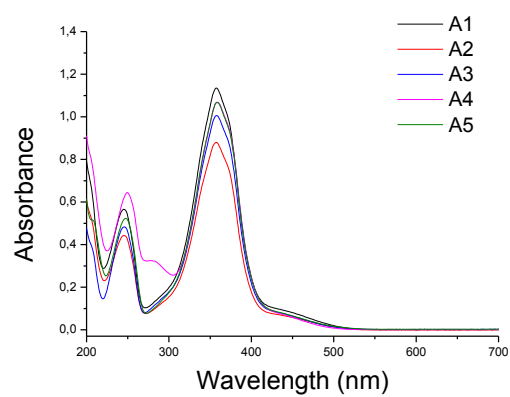


DSC thermograms of t-A0

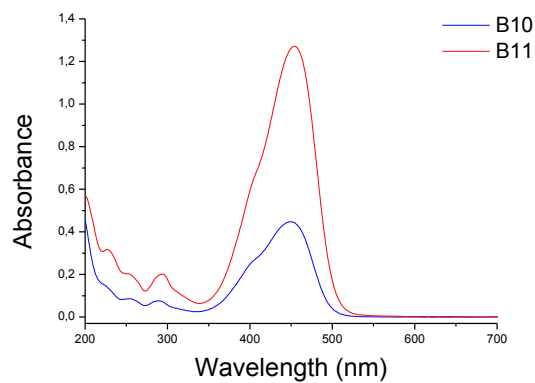


Appendix-g UV-Vis spectra of azo compounds

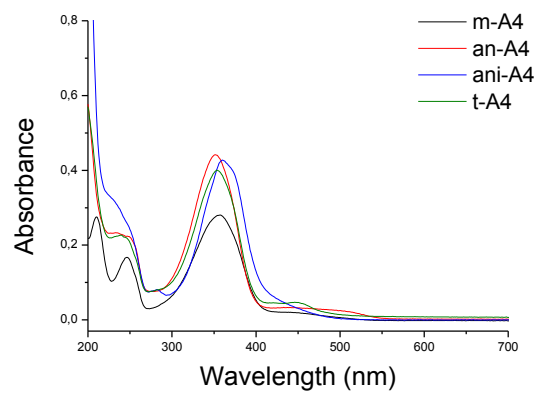
UV-Vis spectrum of A1, A2, A3, A4



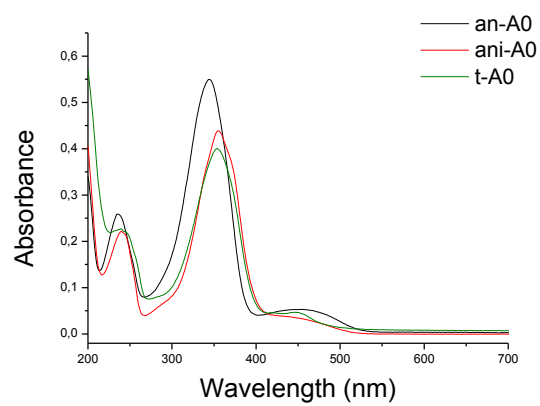
UV-Vis spectrum of B10 and B11 and A5 in acetonitrile in ethanol



UV-Vis spectrum of m-A4, an-A4, ani-A4 and t-A4 in acetonitrile

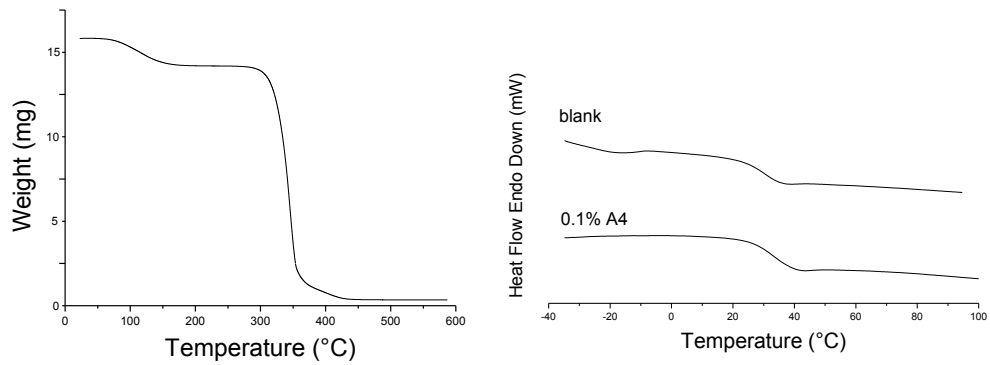


UV-Vis spectrum of an-A0, ani-A0 and t-A0 in acetonitrile

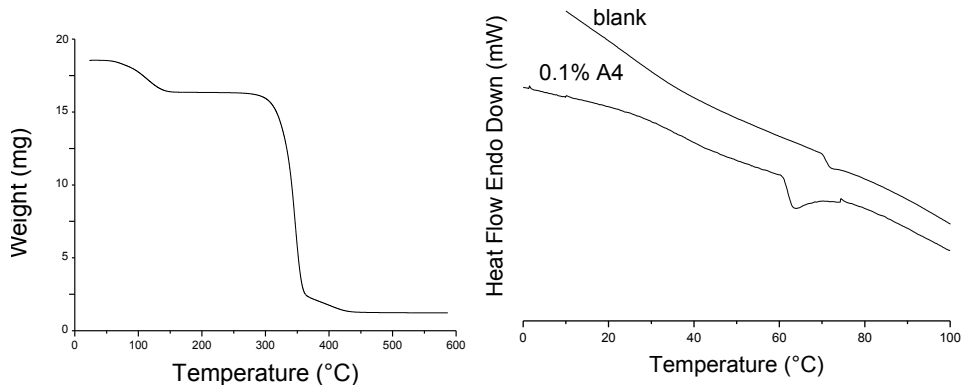


Appendix-h Thermal characterization of thin films

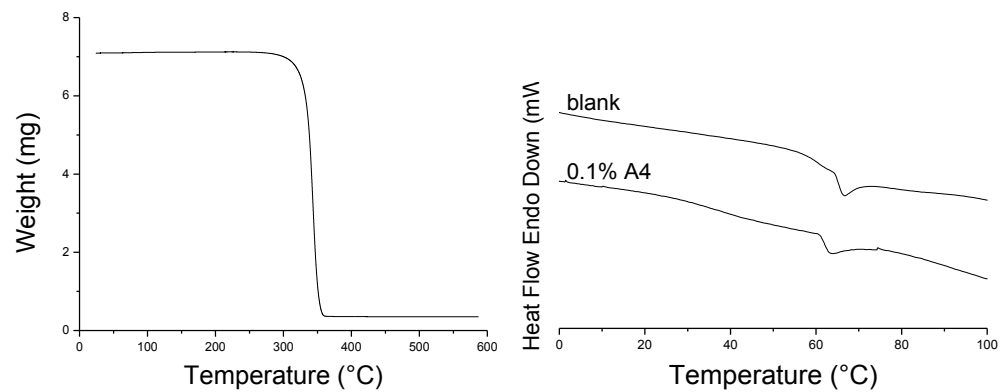
Thermograms from TGA and DSC analyses on PLA 4060D with Tween 80 and 0.1% of A4 films prepared by solvent casting:



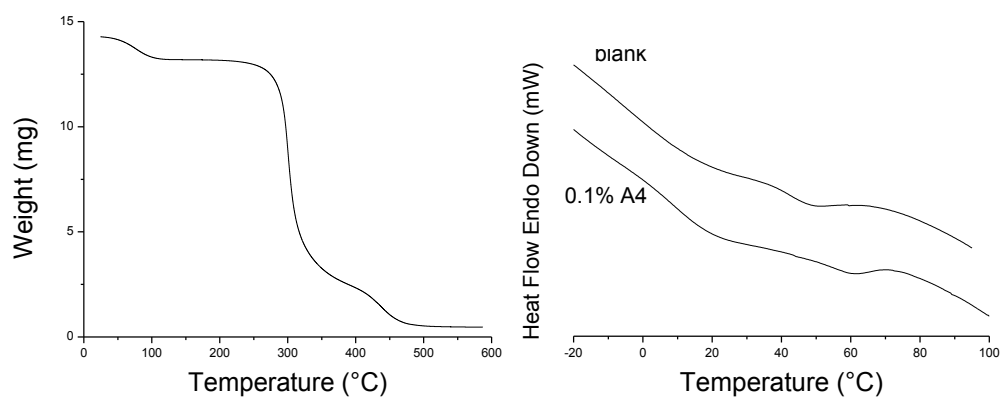
Thermograms from TGA and DSC analyses on PLA 4060D/4032D with Tween 80 and 0.1% of A4 prepared by solvent casting



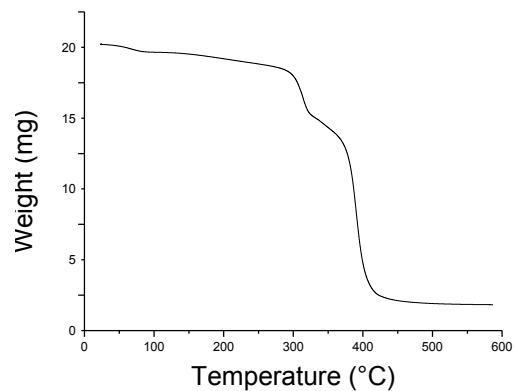
Thermograms from TGA and DSC analyses on PLA4032D and 0.1% of A4 prepared by mold casting



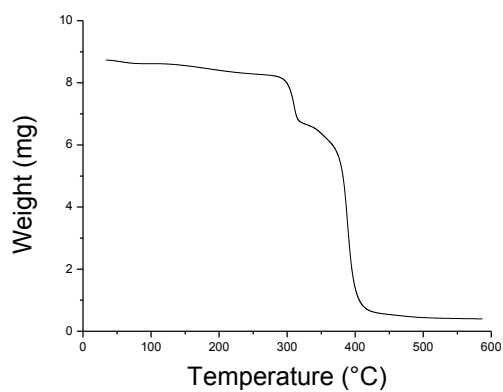
Thermograms from TGA and DSC analyses on of PVA with PEG 400 and 0.1% of A4 prepared by solvent casting



Thermogram from TGA of Mater-Bi CF03A with PEG 400 and 0.1% of A4 prepared by solvent casting



Thermogram from TGA of Mater-Bi CF03A with 0.1% of A4 prepared by mold casting method



Abbreviations, Acronyms and Symbols

$^1\text{H NMR}$	Proton Nuclear magnetic resonance
A1	4'-hydroxy-(4-hydroxy-3-ethyl)-azobenzene
A2	4'-hydroxy-(4-hydroxy-3-allyl)-azobenzene
$A_{280\text{nm}}$	Absorbance measured at 280 nm
A3	4'-hydroxy-(4-hydroxy-3-propyl)-azobenzene
A4	4'-hydroxy-(4-hydroxy-3,5-dimethyl)-azobenzene
$A_{403\text{nm}}$	Absorbance measured at 403 nm
A5	4'-hydroxy-(4-hydroxy-3-methyl-5-allyl)-azobenzene
ABC	ATP-Binding Cassette
ABTS $^{\cdot-}$	ABTS $^{2-}$ oxidation product
ABTS $^{2-}$	2,2'-Azino-bis(3-ethylbenzothiazoline-6-sulfonic acid) diammonium salt
ADMET	Absorption, Distribution, Metabolism, Excretion, Toxicity
AlogP98	Logarithm of the partition coefficient between n-octanol and water
ALY	peptide used as template (ALYLAIKRR)
AMP	Antimicrobial peptide
an-A0	4'-hydroxy-azobenzene
an-A4	4-hydroxy-3,5-dimethyl-azobenzene
ani-A0	4'-hydroxy-4-methoxy-azobenzene
ani-A4	4'-methoxy-(4-hydroxy-3,5-dimethyl)-azobenzene
APD	Antimicrobial Peptide Database
Arg	Arginine (R)
azoALY	Analogue of ALY peptide with azo-amino-acid into sequence
azoPhe	Phenylalanine-4'-azobenzene
B10	4'-hydroxy-(2-hydroxy-4-dimethylamino)-azobenzene

B11	4'-hydroxy-(2-hydroxy-4-diethylamino)-azobenzene
BBB	Blood Brain Barrier
BLAST	Basic Local Alignment Search Tool
CAMP	Collection of Anti-Microbial Peptides
CAP	Catabolite Activator Protein
CFU	Colony Forming Unit
CH ₃ CN	Acetonitrile
CHCl ₃	Chloroform
CL	Cardiolipin
CNS	Central Nervous System
CPP	Cell Penetrating Peptides
Cryo-TEM	Cryo Transmission Electron Microscopy
CV	Crystal Violet
CYP2D6	Cytochrome P450 2D6
d	Doublet (NMR signal)
dA414nm	Absorbance at 414 nm derivative
DCM	Dichloromethane
DIEA	N,N-Diisopropylethylamine
DiI	1,1'-Dioctadecyl-3,3,3',3'-tetramethylindocarbocyanine perchlorate
DIWV	Dipeptide Instability Weight Value
DLS	Dynamic Light Scattering
DMF	N,N-Dimethylformamide
DMSO	Dimethylsulfoxide
DMSO-d ₆	Hexadeuterodimethyl sulfoxide
DNA	Deoxyribonucleic acid
DPG	Diphosphatidylglycerol
DSC	Differential Scanning Calorimetry
DSC	Discrimination of protein Secondary structure Class

dt	Time derivative
ESI-MS	Electro Spray Ionization Mass Spectrometry
Et ₃ SiH	Triethylsilane
F1-ATPase	F1 portion of ATP synthase
FAT-VET	Freezing and thawing extruded vesicles
FDA	Food and Drug Administration
Fmoc	Fluorenylmethyloxycarbonyl chloride
Fmoc-AzoTyr	Azo-amino acid 3-(p-tolyldiazenyl)-N-Fmoc-tyrosine
GUV	Giant unilamellar vesicle
H ₂ O ₂	Hydrogen peroxide
HBTU	O-(Benzotriazol-1-yl)-N,N,N',N'-tetramethyluronium hexafluorophosphate
HCl	Hydrochloric acid
HEPES	4-(2-hydroxyethyl)-1-piperazineethanesulfonic acid
HOBt	N-Hydroxybenzotriazole
HRPC	Horseradish peroxidase isoenzyme C
ID	Identify number
II	Instability index
ITO	Indium Tin Oxide
LLDPE	Linear low-density polyethylene
LPS	Lipopolysaccharide
LUVET	Large unilamellar vesicle by extrusion techniques
Lys	Lysine (k)
m	Multiplet (NMR signal)
m-	Meta
m-A4	3'-hydroxy-(4-hydroxy-3,5-dimethyl)-azobenzene
mbar	Millibar
MDR-TB	Multidrug-resistant tuberculosis
MES	4-Morpholineethanesulfonic acid

MHB	Mueller Hinton Broth
MIC ₀	Minimum Inhibitory Concentration required to inhibit the growth of 100% of organisms
MIC ₅₀	Minimum Inhibitory Concentration required to inhibit the growth of 50% of organisms
MLP	Molecular Lipophilicity Potential
MLV	multilamellar vesicles
mM	Millimolar
MOPS	4-Morpholinepropanesulfonic acid
MRSA	Methicillin-resistant Staphylococcus aureus
mW	Molecular weight
NaHCO ₃	Sodium bicarbonate
NaNO ₂	Sodium nitrite
NaOH	Sodium hydroxide
NCBI	National Center for Biotechnology Information
nM	Nanomolar
nm	Nanometer
OD	Optical Density
p-	para-
PBS	Phosphate buffered saline
PC	Phosphatidylcholine
PDB	Protein Data Bank
PdI	Polydispersity Index
PDMS	Polydimethylsiloxane
PE	Phosphatidylethanolamine
PEG400	Polyethylene glycol 400
PG	Phosphatidylglycerol
PI	Phosphatidylinositol
pI	Isoelectric point

pKa	Negative logarithm of the ionization constant (K) of an acid
PLA	Poly(lactic acid)
pM	Picomolar
POPC	1-palmitoyl-2-oleoyl-sn-glycero-3-phosphocholine
POPG	1-palmitoyl-2-oleoyl-sn-glycero-3-phospho-(1'-rac-glycerol) (sodium salt)
PP	Polypropylene
Pro	Proline (P)
PS	Phosphatidylserine
PS	Polystyrene
PSA_2D	Polar surface area
PVA	Poly(vinyl alcohol)
QSAR	Quantitative structure-activity relationship
r_i	Inner radius
RNA	Ribonucleic acid
r_o	Outer radius
RP-HPLC	Reversed phase High performance liquid chromatography
RPMI	Roswell Park Memorial Institute
RSS	Rich Site Summary
RZ	Reinheitszahl
s	Singlet (NMR signal)
SM	Sphingomyelin
st. dev.	Standard deviation
t	Triplet (NMR signal)
t-A0	4'-hydroxy-4-methyl-azobenzene
t-A4	4'-methyl-(4-hydroxy-3,5-dimethyl)-azobenzene
T_c	Crystallization temperature
T_d	Degradation temperature
TFA	Trifluoroacetic acid

T_g	Glass transition temperature
TGA	Thermal gravimetric analysis
T_m	Melting temperature
Trp	Tryptophan (W)
Tween80	Polyoxyethylenesorbitan monooleate
XTT	2,3-bis (2-methoxy-4-nitro-5-sulfophenyl)-2H-tetrazolium-5-carboxanilide
YADAMP	Yet another database of antimicrobial peptides
YPD	Yeast Extract Peptone Dextrose
Z-Ave	Mean Particle Size
δ	NMR chemical shift (ppm)
ΔG	Free energy of binding
ΔH_c	Crystallization enthalpy
ΔH_m	Melting enthalpy
ϵ_{\max}	Molar extinction coefficient
λ_{\max}	Wavelength at the principal absorption maximum
μ_H	Hydrophobic dipole moment
μM	Micromolar
μm	Micrometer

Reference

1. ECDC/EMA, *The bacterial challenge - time to react*. *Ejhp Practice*, 2009. **15**(5): p. 15-15.
2. Marr, A.K., W.J. Gooderham, and R.E.W. Hancock, *Antibacterial peptides for therapeutic use: obstacles and realistic outlook*. *Current Opinion in Pharmacology*, 2006. **6**(5): p. 468-472.
3. Zasloff, M., *Antimicrobial peptides of multicellular organisms*. *Nature*, 2002. **415**(6870): p. 389-395.
4. Zaiou, M., *Multifunctional antimicrobial peptides: therapeutic targets in several human diseases*. *Journal of Molecular Medicine-Jmm*, 2007. **85**(4): p. 317-329.
5. Jenssen, H., P. Hamill, and R.E.W. Hancock, *Peptide antimicrobial agents*. *Clinical Microbiology Reviews*, 2006. **19**(3): p. 491-+.
6. Epanand, R.M. and H.J. Vogel, *Diversity of antimicrobial peptides and their mechanisms of action*. *Biochimica Et Biophysica Acta-Biomembranes*, 1999. **1462**(1-2): p. 11-28.
7. Brogden, K.A., *Antimicrobial peptides: Pore formers or metabolic inhibitors in bacteria?* *Nature Reviews Microbiology*, 2005. **3**(3): p. 238-250.
8. Park, C.B., et al., *Structure-activity analysis of buforin II, a histone H2A-derived antimicrobial peptide: The proline hinge is responsible for the cell-penetrating ability of buforin II*. *Proceedings of the National Academy of Sciences of the United States of America*, 2000. **97**(15): p. 8245-8250.
9. Romeo, D., et al., *Structure and bactericidal activity of an antibiotic dodecapeptide purified from bovine neutrophils*. *J Biol Chem*, 1988. **263**(20): p. 9573-5.
10. Tsai, H. and L.A. Bobek, *Human salivary histatins: promising anti-fungal therapeutic agents*. *Crit Rev Oral Biol Med*, 1998. **9**(4): p. 480-97.
11. Schroder, J.M., *The role of keratinocytes in defense against infection*. *Curr Opin Infect Dis*, 2010. **23**(2): p. 106-10.
12. Zasloff, M., *Magainins, a class of antimicrobial peptides from *Xenopus* skin: isolation, characterization of two active forms, and partial cDNA sequence of a precursor*. *Proc Natl Acad Sci U S A*, 1987. **84**(15): p. 5449-53.
13. Imura, Y., N. Choda, and K. Matsuzaki, *Magainin 2 in action: distinct modes of membrane permeabilization in living bacterial and mammalian cells*. *Biophys J*, 2008. **95**(12): p. 5757-65.

14. Zanetti, M., *The role of cathelicidins in the innate host defenses of mammals*. *Curr Issues Mol Biol*, 2005. **7**(2): p. 179-96.
15. Wang, Y.P., et al., *Snake Cathelicidin from Bungarus fasciatus Is a Potent Peptide Antibiotics*. *Plos One*, 2008. **3**(9).
16. Uzzell, T., et al., *Hagfish intestinal antimicrobial peptides are ancient cathelicidins*. *Peptides*, 2003. **24**(11): p. 1655-1667.
17. Oren, Z., et al., *Structure and organization of the human antimicrobial peptide LL-37 in phospholipid membranes: relevance to the molecular basis for its non-cell-selective activity*. *Biochem J*, 1999. **341** (Pt 3): p. 501-13.
18. Wimley, W.C., M.E. Selsted, and S.H. White, *Interactions between Human Defensins and Lipid Bilayers - Evidence for Formation of Multimeric Pores*. *Protein Science*, 1994. **3**(9): p. 1362-1373.
19. Selsted, M.E., et al., *Primary Structures of Mcp-1 and Mcp-2, Natural Peptide Antibiotics of Rabbit Lung Macrophages*. *Journal of Biological Chemistry*, 1983. **258**(23): p. 4485-4489.
20. Ganz, T., et al., *Defensins - Natural Peptide Antibiotics of Human-Neutrophils*. *Journal of Clinical Investigation*, 1985. **76**(4): p. 1427-1435.
21. Tang, Y.Q., et al., *A cyclic antimicrobial peptide produced in primate leukocytes by the ligation of two truncated alpha-defensins*. *Science*, 1999. **286**(5439): p. 498-502.
22. Hancock, R.E.W. and A. Rozek, *Role of membranes in the activities of antimicrobial cationic peptides*. *Fems Microbiology Letters*, 2002. **206**(2): p. 143-149.
23. Yeaman, M.R. and N.Y. Yount, *Mechanisms of antimicrobial peptide action and resistance*. *Pharmacol Rev*, 2003. **55**(1): p. 27-55.
24. Cronan, J.E., *Bacterial membrane lipids: Where do we stand?* *Annual Review of Microbiology*, 2003. **57**: p. 203-224.
25. Hancock, R.E., *Cationic peptides: effectors in innate immunity and novel antimicrobials*. *Lancet Infect Dis*, 2001. **1**(3): p. 156-64.
26. Jiang, Z.Q., et al., *Effects of Hydrophobicity on the Antifungal Activity of alpha-Helical Antimicrobial Peptides*. *Chemical Biology & Drug Design*, 2008. **72**(6): p. 483-495.
27. Madigan, M.T., *Brock biology of microorganisms*. 13th ed. 2012, San Francisco: Benjamin Cummings. xxviii, 1043, 77 p.
28. Tytler, E.M., et al., *Molecular-Basis for Prokaryotic Specificity of Magainin-Induced Lysis*. *Biochemistry*, 1995. **34**(13): p. 4393-4401.
29. Matsuzaki, K., *Why and how are peptide-lipid interactions utilized for self-defense? Magainins and tachyplepsins as archetypes*. *Biochimica et Biophysica Acta (BBA) - Biomembranes*, 1999. **1462**(1-2): p. 1-10.
30. Epand, R.F., et al., *Amphipathic Helical Cationic Antimicrobial Peptides Promote Rapid Formation of Crystalline States in the*

- Presence of Phosphatidylglycerol: Lipid Clustering in Anionic Membranes*. Biophysical Journal, 2010. **98**(11): p. 2564-2573.
31. Yang, L., et al., *Crystallization of antimicrobial pores in membranes: Magainin and protegrin*. Biophysical Journal, 2000. **79**(4): p. 2002-2009.
 32. Powers, J.P.S. and R.E.W. Hancock, *The relationship between peptide structure and antibacterial activity*. Peptides, 2003. **24**(11): p. 1681-1691.
 33. Mihajlovic, M. and T. Lazaridis, *Antimicrobial peptides in toroidal and cylindrical pores*. Biochimica Et Biophysica Acta-Biomembranes, 2010. **1798**(8): p. 1485-1493.
 34. Huang, H.W., *Molecular mechanism of antimicrobial peptides: the origin of cooperativity*. Biochim Biophys Acta, 2006. **1758**(9): p. 1292-302.
 35. Koo, J.C., et al., *Pn-AMP1, a plant defense protein, induces actin depolarization in yeasts*. Plant and Cell Physiology, 2004. **45**(11): p. 1669-1680.
 36. Salvatore, M., et al., *alpha-defensin inhibits influenza virus replication by cell-mediated mechanism(s)*. Journal of Infectious Diseases, 2007. **196**(6): p. 835-843.
 37. Buck, C.B., et al., *Human alpha-defensins block papillomavirus infection*. Proceedings of the National Academy of Sciences of the United States of America, 2006. **103**(5): p. 1516-1521.
 38. McGwire, B.S., et al., *Killing of African trypanosomes by antimicrobial peptides*. J Infect Dis, 2003. **188**(1): p. 146-52.
 39. Peschel, A., et al., *Inactivation of the dlt operon in Staphylococcus aureus confers sensitivity to defensins, protegrins, and other antimicrobial peptides*. J Biol Chem, 1999. **274**(13): p. 8405-10.
 40. Otto, M., *Bacterial evasion of antimicrobial peptides by biofilm formation*. Curr Top Microbiol Immunol, 2006. **306**: p. 251-8.
 41. Nikaido, H., *Multidrug efflux pumps of gram-negative bacteria*. J Bacteriol, 1996. **178**(20): p. 5853-9.
 42. Maloy, W.L. and U.P. Kari, *Structure-activity studies on magainins and other host defense peptides*. Biopolymers, 1995. **37**(2): p. 105-22.
 43. Dennison, S.R. and D.A. Phoenix, *Influence of C-Terminal Amidation on the Efficacy of Modelin-5*. Biochemistry, 2011. **50**(9): p. 1514-1523.
 44. Hwang, H., et al., *Reduction of Helical Content by Insertion of a Disulfide Bond Leads to an Antimicrobial Peptide with Decreased Hemolytic Activity*. Chemmedchem, 2013. **8**(1): p. 59-62.
 45. Strandberg, E., et al., *Influence of C-terminal amidation on the antimicrobial and hemolytic activities of cationic alpha-helical peptides*. Pure and Applied Chemistry, 2007. **79**(4): p. 717-728.

46. Ganz, T., *Defensins and host defense*. Science, 1999. **286**(5439): p. 420-1.
47. Kreil, G., *D-amino acids in animal peptides*. Annu Rev Biochem, 1997. **66**: p. 337-45.
48. Tew, G.N., et al., *De novo design of biomimetic antimicrobial polymers*. Proceedings of the National Academy of Sciences of the United States of America, 2002. **99**(8): p. 5110-5114.
49. Nguyen, L.T., et al., *Serum stabilities of short tryptophan- and arginine-rich antimicrobial peptide analogs*. PLoS One, 2010. **5**(9).
50. Tam, J.P., Y.A. Lu, and J.L. Yang, *Correlations of cationic charges with salt sensitivity and microbial specificity of cystine-stabilized beta-strand antimicrobial peptides*. Journal of Biological Chemistry, 2002. **277**(52): p. 50450-50456.
51. *ClinicalTrials.gov*. Available from: <http://clinicaltrials.gov>.
52. Piotto, S.P., et al., *YADAMP: yet another database of antimicrobial peptides*. Int J Antimicrob Agents, 2012. **39**(4): p. 346-51.
53. *UniProtKB/Swiss-Prot*. Available from: <http://www.uniprot.org/uniprot>
54. Wang, G., X. Li, and Z. Wang, *APD2: the updated antimicrobial peptide database and its application in peptide design*. Nucleic Acids Res, 2009. **37**(Database issue): p. D933-7.
55. Thomas, S., et al., *CAMP: a useful resource for research on antimicrobial peptides*. Nucleic Acids Res, 2010. **38**(Database issue): p. D774-80.
56. *NCBI*. Available from: <http://www.ncbi.nlm.nih.gov/taxonomy>.
57. Lehninger, A.L., D.L. Nelson, and M.M. Cox, *Lehninger principles of biochemistry*. 5th ed. 2008, New York: W.H. Freeman.
58. Gasteiger, E., et al., *Protein Identification and Analysis Tools on the ExPASy Server*, in *The Proteomics Protocols Handbook*, J. Walker, Editor. 2005, Humana Press. p. 571-607.
59. Bjellqvist, B., et al., *Reference points for comparisons of two-dimensional maps of proteins from different human cell types defined in a pH scale where isoelectric points correlate with polypeptide compositions*. Electrophoresis, 1994. **15**(3-4): p. 529-39.
60. Boman, H.G., *Antibacterial peptides: basic facts and emerging concepts*. J Intern Med, 2003. **254**(3): p. 197-215.
61. Radzicka, A. and R. Wolfenden, *Comparing the Polarities of the Amino-Acids - Side-Chain Distribution Coefficients between the Vapor-Phase, Cyclohexane, 1-Octanol, and Neutral Aqueous-Solution*. Biochemistry, 1988. **27**(5): p. 1664-1670.
62. Tossi A, S.L., Giangaspero A. , *New consensus hydrophobicity scale extended to non-proteinogenic amino acids*. Peptides 2002.

- Proceedings of the Twenty-Seventh European Peptide Symposium. Napoli, Italy: Edizioni Ziino, 2002: p. 416–7.
63. Kyte, J. and R.F. Doolittle, *A simple method for displaying the hydropathic character of a protein*. J Mol Biol, 1982. **157**(1): p. 105-32.
 64. Eisenberg, D., et al., *Hydrophobic Moments and Protein-Structure*. Faraday Symposia of the Chemical Society, 1982(17): p. 109-120.
 65. King, R.D. and M.J. Sternberg, *Identification and application of the concepts important for accurate and reliable protein secondary structure prediction*. Protein Sci, 1996. **5**(11): p. 2298-310.
 66. Huang, F. and W.M. Nau, *A conformational flexibility scale for amino acids in peptides*. Angew Chem Int Ed Engl, 2003. **42**(20): p. 2269-72.
 67. Guruprasad, K., B.V.B. Reddy, and M.W. Pandit, *Correlation between Stability of a Protein and Its Dipeptide Composition - a Novel-Approach for Predicting Invivo Stability of a Protein from Its Primary Sequence*. Protein Engineering, 1990. **4**(2): p. 155-161.
 68. Holton, T.A., et al., *CPPpred: prediction of cell penetrating peptides*. Bioinformatics, 2013. **29**(23): p. 3094-6.
 69. O'Neal, E.K. and C.M. Grisham. *Java applet for Helical-Wheel*. Available from: <http://cti.itc.virginia.edu/~cmg/Demo/wheel/wheelApp.html>.
 70. Rotem, S. and A. Mor, *Antimicrobial peptide mimics for improved therapeutic properties*. Biochim Biophys Acta, 2009. **1788**(8): p. 1582-92.
 71. Lienkamp, K. and G.N. Tew, *Synthetic mimics of antimicrobial peptides--a versatile ring-opening metathesis polymerization based platform for the synthesis of selective antibacterial and cell-penetrating polymers*. Chemistry, 2009. **15**(44): p. 11784-800.
 72. Piers, K.L. and R.E. Hancock, *The interaction of a recombinant cecropin/melittin hybrid peptide with the outer membrane of Pseudomonas aeruginosa*. Mol Microbiol, 1994. **12**(6): p. 951-8.
 73. Bai, Y., et al., *Structure-dependent charge density as a determinant of antimicrobial activity of peptide analogues of defensin*. Biochemistry, 2009. **48**(30): p. 7229-39.
 74. Ireland, D.C., et al., *Isolation, sequencing, and structure-activity relationships of cyclotides*. J Nat Prod, 2010. **73**(9): p. 1610-22.
 75. Jagadish, K. and J.A. Camarero, *Cyclotides, a promising molecular scaffold for peptide-based therapeutics*. Biopolymers, 2010. **94**(5): p. 611-6.
 76. Franzman, M.R., et al., *Targeted antimicrobial activity of a specific IgG-SMAP28 conjugate against Porphyromonas gingivalis in a mixed culture*. Int J Antimicrob Agents, 2009. **33**(1): p. 14-20.

77. Leupold, E., H. Nikolenko, and M. Dathe, *Apolipoprotein E peptide-modified colloidal carriers: the design determines the mechanism of uptake in vascular endothelial cells*. *Biochim Biophys Acta*, 2009. **1788**(2): p. 442-9.
78. Guyomard, A., et al., *Incorporation of a Hydrophobic Antibacterial Peptide into Amphiphilic Polyelectrolyte Multilayers: A Bioinspired Approach to Prepare Biocidal Thin Coatings*. *Advanced Functional Materials*, 2008. **18**(5): p. 758-765.
79. Gorostiza, P. and E.Y. Isacoff, *Optical switches for remote and noninvasive control of cell signaling*. *Science*, 2008. **322**(5900): p. 395-9.
80. Mayer, G. and A. Heckel, *Biologically active molecules with a "light switch"*. *Angew Chem Int Ed Engl*, 2006. **45**(30): p. 4900-21.
81. Szymański, W., et al., *Reversible Photocontrol of Biological Systems by the Incorporation of Molecular Photoswitches*. *Chemical Reviews*, 2013. **113**(8): p. 6114-6178.
82. Schierling, B., et al., *Controlling the enzymatic activity of a restriction enzyme by light*. *Proc Natl Acad Sci U S A*, 2010. **107**(4): p. 1361-6.
83. Tochitsky, I., et al., *Optochemical control of genetically engineered neuronal nicotinic acetylcholine receptors*. *Nat Chem*, 2012. **4**(2): p. 105-11.
84. Bonardi, F., et al., *Light-induced control of protein translocation by the SecYEG complex*. *Angew Chem Int Ed Engl*, 2010. **49**(40): p. 7234-8.
85. Stein, M., et al., *Azo-propofols: photochromic potentiators of GABA(A) receptors*. *Angew Chem Int Ed Engl*, 2012. **51**(42): p. 10500-4.
86. Piotto, S., et al., *Small azobenzene derivatives active against bacteria and fungi*. *Eur J Med Chem*, 2013. **68**: p. 178-84.
87. Kumar, G.S. and D.C. Neckers, *Photochemistry of azobenzene-containing polymers*. *Chemical Reviews*, 1989. **89**(8): p. 1915-1925.
88. de Lange, J.J., J.M. Robertson, and I. Woodward, *X-Ray Crystal Analysis of Trans-Azobenzene*. *Proceedings of the Royal Society of London. Series A. Mathematical and Physical Sciences*, 1939. **171**(946): p. 398-410.
89. Bose, M., et al., *The Incorporation of a Photoisomerizable Amino Acid into Proteins in E. coli*. *Journal of the American Chemical Society*, 2005. **128**(2): p. 388-389.
90. Jaffé, H.H. and M. Orchin, *Theory and applications of ultraviolet spectroscopy*. 1962, New York,: Wiley. 624 p.
91. Ishibashi, J., et al., *Purification, cDNA cloning and modification of a defensin from the coconut rhinoceros beetle, Oryctes rhinoceros*. *Eur J Biochem*, 1999. **266**(2): p. 616-23.
92. Stewart, J.M. and J.D. Young, *Solid phase peptide synthesis*. 2nd ed. 1984, Rockford, Ill.: Pierce Chemical Co. xvi, 176 p.

93. Maget-Dana, R., et al., *The secondary structure of the insect defensin A depends on its environment. A circular dichroism study.* Biochimie, 1995. **77**(4): p. 240-4.
94. Welinder, K.G. and L.B. Smillie, *Amino acid sequence studies of horseradish peroxidase. II. Thermolytic peptides.* Can J Biochem, 1972. **50**(1): p. 63-90.
95. Welinder, K.G., *Plant peroxidases: structure-function relationships*, in *Plant Peroxidases 1980-1990. Topics and Detailed Literature on Molecular, Biochemical, and Physiological Aspects*, C. Penel, Gaspar, T., Greppin, H., Editor. 1992: University of Geneva. p. 1-24.
96. Morita, Y., et al., *Purification, crystallization, and characterization of peroxidase from Coprinus cinereus.* J Biochem, 1988. **103**(4): p. 693-9.
97. Haschke, R.H. and J.M. Friedhoff, *Calcium-related properties of horseradish peroxidase.* Biochem Biophys Res Commun, 1978. **80**(4): p. 1039-42.
98. Shannon, L.M., E. Kay, and J.Y. Lew, *Peroxidase isozymes from horseradish roots. I. Isolation and physical properties.* J Biol Chem, 1966. **241**(9): p. 2166-72.
99. Pace, C.N., et al., *How to Measure and Predict the Molar Absorption-Coefficient of a Protein.* Protein Science, 1995. **4**(11): p. 2411-2423.
100. Veitch, N.C., *Horseradish peroxidase: a modern view of a classic enzyme.* Phytochemistry, 2004. **65**(3): p. 249-259.
101. Childs, R.E. and W.G. Bardsley, *The steady-state kinetics of peroxidase with 2,2'-azino-di-(3-ethyl-benzthiazoline-6-sulphonic acid) as chromogen.* Biochem J, 1975. **145**(1): p. 93-103.
102. Chan, Y.H.M. and S.G. Boxer, *Model membrane systems and their applications.* Current Opinion in Chemical Biology, 2007. **11**(6): p. 581-587.
103. Walde, P., et al., *Giant Vesicles: Preparations and Applications.* Chembiochem, 2010. **11**(7): p. 848-865.
104. Cevc, G., *Phospholipids handbook.* 1993, New York: Marcel Dekker, Inc. xi, 988 p.
105. Olson, F., et al., *Preparation of Liposomes of Defined Size Distribution by Extrusion through Polycarbonate Membranes.* Biochimica Et Biophysica Acta, 1979. **557**(1): p. 9-23.
106. Mayer, L.D., M.J. Hope, and P.R. Cullis, *Vesicles of Variable Sizes Produced by a Rapid Extrusion Procedure.* Biochimica Et Biophysica Acta, 1986. **858**(1): p. 161-168.
107. Nayar, R., M.J. Hope, and P.R. Cullis, *Generation of Large Unilamellar Vesicles from Long-Chain Saturated Phosphatidylcholines by Extrusion Technique.* Biochimica Et Biophysica Acta, 1989. **986**(2): p. 200-206.

108. Walde, P. and S. Ichikawa, *Enzymes inside lipid vesicles: preparation, reactivity and applications*. Biomol Eng, 2001. **18**(4): p. 143-77.
109. Koynova, R. and M. Caffrey, *Phases and phase transitions of the phosphatidylcholines*. Biochim Biophys Acta, 1998. **1376**(1): p. 91-145.
110. Wiedmann, T., A. Salmon, and V. Wong, *Phase behavior of mixtures of DPPC and POPG*. Biochim Biophys Acta, 1993. **1167**(2): p. 114-20.
111. Angelova, M.I. and D.S. Dimitrov, *Liposome Electroformation*. Faraday Discussions, 1986. **81**: p. 303-+.
112. Angelova, M.I., et al., *Preparation of Giant Vesicles by External Ac Electric-Fields - Kinetics and Applications*. Trends in Colloid and Interface Science Vi, 1992. **89**: p. 127-131.
113. Robinson, T., et al., *Microfluidic trapping of giant unilamellar vesicles to study transport through a membrane pore*. Biomicrofluidics, 2013. **7**(4).
114. Matsuzaki, K., et al., *Magainin 1-Induced Leakage of Entrapped Calcein out of Negatively-Charged Lipid Vesicles*. Biochimica Et Biophysica Acta, 1989. **981**(1): p. 130-134.
115. Matsuzaki, K., et al., *Interactions of an antimicrobial peptide, tachyplesin I, with lipid membranes*. Biochim Biophys Acta, 1991. **1070**(1): p. 259-64.
116. Porstmann, B., et al., *Temperature dependent rise in activity of horseradish peroxidase caused by non-ionic detergents and its use in enzyme-immunoassay*. Clin Chim Acta, 1981. **109**(2): p. 175-81.
117. Gregoriadis, G., *Liposome technology*. 2nd ed. 1993, Boca Raton, Fla.: CRC Press.
118. Tahara, Y. and Y. Fujiyoshi, *A new method to measure bilayer thickness: cryo-electron microscopy of frozen hydrated liposomes and image simulation*. Micron, 1994. **25**(2): p. 141-9.
119. Cornell, B.A., J. Middlehurst, and F. Separovic, *The Molecular Packing and Stability within Highly Curved Phospholipid-Bilayers*. Biochimica Et Biophysica Acta, 1980. **598**(2): p. 405-410.
120. Mitchell, D.J. and B.W. Ninham, *Micelles, vesicles and microemulsions*. Journal of the Chemical Society, Faraday Transactions 2: Molecular and Chemical Physics, 1981. **77**(4): p. 601-629.
121. Dickey, A. and R. Faller, *Examining the contributions of lipid shape and headgroup charge on bilayer behavior*. Biophys J, 2008. **95**(6): p. 2636-46.
122. Tang, H., M. Kays, and A. Prince, *Role of Pseudomonas aeruginosa pili in acute pulmonary infection*. Infect Immun, 1995. **63**(4): p. 1278-85.

123. Liu, C., et al., *Clinical practice guidelines by the infectious diseases society of america for the treatment of methicillin-resistant Staphylococcus aureus infections in adults and children: executive summary*. Clin Infect Dis, 2011. **52**(3): p. 285-92.
124. Bradamante, S., L. Barengi, and A. Villa, *Cardiovascular protective effects of resveratrol*. Cardiovasc Drug Rev, 2004. **22**(3): p. 169-88.
125. Athar, M., et al., *Resveratrol: a review of preclinical studies for human cancer prevention*. Toxicol Appl Pharmacol, 2007. **224**(3): p. 274-83.
126. Zamin, L.L., et al., *Protective effect of resveratrol against oxygen-glucose deprivation in organotypic hippocampal slice cultures: Involvement of PI3-K pathway*. Neurobiol Dis, 2006. **24**(1): p. 170-82.
127. Baur, J.A. and D.A. Sinclair, *Therapeutic potential of resveratrol: the in vivo evidence*. Nat Rev Drug Discov, 2006. **5**(6): p. 493-506.
128. Leiro, J.M., et al., *The anti-inflammatory activity of the polyphenol resveratrol may be partially related to inhibition of tumour necrosis factor- α (TNF- α) pre-mRNA splicing*. Molecular Immunology, 2010. **47**(5): p. 1114-1120.
129. Filip, V., et al., *Resveratrol and its antioxidant and antimicrobial effectiveness*. Food Chemistry, 2003. **83**(4): p. 585-593.
130. Paulo, L., et al., *Antimicrobial activity and effects of resveratrol on human pathogenic bacteria*. World Journal of Microbiology and Biotechnology, 2010. **26**(8): p. 1533-1538.
131. Taguri, T., T. Tanaka, and I. Kouno, *Antimicrobial activity of 10 different plant polyphenols against bacteria causing food-borne disease*. Biol Pharm Bull, 2004. **27**(12): p. 1965-9.
132. Gledhill, J.R., et al., *Mechanism of inhibition of bovine F1-ATPase by resveratrol and related polyphenols*. Proc Natl Acad Sci U S A, 2007. **104**(34): p. 13632-7.
133. Accelrys, *Discovery Studio 2.5*. Available from: <http://accelrys.com/products/discovery-studio/>.
134. Cheng, A. and K.M. Merz, *Prediction of Aqueous Solubility of a Diverse Set of Compounds Using Quantitative Structure–Property Relationships*. Journal of Medicinal Chemistry, 2003. **46**(17): p. 3572-3580.
135. Egan, W.J. and G. Lauri, *Prediction of intestinal permeability*. Advanced Drug Delivery Reviews, 2002. **54**(3): p. 273-289.
136. Susnow, R.G. and S.L. Dixon, *Use of Robust Classification Techniques for the Prediction of Human Cytochrome P450 2D6 Inhibition*. Journal of Chemical Information and Computer Sciences, 2003. **43**(4): p. 1308-1315.
137. Cheng, A. and S. Dixon, *In silico models for the prediction of dose-dependent human hepatotoxicity*. Journal of Computer-Aided Molecular Design, 2003. **17**(12): p. 811-823.

138. Merino, E., *Synthesis of azobenzenes: the coloured pieces of molecular materials*. Chem Soc Rev, 2011. **40**(7): p. 3835-53.
139. Acierno, D., et al., *Synthesis and Characterization of Segmented Liquid Crystalline Polymers with the Azo Group in the Main Chain*. Macromolecules, 2004. **37**(17): p. 6418-6423.
140. Bruice, P.Y., *Organic chemistry*. 4th ed. 2004, Upper Saddle River, NJ: Pearson/Prentice Hall. xxxvi, 1228, 74 p.
141. CLSI, *Approved Standard-Third Edition, in Reference method for broth dilution antifungal susceptibility testing of yeasts*; . 2008, Clinical and Laboratory Standards Institute, Wayne, PA.
142. Patton, T., et al., *Use of a spectrophotometric bioassay for determination of microbial sensitivity to manuka honey*. J. Microbiol. Methods, 2006. **64**(1): p. 84-95.
143. da Silva, W., et al., *Improvement of XTT assay performance for studies involving Candida albicans biofilms*. Braz Dent J. , 2008. **19**(4): p. 364-369.
144. Jin, Y., et al., *Biofilm-forming ability of Candida albicans is unlikely to contribute to high levels of oral yeast carriage in cases of human immunodeficiency virus infection*. J Clin Microbiol. , 2003. **41**: p. 2961-7.
145. Weber, K., B. Schulz, and M. Ruhnke, *Resveratrol and its antifungal activity against Candida species*. Mycoses, 2011. **54**(1): p. 30-33.
146. Kenawy el, R., S.D. Worley, and R. Broughton, *The chemistry and applications of antimicrobial polymers: a state-of-the-art review*. Biomacromolecules, 2007. **8**(5): p. 1359-84.
147. Hook, A.L., et al., *Combinatorial discovery of polymers resistant to bacterial attachment*. Nat Biotechnol, 2012. **30**(9): p. 868-75.
148. Muñoz-Bonilla, A. and M. Fernández-García, *Polymeric materials with antimicrobial activity*. Progress in Polymer Science, 2012. **37**(2): p. 281-339.
149. Quintavalla, S. and L. Vicini, *Antimicrobial food packaging in meat industry*. Meat Sci, 2002. **62**(3): p. 373-80.
150. Vroman, I. and L. Tighzert, *Biodegradable Polymers*. Materials, 2009. **2**(2): p. 307-344.
151. Mohee, R., et al., *Biodegradability of biodegradable/degradable plastic materials under aerobic and anaerobic conditions*. Waste Manag, 2008. **28**(9): p. 1624-9.
152. Garlotta, D., *A Literature Review of Poly(Lactic Acid)*. Journal of Polymers and the Environment, 2001. **9**(2): p. 63-84.
153. Bastioli, C., *Properties and applications of Mater-Bi starch-based materials*. Polymer Degradation and Stability, 1998. **59**(1-3): p. 263-272.

154. Rosen, S.L., *Fundamental principles of polymeric materials*. 2nd ed. SPE monographs, 1993, New York: Wiley. xvi, 420 p.
155. Letcher, T.M., *Solubility of plasticizers, polymers and environmental pollution*, in *Thermodynamics, solubility, and environmental issues*. 2007, Elsevier. p. 397-407.
156. Piotto, S., et al., *Novel antimicrobial polymer films active against bacteria and fungi*. *Polymer Composites*, 2013. **34**(9): p. 1489-1492.
157. Concilio, S., et al., *Antimicrobial polymer films for food packaging*, in *6th International Conference on Times of Polymers (Top) and Composites*. 14-16 june, 2012. p. 256-258.
158. Galya, T., et al., *Antibacterial poly(vinyl alcohol) film containing silver nanoparticles: Preparation and characterization*. *Journal of Applied Polymer Science*, 2008. **110**(5): p. 3178-3185.



Dipartimento di farmacia
Via Giovanni Paolo II, 132 - 84084 -
Fisciano (SA)